Università degli Studi della Tuscia di Viterbo
in convenzione con il Centro di Ricerca ENEA Frascati

Corso di Dottorato di Ricerca in

Ingegneria degli ecosistemi e sistemi produttivi - XXX Ciclo

STUDY OF MULTI-TUBE PD-AG MEMBRANE REACTOR FOR ULTRA-PURE HYDROGEN ISOTOPES SEPARATION IN NUCLEAR FUSION FUEL CYCLE

(**s.s.d. ING-IND/09**)

Tesi di dottorato di:
Dott. Marco INCELLI

Coordinatore del corso
Prof. Silvio FRANCO
Firma ……..

Tutore
Prof. Maurizio Carlini
Firma ……

A.A. 2016/17

Table of Contents

List of Tables

List of Figures

Abstract and scope

Nuclear fusion power is one of the most challenging and promising worldwide project for future carbon-free energy production. Currently, few experimental fusion machines, so called tokamak, have been built in order to investigate the fusion feasibility. A demonstrative fusion power reactor (DEMO) is planned to be constructed in the next decades. Fusion reactors will perform the D-T (Deuterium-Tritium) reaction. Deuterium is widely available in nature while tritium is present in few traces due to its fast-decay (12.6 year). Therefore, it has to be produced in situ by high-energy neutron (originated by the DT reaction) interaction with lithium-based materials, called Breeding Blanket (BB).

Four BB concepts (solids and liquids) are investigated within the EUROfusion programme for their possible implementation in DEMO together with their own tritium extraction systems.

Concerning the solid Breeding Blanket concept, named Helium Cooled Pebble Bed (HCPB), a Helium stream will be used to purge tritium from the lithium-base pebble beds. Inside the Helium purge stream, Tritium will be present in form of Q_2 and/or Q_2O (with Q=H, D, T) in few traces. For this purpose, two main Tritium Extraction and Recovery Systems (TERS) have been identified for the DEMO HCPB: 1) the reference solution, which is based on molecular sieve and cold trap separation technologies and 2) the backup solution, which is based on membrane separation technologies. In particular, the backup solution foresees a pre-concentration stage, which reduces the helium content in the tritiated gas stream, a Pd-Ag permeator that separates the hydrogen isotopes (Q_2) in the gas phase and a Catalytic Membrane Reactor (CMR), which recovers the hydrogen isotopes in the oxidized phase (Q_2O). The aim of this thesis is to experimentally investigate the feasibility of the tritium extraction system based on the membranes technologies that are very attractive because of their long durability, stability and the continuous operation which allow to reduce the tritium inventory.

The dissertation presents the experimental performances of a Pd-Ag permeator and a Catalytic Membrane Reactor for hydrogen isotopes recovery in gas (Q_2) and liquid phase (Q_2O), respectively. In ENEA Frascati, a single-membrane module facility has been built to assess the performances in hydrogen separation and in heavy water decontamination operated through Water Gas Shift (WGS) and Isotopic Swamping (IS) reactions. Several tests have been carried out in order to

examine in depth the hydrogen permeation performances in different operating conditions (temperature, pressure, He/H_2 ratio). The permeation tests confirm that, at high He/H_2 flow ratio, the ability in hydrogen separation dramatically decreases till to become useless at He/H_2 more than 50. Therefore, in case of the HCPB in which the He/H_2 feed flow ratio is much higher, a pre-concentration stage is necessary to reduce the He/H_2 feed flow ratio. Concerning the reaction tests, different catalysts, one laboratory-made and one commercial, have been tested and compared by performing WGS and IS. In case of WGS, one of most critical issue is the by-product formation (particularly methane) that must be avoided. Several experiments have been carried out with encouraging results. The reaction tests demonstrate the possibility of performing high hydrogen reaction and separation rates (up to 80% of total efficiency in a single step) with a very low methane production (measured between $0.4\%_{mol}$ and $1.7\%_{mol}$) at low pressure (1-3 bar) and temperature (573-623 K). Regarding the IS reaction, lower but still good performances have been reached (about 60%). The catalyst comparison demonstrates the critical role of the catalyst choice that hugely influence the process performances. In addition, also the effect of the operating parameters (i.e. temperature, pressures and feed flow rates) on the reaction efficiency and methane formation has been experimentally evaluated. Based on the design and the testing of the single Pd-Ag module, successively a mechanical design of a 10-tube membrane module has been assessed. The multi-tube membrane reactor has been manufactured and integrated in a new experimental facility, which have been also designed and commissioned to test the middle-scale membrane apparatus under DEMO-relevant conditions. Particularly the results of the previous experimental activity on the single membrane were useful for the identification of specific operating parameters and the assessment of the permeation and reaction procedures that allowed to correctly operate the new middle-scale system.

Future tests on middle-scale reactors, in view of DEMO, are necessary to validate the scalability of the single-tube performances and allow to gain experience on the engineering and operation procedure. Furthermore, in case of a good scalability of the single-tube, a ready (back-up) solution will be available in few years for the tritium extraction system of the HCPB DEMO blanket. On the contrary, if the scalability would affect the tritium removal performances in Pd-Ag membrane separation and reaction, the work presented could be a primary step towards a better optimization of the multi-tube engineering concept.

1. The fuel cycle of fusion reactor

Nuclear fusion power is one of the most challenging and promising options for future carbon-free energy production. A great deal of combined efforts is underway in order to assess the feasibility and demonstrate the capability of large-scale power production. Few experimental fusion machines (tokamaks), consisting in a toroidal vacuum chamber where a burning plasma of hydrogen isotopes is magnetically confined, were built (JET in Culham, UK) or are under construction (ITER in Catarache, FR), while a fusion power reactor (DEMO) is planned to be constructed in the next decades as foresees by the European fusion roadmap of H2020 [1]. So far, JET is the main and largest operating fusion device and its scientific purpose is focused on the preparation of ITER operation and safety. It has been recently upgraded introducing an ITER-like first wall which is under testing in several campaign [6, 7]. ITER is the halfway reactor aimed at assesses some plasma configuration, operational procedure and technologies in view of DEMO. This last one is under design and it will be the demonstrative fusion power plant. It currently represents the single step between ITER and a commercial reactor [4].

The D-T reaction is the reference reaction for the first-generation fusion reactor. The main reasons is that it exhibit the higher cross section (which is the main parameter for the reaction rate) at lower energy or plasma temperature as shown in Figure 1.

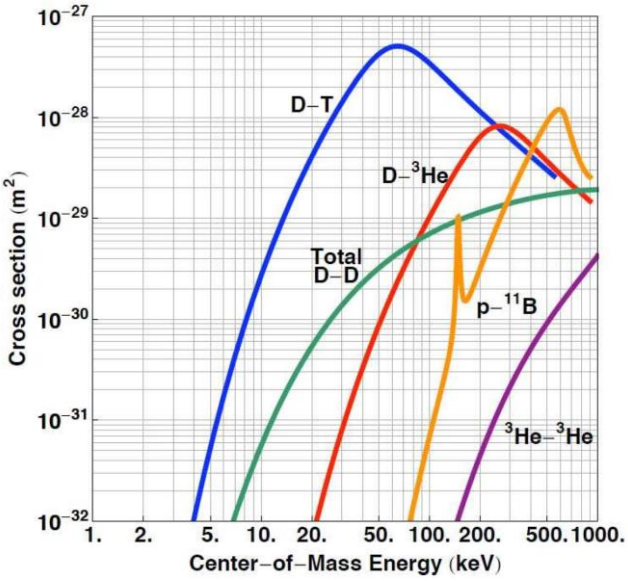

Figure 1. Cross sections of the main potential fusion reactions

The fusion of the deuterium and tritium nuclei generates a Helium nuclide and a fast neutron (14.1 MeV). The reaction is shown in (1)

$$ {}_{1}^{2}D + {}_{1}^{3}T \rightarrow {}_{2}^{4}He(3.5\,MeV) + {}_{0}^{1}n(14.1\,MeV) \quad (1) $$

Where *D* and *T* are Deuterium and Tritium, *He* is Helium and *n* is the neutron. As shown in Figure 1 the D-T cross section reaches acceptable values around plasma temperature of 10 KeV (~ 10^8 °C) while around 100 keV (10^9 °C) the cross section increases of almost five order of magnitudes. In this temperature range, the D-T reaction has the highest ignition potential. The D-T reaction delivers 80% of its power in the 14-MeV neutron, which energy will be converted and recovered in the breeding blanket and 20% in the charged alpha particle. The neutrons absorption in the breeding blanket will generate tritium from lithium and thermal energy (from ~2 to 4.8 MeV) by exothermic reactions. The significant fraction of the alpha energy will be converted to electromagnetic radiation, deposited at the first wall, and transferred to the thermal recovery system [5].

Although the reference fusion fuels are D and T, alternative fusion reactions could be taken into account for the next generation reactor (Figure 2). It is the case of tokamaks burning in a catalysed D-D mode, which look promising (first-generation reactor). The environmental impacts of a D-T fuelled reactor will be related to the radioactivity of the tritium and the activation and radiation damage of materials due to 14-MeV neutrons, and the absolute requirement for breeding tritium fuel.

On the other hand, advanced fusion reactors may require start-up scenarios involving the use of small amounts of D-T fuel for high and fast ignition, while less reactive but, perhaps, more environmentally and economically acceptable fuels may be used.

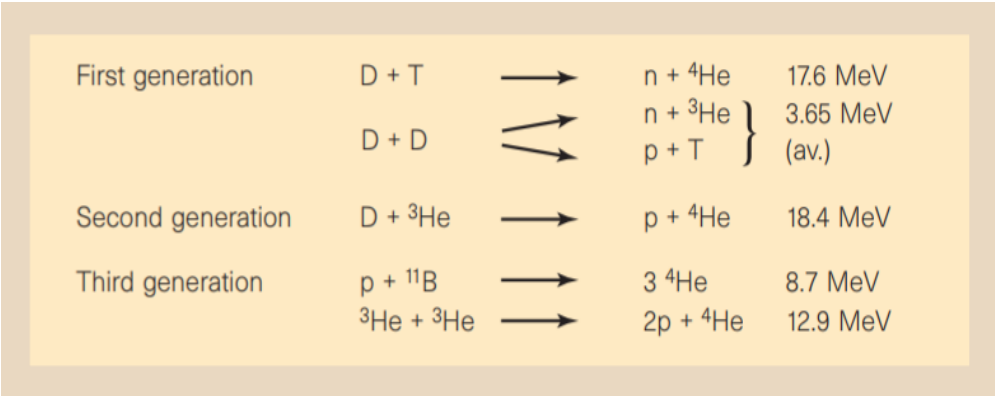

Figure 2. Main nuclear fusion reactions in the future power plants [6]

ITER (International Thermonuclear Experimental Reactor) and DEMO (DEMOnstrating fusion power reactor) will perform the D-T reaction and DEMO will become the reference experimental reactor for the first generation reactor.

The second-generation (D-^{3}He) reaction is very interesting because it does not require breeding and recovering tritium. It is characterised by a very low presence of fusion neutrons but it is not completely a “neutron-free” reaction, due to D-D side reactions, which generates 2.45 MeV neutrons and T inducing the D-T reaction. Other interesting aspects of this reaction are the possibility to obtain electrical power by direct energy conversion of proton without using a thermodynamic cycle with a turbine. The “only” drawbacks are the availability of ^{3}He and the difficulty to achieve the burning plasma conditions [7].

Power Plants based on nuclear fusion concept must be self-sufficient in term of tritium production and fuels accountancy.

The main fuels involved in nuclear reactions will be deuterium (extracted from water) and tritium (produced in situ) both processed, in spite of fission nuclear fuel, in a closed fuel cycle. In particular, deuterium will be extracted from seawater in a simple and well-proven industrial process. The process simply consists in "Heavy water" separation from light water, or D_2O in which D is deuterium, and then the electrolysis allows to obtain and separate D_2 in gaseous phase [8]. As mentioned in [9], since 1930s, the natural concentration of deuterium was estimated to be:

- D/^{1}H = 1/4000 by measuring the intensity of Balmer lines in the spectrum of natural hydrogen
- D/^{1}H = 1/5000 by means of mass spectrometry
- D/^{1}H = 1/6200 on the basis of density differences between natural and depleted waters (current reference value)

It means that the concentration of the deuterium in the water is 0.016%[10].

Differently, tritium will be produced in lithium-based breeding blanket which consists in an thick layer (about 1 m) mounted on the plasma-facing side of the chamber.

Inside the Tokamak, the fuel that is expected to be burnt, will be a very small fraction of the entire fuel injected. The tritium burn-up fraction, interpreted as the fraction of burnt fuel and the one injected in the vacuum chamber, will be around 1%, or less in

ITER and few percentage (less than 5%) in DEMO [11]. Therefore, a huge quantity of fuel has to be recovered and purified.

Additionally, the fuel cycle should be designed according to:

- Fuel cost control and tritium accountancy
- Tritium inventory minimization
- Radiation losses minimization
- Fulfilment of the stability on neutron irradiation
- Condensable fuel, exhaust product and ashes management

Finally, the technologies and the processes to be adopted in the fuel cycle dramatically changes depending on the mixture content in the exhaust and the breeding blanket concept. Therefore, in order to fulfil all these requirements, the fusion fuel cycles characterization is becoming one of the most important challenges for fusion feasibility. Up to now, recirculation of unburned tritium is one of the major problems of the D-T fusion reactors [5].

1.2 The Issue of Tritium

Tritium (from greek "tritos", the third) is the radioactive isotope of hydrogen. It is a weak β^- emitter (penetration in air ~6 mm and in metals less than 1 mm) with a mid-short half-life (τ) of 12.3 years, which makes it very rare on earth (few traces). Hydrogen isotopes, in general, are a colourless, odourless, tasteless and non-metallic. When the three hydrogen isotopes gases are mixed, six different isotopologues appear: H_2, HD, HT, D_2, DT, and T_2. Conventionally molecular hydrogen isotopes will be cited as Q_2 (with Q = H, D, or T) and oxide form as Q_2O (meaning H_2O, HDO, HTO, D_2O, DTO, T_2O).

1.2.1 Tritium Properties

Table 1 reports the general properties of hydrogen deuterium and tritium. The difference among them is due to the comparable mass of neutron and hydrogen, which implies large mass differences among hydrogen isotopes. The isotopic effects, meant as the differences of those physical properties, are much more pronounced than the isotopic effects of any other elements.

Like hydrogen, tritium is highly reactive in:

- Giving/Accepting electrons
- Metal interaction (dissolution, diffusion, permeation etc.)
- Thermodynamics and kinetics (isotope effect influence)
- Explosion risks (Highly combustible diatomic gas Q_2) with a concentration in air between 4 and 75%

Regarding tritium, the radioactivity, therefore the decay type and the energy emission promote the radiochemical reaction.

Table 1. Hydrogen isotopes: comparison of the general properties [12]

	H_2	D_2	T_2
Abundance (in atomic form)	99.985 %	0.016 %	10^{-18}
Density (kg m^{-3}) at STP (0 °C, 101.325 kPa)	0.08988	0.180	0.2705
Heat of vaporization (kJ mol^{-1})	0.904	1.24	1.39
Boiling point (BP) (K)	20.271	23.67	25.04
Liquid density at BP (kg m^{-3})	70.99	163.83	255.6
Heat of fusion (kJ mol^{-1})	0.117	0.197	0.250
Melting point (MP) (K)	13.99	18.73	20.62
Solid density at M.P. (kg m^{-3})	86.3	196.7	45.35 mol L^{-1}
Triple point (TP)	13.804 K (7.030 kPa)	18.69 K (17.13 kPa)	20.62 K (21.6 kPa)
Critical point (CP)	32.976 K (1.293 MPa)	38.26 K (1.65 MPa)	40.44 K (1.85 MPa)
Density at CP (mol m^{-3})	15,200	16,700	17,700
Solid heat capacity at TP (J mol^{-1} K^{-1})	6.2	11.8	16.1

Bond energy (kJ mol^{-1})	435.9	443.4	446.9

Tritium, like hydrogen, can be found in different forms:

- Molecurar (Q_2)
- Oxidised (Q_2O)
- Bound (i.e. CQ_4, R-Q, Q_2O_2 etc.)

As reported in [13], Hydrogen is present in almost all materials. Tritium atoms will exchange with hydrogen atoms to form tritiated molecules. This behaviour is particularly prevalent in the biological systems in which hydrogen, deuterium and tritium are readily absorbed in the tissues and they are retained for decades. Oxidised form of tritium, although corrosive because of the radiolysis, are estimated to be 25000 time more hazardous than gaseous tritium inhalation because of the strong interaction between the skin and the tritiated water. In the same way, tritium can bind in organic [14] or inorganic [15] molecules in order to form tritiated product as i.e. methane (CQ_4) which is one of the common and problematic by-product in fusion fuel cycles.

1.2.2 Tritium availability

As already discussed, Tritium it is very rare in nature because its decay in a short half-life. However, there are different tritium sources, natural or not, which allow to have consistent quantities on earth. Tritium is produced:

- In nature on the high atmosphere and in the Earth's interior
- In Canadian nuclear reactors (CANDU)
- From lithium irradiation by neutrons

Cosmic rays are characterized mostly by high-energy particles such as neutrons, which interact with the upper atmosphere. These interactions permit the formation of many elements in stable or unstable form as described in [16] and [17]. Regarding tritium, cosmic rays are the reason of the primary natural source of tritium on earth. It is continuously generated by Nitrogen as shown in (2) and (3):

$$^{14}_{7}N + ^{1}_{0}n \rightarrow ^{12}_{6}C + ^{3}_{1}H - 4.3\ MeV \qquad (2)$$

$$^{14}_{7}N + ^{1}_{0}n \rightarrow 3^{4}_{2}He + ^{3}_{1}H - 11.5\ MeV \qquad (3)$$

The same Tritium (T) rapidly reacts with the oxygen in the air in order to form Q_2O (mostly HTO) blended in the atmosphere as humidity or suspended particle. Consequently, due to the T decays with half-life of 12.3 years, tritium decays about 5% per year, therefore a balance of the amount of T is established with the production and the decay. This mechanism assesses the concentration of tritium around 10^{-18} in natural hydrogen (T/H). This concentration, which is quite constant on earth, allows to estimate the total abundance of T around of several kg [18]. Actually, the nuclear weapon tests performed since 50s have been introduced in the atmosphere artificial tritium, which is much more than the natural background.

Tritium is produced through fission of natural uranium ores. The natural production rate is conventionally estimated around 0.18 kg y^{-1} [19]. Some studies confirm that an additional tritium source could be the earth's mantle in which nuclear fusion reactions occur. In particular according with [20], the Tritium measured in the lake bottom is 10% higher than natural background on lake surface. The authors assert that "… the ^{3}He and ^{3}H might be all from the mantle source, and produced by the supposed natural-nuclear-fusion, which might occur in an environment rich in water (H) and (U + Th) at high temperature and high pressure in the deep Earth." with the exclusion of nuclear tests or other nuclear reactions.

Artificial source of tritium can be attributable to nuclear fission reactors, in particular CANDUs reactors and nuclear weapons tests.

Due to the strategic importance of tritium for nuclear weapons, few nuclear fission reactors are dedicated to tritium production for military purpose while several civil fission reactors such as the Canadian PWR (Pressurized heavy Water Reactor) also called CANDU (CANada Deuterium Uranium) produce tritium because they use heavy water as neutron moderator (4):

$$D + n \rightarrow T + 6.25\ MeV \qquad (4)$$

Within the CANDU reactor more than 97% of tritium is bred in the moderator system under thermal neutron flux and a small part permeates in the coolant (~5%).

Since 1980s in the world, there are 38 active CANDU reactors, of which 22 built in Canada. The number of active reactor remains approximately constant [21] [22]. For

a typical CANDU 6 reactor, one of these power plants would produce about 130 g T^{-1} y^{-1} (average lifetime 50 year). Afterwards, two tritium removal facilities which are the Darlington Tritium Removal Facility (DTRF) and the Wolsong tritium removal facility (WTRF), achieve the tritium extraction capability of 3.27 kg yr^{-1} only in Canada [21]. Commercial light water reactors are releasing T around 1 g/year/reactor. Most important tritium extraction facilities are at Savannah River (US), Grenoble (France, 1972), Mound (US, 1986), Darlington (Canada, 1988), and Chalk River (Canada, 1988) with 95-97% of removal efficiency [19].

Tritium became part of the hydrological cycle; the distribution in the environment was estimated to be ~0.5% in the atmosphere, ~12 % in continental waters, and ~87.5% in oceans [17].

Tritium can be produced in some fission reactor (LWR, PWR or CANDU) or by neutron irradiation of lithium or boron.

Lithium is the lightest metal in nature and one of the most common metal especially in hard rocks. It is reference metal for battery energy storage (^{7}Li which is the 92.5% of the total lithium) and it is widely used in nuclear reactor for tritium production (^{6}Li with an abundance of 7.5%).

Tritium can be produced by neutron absorption in Li-based or B-based materials. These nuclear reactions are now performed in some light or heavy water fission reactors by using a special rod containing ^{6}Li, or ^{10}B. The reactions of interest are:

$$^{10}_{5}B + ^{1}_{0}n \rightarrow 2\ ^{4}_{2}He + ^{3}_{1}H \qquad (5)$$

$$^{6}_{3}Li + ^{1}_{0}n \rightarrow ^{3}_{1}H + ^{4}_{2}He + 4.8\ MeV \qquad (6)$$

Regarding the lithium, the same nuclear reaction will produce tritium in nuclear fusion devices. Differently from ^{7}Li, ^{6}Li has a very high thermal neutron cross-section as shown in Figure 3, while the breeding cross-section of ^{7}Li is significant only for fast reactions.

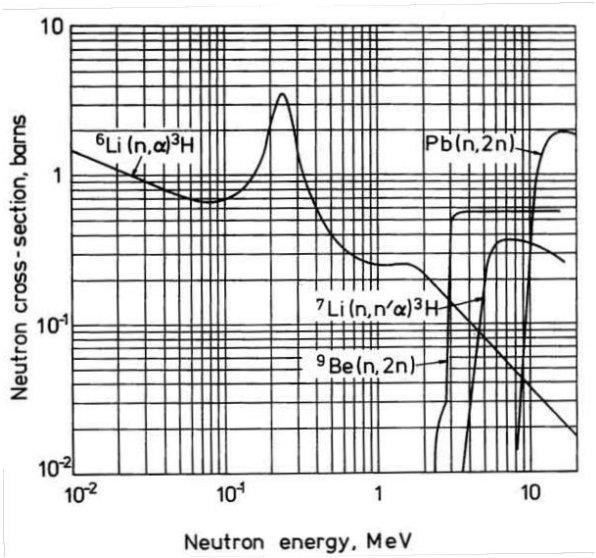

Figure 3. Neutron cross-section for tritium breeding (Source: National Physical Laboratory)

Dedicated military reactors produce several kilograms of tritium (which inventory is unavailable) by using $LiAlO_2$ or LiAl fuelled rods.

Tritium can be produced also in commercial nuclear fission power plants, as well described in [23]. As confirmed in [19], the exact amount is limited by requirements on criticality, flux profile, and electricity production. Since ^{6}Li has a very high cross-section, it burns out quickly. This means that the lithium must be located where it can be readily and easily removed, or moved during the operations. On the other hand, replacing the rods in LWRs more frequently would be major expensive. Just to give an example, in this scenario, estimation of tritium production by LWRs (Light Water Reactors) is about 0.1 kg T GWe^{-1} y^{-1} with a cost of 2-3 times more than the current price.

The possibility of using lithium in CANDU reactors is surprisingly possible because, apparently, the tritium production does not affect the power production and the operation could be more affordable. Nevertheless, the major practical limitation is the time required to adequately develop and test a new 'fuel' bundle and nuclear procedure[19].

According to [21], the total T inventory for military use is estimated to be around 600 kg at maximum during the early 1970s. After ‘50s nuclear tests, the total amount of tritium in the atmosphere was estimated to be around 500 kg [19]. The USA inventory has been estimated [24] at 40 kg in 2003 while, for Russia the inventory was about 66 kg in 1991, even though the US DOE (Department of Energy) has

published a tritium management plan [25] in which they declared that the number of nuclear US warheads has declined [26].

Nevertheless, the US tritium stockpile is not sufficient, and the DOE has started producing fresh tritium by irradiating tritium-producing burnable absorber rods containing lithium aluminate ceramic pellets in a single light water reactor. They expect to use up to three Tennessee Valley Authority (TVA) reactors for this purpose, to fulfil a maximum production requirement of 2800 g per 18-month cycle. Use of the second reactor would likely begin in the early 2020s. In short, the US government intends to produce only as much tritium as it believes it needs to maintain its nuclear warheads with an adequate reserve.

Therefore, tritium production itself to satisfy the nuclear fusion requirement is not only a problem in term of technology or infrastructure but it involves political and military strategies and this is strictly related to the economic and social solidity of all countries. This is confirmed also in [26] in which the authors declare that "Lack of tritium cannot be considered a fundamental problem, since it can be generated in any fission reactor even though the technical, political and economic issues are significant."

Next-generation fusion devices like ITER and especially DEMO, may consume several kilogrammes of tritium per year [1]. Currently, around 100 g of T is produced per year in a standard CANDU reactor and 20–25 kg T (mainly from Canada) will be available for operation of ITER[12].

This corresponds to the initial required amount for ITER start-up operation (D-T Reactions, T inventory in materials, T in tritium plant). This means that at present we have no T reserves for DEMO, which is foreseen for 2050s in the European fusion roadmap.

During these decades, tritium market will completely change due to the huge increasing of fuel requirement. The supply of tritium for fusion will depend on the availability of man-made sources [21].

Nevertheless, the tritium supply is a very critical issue for DEMO but even more for further fusion devices. This aspect is evident considering that, by assuming 10 year delay in ITER and therefore in DEMO (2060) and considering the half-life of tritium, in 2060 tritium stocks will be very small, surely not relevant for the next fusion machines. This is confirmed in [27] in which it is declared that the definition of the

timeline for tritium supply is very important for DEMO, which must breed tritium from the very beginning and use about 5-10 kg amount of tritium for start-up operations and produce its own tritium well before 2060.

Fusion should be developed in order to take advantage of the unique historical opportunity in which tritium is available. In this short timeline, the development of D-T fusion and alternative fusion reactions must be carefully planned worldwide taking into account tritium availability as well as the development and deployment of more efficient and performant breeding component [26].

1.2.3 Tritium measurements

Although Tritium chemistry is similar to that of other hydrogen isotopes, a number of significant differences arise because of the different mass of the different hydrogen isotopes. The tritium measurement techniques can follow two different approaches:

- Tritium's decay detection
- Tritium's physical and chemical properties

Basing on radioactive properties, tritium can be detected and measured via:

a. Beta Induced X-ray Spectroscopy (BIXS)
b. Scintillation
c. Ionisation Chambers
d. Solid State Detectors
e. Calorimetry and Bolometers
f. Less-well established techniques (Cherenkow Radiation, Tritium imaging plate)

On the contrary, basing on physical and chemical properties, tritium is measured through:

a. Mass Spectroscopy
b. Raman Spectroscopy
c. Gas Chromatography
d. Nuclear Magnetic Resonance (NMR)
e. Spectroscopy Techniques (Infrared, Visible and Ultraviolet)
f. Photoacoustic Spectroscopy

The main methods for hydrogen isotopes measurement are listed in Table 2 considering the measurement range, time for analysis, advantages and disadvantages. The measurement methods highlighted in grey are used in TLK (tritium Laboratory Karlsruhe) in Germany.

Although there are different technologies for tritium measurement, only some of them could be suitable or investigable for tritium plants and nuclear fusion power plants. The reason can be summarized in the limitations of the specific technology and the possibility to go beyond them. The study [28] gives a wide overview of the promising techniques for tritium measurement in the future fusion device. Therefore, only few of the techniques listed in Table 2 are described in this dissertation.

Mass spectroscopy is a powerful and widely used tool for monitoring tritium because it is able to measure the mass differences between elements and their isotopes. It has the ability to detect a large range of particles, not just determine tritium content, and could be used for inline and real time measurements[29].

Table 2. List of the main methods for tritium measurement including the operative range, time for analysis, advantages and limitation. In grey are underlined the major tritium detection methods used at the Tritium Laboratory Karlsruhe (TLK)

Name	Measurement range (Bq/m^3)	Time for analysis (s)	Advantages	Limitation	Ref.
Calorimetry	10^9–10^{16} Bq (total activity)	3x 10^4–7×10^5	Calibration without tritium providing absolute accuracy	• Time for measurement • high detection limit	[29]
Ionization Chamber	10^4–10^{17}	15	• Wide range of activity • Real-time and in/on-line	Sensitive to gas composition	[29]
β-decay induced X-ray (BIXS) spectroscopy	10^8–10^{17}	120–1200	• Simple, in-line • detector commercially available	Detection limit depends on measurement time	[29]

Gas Chromatography	10^{10}–10^{17}	2700–5400	Full chemical and isotopic composition	Time for analysis and cryogenic temperature	[29]
Mass Spectrometer	10^{12}–10^{17}	10	Real-time and in-line, commercially available	Many isobaric interferences make interpretation difficult	[29]
Laser Raman Spectroscopy	3×10^{11}–10^{17}	2–1000	Near to real time, in/on-line, can avoid calibration if pure Q_2	Detection limit depends on measurement time	[29]
Infra-Red (FTIR) Spectroscopy	10^{12}–10^{17}	10-120	• Non-destructive analysis • Commercially available	Difficult to determine hydrogen isotopologues	[28]
Nuclear Magnetic Resonance (NMR)	10^{5}-10^{17}	1-10	High tritium sensitivity	Strong magnetic field	[28]
PhotoAcoustic Spectroscopy	10^{5}-10^{17}	1-5	• High sensitivity • Commercially available • Non-destructive • Fast measurements	• one chemical product detection at a time • Noise for in-line monitoring	[28]
Scintillation	10^{4}–10^{17}	100-200	• Cheap and Mature technology • Real time monitoring • Low pressure, temperature and humidity dependency	• Waste production • Contamination effects	[28]

Laser Raman spectroscopy and, in particular, Vibrational Raman Spectroscopy is a very useful technique for detecting a wide range of molecules. Qualitative analysis of gases can be achieved with Raman shifted light, with quantitative information being obtained by the signal intensities.

Gas chromatography (GC) is a very useful tool for full chemical and isotopic determination of gases.
At Tritium laboratory Karlsruhe (TLK), gas chromatography is probably the most used analytical technique to characterise gaseous mixtures that contain tritium [29]. A good agreement for hydrogen isotopes was found by measuring deuterium and tritium in different pre-calibrated concentration with a 5% of accuracy [30].
Some R&D progress on tritium technologies stated the development of a real time monitoring system for isotopic compositions of hydrogen gas by adopting micro gas chromatography (μGC) as a candidate for a DEMO analysis system [31]. At TLK, μGC is also being developed to reduce the measurement times to 5 minutes (instead of 45-90 minutes). Nevertheless, this method remain a slow method especially for multiple runs, so, in view of DEMO, this aspect would severely affects the responding time for tritium level.
NMR (Nuclear Magnetic Resonance) could be a real possibility for tritium detection because Tritium has the highest sensitivity on magnetic resonance than all molecules. The different gyromagnetic ratio to protium allows NMR to clearly distinguish tritium to protium, although it has the same spin. This means that the resonant frequency is slightly higher for tritium. On the other hand, deuterium has a spin of 1, and has a weak NMR signal.

Fourier Transform Infra-Red (FTIR) spectroscopy is an analytical technique that can be used to determine the composition of gaseous or liquid sample using electromagnetic radiation from the infrared region of the spectrum (approximately between 1 and 1000 μm). This covers a wide range of spectroscopic techniques, which most are based on absorption spectroscopy. FTIR analysis is very fast but it has a low accuracy especially in measuring tritiated/heavy water.
Photons spectroscopy technique can be used for detection of very low gas concentrations (parts per billion or maybe even parts per trillion). The concept is relatively simple, cheaper, and commercially available. It is extremely sensitive so that could be used for trace tritium measurements in a fusion plant. A drawback of

photoacoustic spectroscopy is that often only one chemical can be detected at one time [32].

1.3 Scope and architecture of the fuel cycle

As mentioned in the introduction, the fuel cycle is one of the most important systems for next fusion device because it has to fulfil several and critical requirements aimed to tritium self-sufficiency.

Two parameters strongly influence the design of the fuel cycle: the tritium Burn-Up Fraction (BUF) and the Tritium Breeding Ratio (TBR). The first defines the duty of the inner fuel cycle that has to recover and purify the unburned tritium, while the latter determines the dimension of the outer fuel cycle in which the tritium produced in the blanket has to be recovered [7].

Conventionally, the tritium Burn-Up Fraction (BUF) or the f_{burnup}, meant as the probability that a tritium nucleus injected into a reactor is fused before escaping from the confinement region, is the main factor used to estimate the entity of recirculation required for a specific tokamak. It can be defined as:

$$f_{burnup} = \frac{\Gamma_\alpha}{\Gamma_T} \qquad (7)$$

Where Γ_α is the fusion reaction production rate of alpha particles and Γ_T is the fueling rate of tritons from all external sources such as gas injectors, pellets, and neutral beams [33]. Just to give an example, BUF in ITER will be 0.3% while it is expected to reach less than 5% in DEMO[21]. The small burn-up fraction in the vacuum vessel, requires a closed loop along with all the auxiliary systems necessary for the safe handling of tritium [34]. This means that a huge quantity of tritium should be accurately recovered and purified. In this sense, ITER will be the first fusion device, which boasts a closed fuel cycle.

From a simple calculation, 56 kg of T should be burnt per GW y^{-1} of fusion power (GW_{th}) for a D-T reactor. A third part of the fusion power is converted to electric power (GW_e)

The inventory is interpreted as the quantity of tritium on one side (inner cycle) in vessel components and in the tritium plant and, on the other side (the outer cycle), in the Breeding Blanket (BB) and the extraction system. Concerning the inner cycle,

the inventory can be identified in the tritium absorbed and trapped in Plasma Facing Components (PFCs), in the dust and in the tritium plant. A significant part of the in-vessel retained tritium inventory in ITER is accumulated in cryopumps. According to the current pumping system concepts, the absence of cryopumps will significantly reduce eliminate this inventory in DEMO, [35].

Inventory has to be as lower as possible in order to minimise the tritium loss and reduce the risk of possible dangerous scenarios, tritium contamination or tritium release in the atmosphere. Concerning the BB, in the blanket modules will coexists three isolated systems: the cooling system, the extraction system and the vessel. The plasma-facing components will operate at high temperature, above 500°C in DEMO, and the risk of tritium permeation in coolant is consistent. Therefore, multiple permeation barriers are essential for the confinement and safe handling of tritium [34] as well as the Atmosphere and Vent Detritiation Systems (ADS/VDS) which are crucial elements in the concept for preventing environmental losses. The environmental and safety aspect strongly affect the total cost due to tritium (currently 30000 \$ g^{-1}) and processing costs.

Therefore, the fuel cycle should achieve:

- High tritium recovery from Vacuum Vessel (VV) and high purification efficiency in the tritium plant and guarantee the fuel recirculation in a small processing time (around 1 hour)
- safety requirement
- high tritium production rate from BB
- minimization of tritium purification and extraction costs
- maximum reliability
- minimum inventory
- highest overall efficiency in order to minimise the environmental losses

In view of future power plants based on D-T reaction, a further challenge consists in handling large flows with a low tritium content and ensure to provide and handle the start-up inventory, which shall be small, and reduce the processing time [36]. Any fusion reactor should breed T in its blanket system and the T breeding should have enough margins to compensate T inventory in its tritium systems, the 5 %/year decay (fuel self-efficiency) and the reserve for new reactors [12].

Figure 4 shows the simplified scheme of a fusion fuel cycle. The fuel cycle is composed of two main parts:

- The outer cycle which is designed to extract tritium from the BB.
- The inner cycle which aim is to recover the unburned fuel (mainly Tritium) and purify and separate Deuterium and Tritium to send them back to the torus.

After the separation from helium, the deuterium/tritium mixture is mingled with the tritium coming from the outer cycle while deuterium is externally supplied and led back into the torus[37].

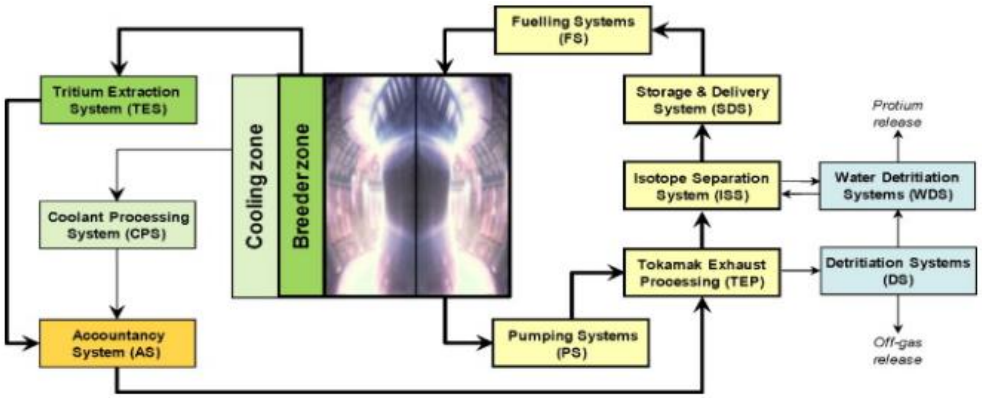

Figure 4. Fusion fuel cycle (bold lines reflect main tritium streams, thin lines mean tritium depleted streams; in yellow: main inner cycle, in blue: infrastructure for tritium handling; in green: breeder loop; in orange: accountancy as interface between blanket loops and inner cycle) [38].

The inner fuel cycle (in yellow) extracts the un-burnt fuel and products (plus other impurities) through a Pumping System, or PS, and route it to the Tritium Exhaust Processing (TEP), which recover the hydrogen isotopes and send them to the Isotope Separation System (ISS), which separates the deuterium from tritium. After separation, both fuels are routed to the Storage & Delivery System (SDS) and then to the Fuelling System (FS) which provide D and T in order to sustain the nuclear fusion reaction.

On the other hand, the outer fuel cycle (in green) extracts tritium from the blanket. The Tritium Extraction System (TES) operates the tritium separation. An Accountancy System (AS in orange) is required to take an accurate and reliable control of the tritium tracking between these the outer and the inner cycle. The AS

also collects tritium from the Coolant Purification System (CPS). This configuration allows to additionally track the tritium permeation in the cooling system.

The performance specifications regarding the inner fuel cycle and part of the outer fuel cycle, including the tritiated water processing, shall be deeply tested in all operational modes. ITER must ensure the reliability and capability of the fuel cycle to fulfil the requirements and be the support of DEMO fuel cycle development and fusion energy mission. Attention is now turning to the design of DEMO, which represents the closed-step reactor capable to demonstrate the net power production from fusion source and it has to demonstrate also to operate with a complete and closed fuel-cycle [39].

Due to different uncertainties on tokamak and plasma specification, the fuel cycle cannot be totally defined. As reported in [36], the European roadmap has defined two DEMO configurations, an early DEMO-1 (producing several 100 MW electric output) with an ITER-like technology, and an advanced DEMO based on new technology and advanced plasma scenarios.

Therefore, ITER should validate different core aspects in order to characterize DEMO tokamak and fuel cycle. A particular focus, strongly related with the fuel cycle characterization, will be given to prove:

- The tritium self-sufficiency for a working breeding blanket concept with a multiplication factor that makes up for the parts of the wall, which are consumed by duct openings (around 10%).
- The long pulse duration in the fuel cycle aimed to a progressive full steady-state operation

It is noteworthy that the fuel cycle' processes and technologies are deeply influenced by the fuel characterization and plasma scenario. Different fuel, or the presence of un-expected product, could cause several changing in the fuel cycle design. For example, the introduction on Plasma Enhancement Gases (PEGs) in a DEMO-like reactor to reduce the power load over the PFCs [40], could entail a modification of a fuel cycle process or technology.

1.3.1 Inner Cycle

Figure 5 shows the block diagram of the inner fuel cycle of a fusion device.

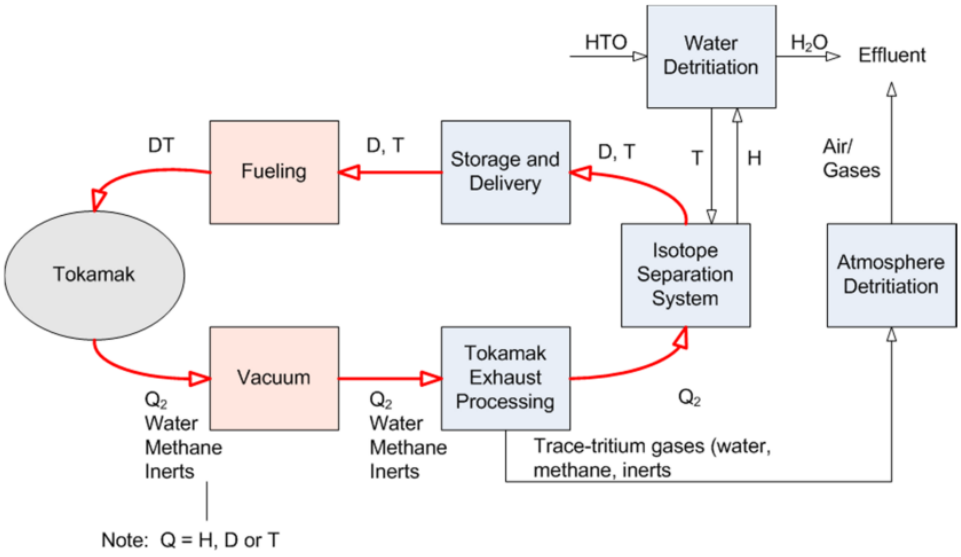

Figure 5. Block diagram of a generic inner fuel cycle [41]. In blue are underline the units that are in the tritium plant while the rest is allocated in the tokamak building.

The inner fuel cycle will be different in ITER and DEMO, especially because a novel pumping system (the metal foil pumps) is under investigation for DEMO, which allows the direct recirculation of most of the unburned tritium. In the follow, we will focus on the main sub-systems, which are all placed in the tritium plant, they are:

- Tokamak Exhaust Processing (TEP)
- Isotopic Separation System (ISS)
- Storage & Delivery System (SDS)
- Water Detritiation System (WDS)
- Atmosphere Detritiation System (ADS).

1.3.1.1 Tokamak Exhaust Processing (TEP)

The TEP is one of the key systems in the tritium plant of ITER and it recalls the concept design of CAPER Facility. This last one has been developed and deeply tested at the Tritium Laboratory Karlsruhe (TLK) [42]. It consists in a fully continuous process based on permeation of hydrogen isotopes through palladium-silver membrane permeator (first process step) which has the capability to perform a high-purity separation of hydrogen isotopes (Q_2) from plasma exhaust gas in the first process stage with an efficiency typically of 95%. The off-gas (or retentate) undergoes a heterogeneously catalysed cracking or conversion reactions (second process step), and counter-current isotopic swamping (third process step) operated

through a PERMCAT [43]. The PERMCAT reactor is the combination of a Pd-Ag permeator with a catalyst bed in order to obtain a very compact device in which chemical reactor and permeation occur simultaneously. In this case, PERMCAT is employed for final clean-up of gases containing tritium (up to about 1%) in different chemical forms such as water, hydrocarbons or molecular hydrogen isotopes [44] by performing the Isotopic Swamping reaction (for more details please refer to [45])

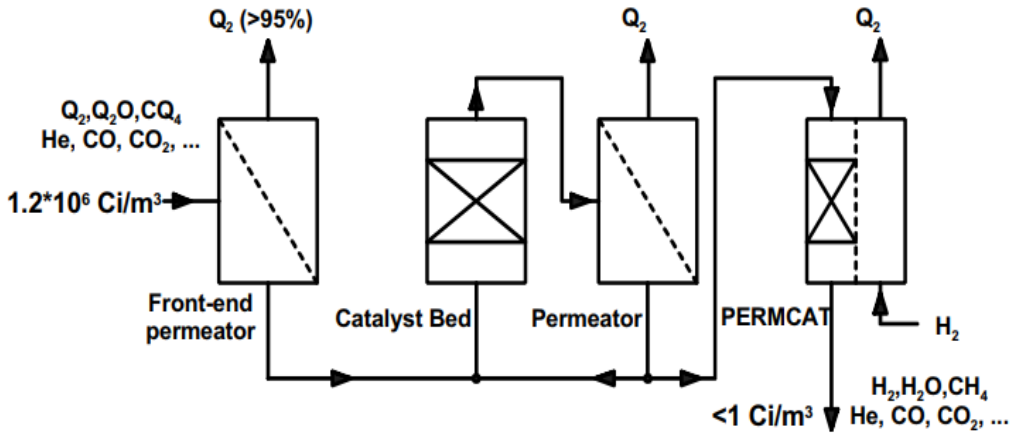

Figure 6. Simplified diagram of the TEP [42]

The incoming gas composition from vacuum vessel could significantly vary due to the uncertainties of tokamak operation or other off-design events such as plasma discharges or gases interaction with PFCs and co-deposits ashes. Consequently, the TEP system has to fulfil many more duties than the tritium plant may suggest [43], rather than operate all the time with well-defined gases. Therefore, in order to test the facility in off-normal condition, in CAPER facility at TLK, a mock-up section were employed for the preparation of gases with different compositions and test the facility with tritium and tritiated impurities [44]. In ITER, tritiated waste gases will be generated and therefore have to be processed t [42]. For this purpose, TEP of ITER has been design as shown in Figure 7.

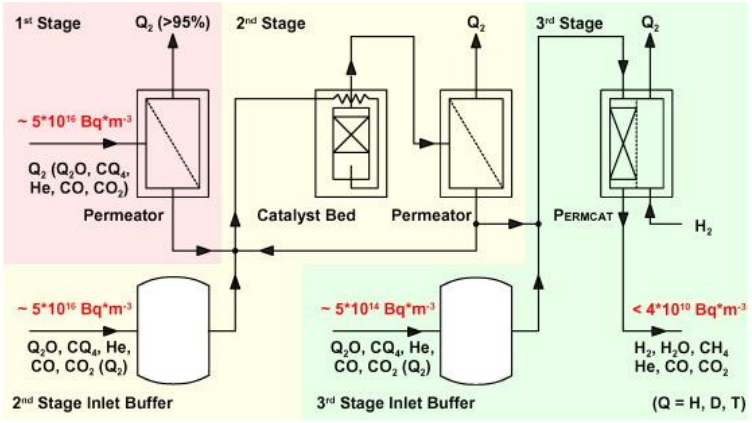

Figure 7. Block diagram of TEP in ITER tritium plant[34]

The exhaust gases pumped out from the vacuum vessel during the pulsed or steady state tokamak operation are routed to the first permeator of the TEP (first stage in Figure 7). The permeator separates the unburnt fuels (tritium isotopomers and deuterium) from the tritiated and non-tritiated impurities or product (such as ^{4}He). The pure Q_2 (permeate) is sent to the ISS for isotopes separation while the retentate (non-permeated gases) is sent to the second stage.

The second stage is represented by a closed loop which involves a catalysed reactor (for cracking or conversion reactions) combined with another Pd-Ag permeator which fulfil the separation of free molecular tritium (or Q_2) obtained by cracking and recombination of tritiated hydrocarbons or tritiated water in the catalytic reactor. As explained in [44] the 2nd stage is dedicated to the impurity processing and it can in principle operate in two different modes:

- The batch mode in which the loop is filled with the gas to be detritiated, cycled for a certain period of time until the tritium level is sufficiently lowered, and then, the loop is emptied
- The continuous mode gas to be detritiated is continuously fed into the closed loop upstream of the catalyst bed and permeator at a flow rate much lower than the loop circulation flow rate, and the loop pressure is kept constant by a continuous withdrawal of gas downstream of the two components.

Continuous mode is easier to control and in comparison to the batch mode may have a higher throughput and on average a reduced tritium inventory[44].

The 3rd step removes almost all of the residual tritium by counter current isotopic swamping and is based on a so-called permeator catalyst (PERMCAT) reactor. The

permeated gas is sent to the ISS while the retentate leaving the TEP is sent to the ADS for further tritium removal. The third stage in CAPER has been tested under several operating conditions. Gases of different compositions have been fed into the PERMCAT, by varying parameters such as impurity, feed flow rate, impurity feed pressure, hydrogen purge flow rate and hydrogen outlet pressure [44].

CAPER can handle a tritium inventory of about 3-5 g and a team of about four people is required for experiments. In the experimental campaigns, the highest measured steady state tritium concentration in the loop was 0.5 g m^{-3}. Such a gas can be easily treated in the downstream PERMCAT, reaching a Decontamination Factor (DF, expressed as the ratio of tritium-inlet to tritium-outlet flow rates) of up to 10^8 with a tritium content of 10^{-4} g m^{-3} (corresponding to 0.4 ppm tritium) downwards the 3rd stage. Only multistage processes like CAPER (and ITER TES) can achieve a tritium content below 1 ppm. The experimental DF required for the TEP system in ITER for a short pulse (450 s) of the D–T burn phase is 10^8 [44] with a final concentration minor or equal to 10^{-4} g m^{-3} in order to route the off-gas to the ADS. Therefore, The TEP concept of ITER has been successfully verified and validated with the CAPER facility

1.3.1.2 Isotope Separation System (ISS)

ISS is designed to accurately separate the hydrogen isotopes coming from the TEP and returning from the WDS. Independent fuelling of D and T is indispensable for plasma burning control via the fuelling system. The ISS is necessary due also to:

- hydrogen presence as an impurity of the fuel which must be separated from D and T
- large amount usage of hydrogen in WDS
- the requirement to have a high tritium separation efficiency (>90%) achievable only with a dedicated facility for hydrogen isotopes

In fusion reactors, the flow rate in the isotope separation system can reach more than 300 mol h^{-1} [12]. Several processes are suitable to perform the isotopic separation of hydrogen, they are:

- gas chromatography
- thermal diffusion
- laser method

- cryogenic distillation

Cryogenic distillation is the only one method which can guarantee at the same time high flow rate and high separation factor[46]. In addition, the cryogenic distillation is a well-known technology and most of the R&D activities on hydrogen isotopes separation have already been completed. Therefore, it has been chosen as the isotope separation system in ITER.

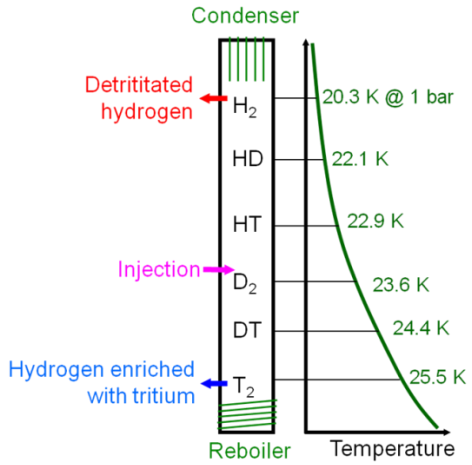

Figure 8. Hydrogen isotopes separation principle (comprehensive of the specific boiling point) in a cryogenic distillation column

In the distillation process, the separation of the hydrogen isotopes phases is possible taking advantage of the different boiling point of H_2, HD, HT, D_2, DT, T_2, as shown in Figure 8. In the same figure are reported the different boiling points of each phase. It is noteworthy that, in order to reach a high purity phase (in this case H_2 D_2, T_2), the columns has to be as long as possible in the way to distinguish the pure phases. In the specific case of hydrogen isotopes, their boiling temperatures are in a very small range (between 20.3 and 25.2 K). This requires a rigorous control of the temperature, which is hard to be respected because of the significant volume of the ISS.

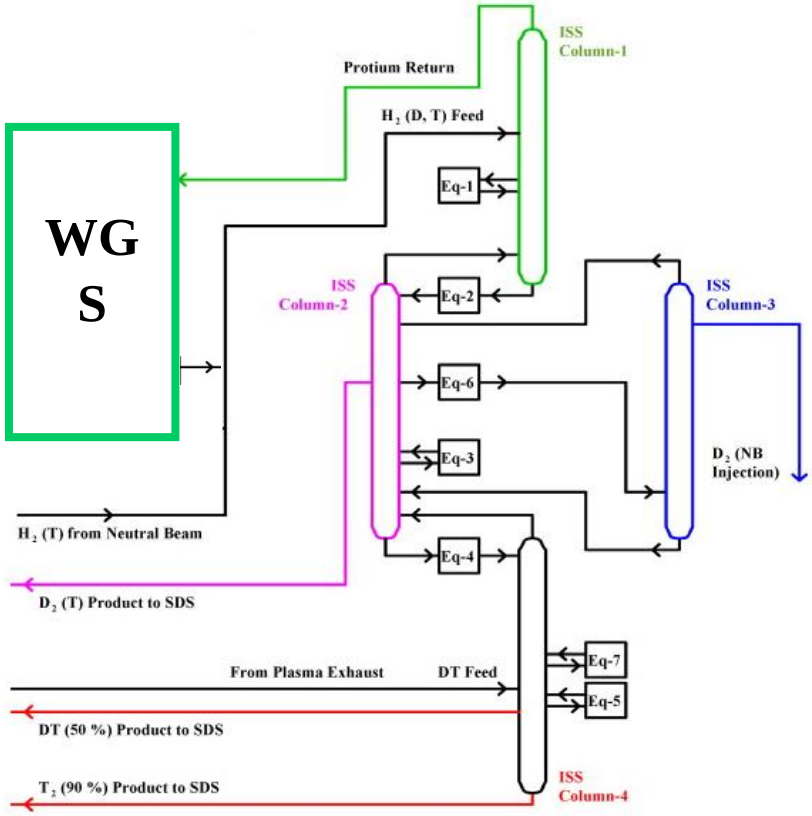

Figure 9. Simplified scheme of ITER ISS [47]

Figure 9 shows a simplified representation of the ISS in ITER. It consists in a cascade of four Cryogenic Distillation columns (CD), which separate hydrogen isotopes coming from TEP and WDS, and send separated phase gas to the SDS. In particular, it transfers three standard products to SDS:

- Tritium with an isotopic purity of 90%;
- Deuterium contaminated with tritium (contamination level <0.6% tritium);
- Deuterium for Neutral Beam (NB) injection (<0.02% tritium, <0.5% protium) [34].

The ISS is the largest component of the entire ITER fuel cycle and it will store most of the tritium inventory of the overall tritium plant. Detailed investigations of various types of ISS column configurations are a key activity for the conceptual design of ISS in DEMO. Under off-normal conditions, the hydrogen isotope inventory of the ISS can be discharged into an ISS expansion tank [43].

ISS is intimately interfaced with the WDS operation that is described in Section 3.1.4.

1.3.1.3 Storage & Delivery System (SDS)

The main purpose of the SDS is to store and to supply the gases needed for the daily operation of a fusion tokamak. The SDS must fulfil the short and long-term tritium storage. In ITER, the Long-Term Storage (LTS) is integrated in the SDS in a separated sub-unit [48].

One function of the SDS is to keep the system safety to prevent tritium release to the working area and environment. Thus, in order to shelter the environment from the tritium treating process most of SDS is located in the glove box (GB) system and surrounded with the inert gas (N_2 or Ar). Table 3 reports the main functions and requirements of the SDS in ITER.

Table 3. Functions & requirements of ITER SDS [34,49]

	Standpoint	***Specification***
Function	1. Safety	Tritium confinement, fire sector, MBA
	2. Tritium accountancy	Tritium inventory estimation
	3. Fueling rate	To keep fueling scenario
Requirements	1. Max. tritium/fire sector	Max. 70 g of tritium
	2. In-bed calorimetry	T_2 accuracy: 3 g/8 h or 1 g/24 h
	3. Fueling rate	Max. 110 Pa m^3/s T_2

The deuterium and tritium storage is realized by using particular Getter Beds (GBs) alloys, which guarantee fast absorption and desorption hydrogenation cycles [50]. The getters are equipped with an in-bed calorimetry to allow to accurately measure the tritium inventory with accuracy of about 1% of the full bed capacity (100 g) in 24 h[48]. During plasma operations, D-T gases must be fuelled with well-defined ratios supplied by different GB. Due to isotope effects, the composition of the hydrogen gas mixture supplied by the getter bed may be different from the one absorbed in the getter and may even change during unloading of the bed [44].

Although there are many metals and alloys, which could be valid candidates for hydrogen isotopes storage, only few of them have suitable properties for safe tritium storage.

Uranium is certainly one of the best candidates for tritium storage. In fact it has a defined stoichiometry (UT_3) which allows desorption of tritium at stable pressures for constant temperatures.

However, uranium is also a strategic fissile fuel and it can create obstructions in the licensing of a fusion machine in certain countries. Therefore, the intermetallic Zr-based alloy was taken in account since the early design of ITER in 1991.

The following equations describe the reactions during absorption (8), desorption (9) and the undesired effect of disproportionation (10):

$$ZrCO + \frac{3}{2} H_2 \rightarrow ZrCoH_3 \qquad (8)$$

$$ZrCOH_3 \rightarrow ZrCo + \frac{3}{2} H_2 \qquad (9)$$

$$2ZrCO + H_2 \rightarrow ZrH_2 + ZrCO_2 \qquad (10)$$

ZrH_2, which is an undesired product due to the disproportionation effect, has a much higher decomposition temperature (more than 700 °C) while $ZrCoH_3$ demonstrated to have a lower decomposition temperature (almost 400°C) [51] but, in both cases, the tritium remains trapped in the bed after several cycles. In order to fix this issue an high vacuum heating was performed but the conclusion was that a fully restore of the original capacity and properties of Zr-C is not achievable[34].

Therefore, after several studies, the conclusion was to adopt Uranium as the main GBs material in SDS [44]. Successively, other studies [51] investigated the possibility to adopt Zr-Co alloy in the Tritium Extraction System of the Test Blanket Module (TBMs) of ITER.

As reported in [48], the SDS stores and supplies deuterium with less than 0.05% tritium for NBI, deuterium with less than 0.6% tritium and tritium gas with 10% deuterium for pellet injection and gas puffing. Isotope mixtures are mainly produced through mass flow controlled combinations of these gases. The deuterium and tritium are received principally from the ISS, from the Long Term Storage or, during off normal operating conditions of the ISS, from the TEP system.

1.3.1.4 Water Detritiation System (WDS)

The WGS is deputed to recover tritium from tritiated water.

The WGS of ITER is based on the Combined Electrolysis and Catalytic Exchange (CECE) process to ensure that the emission level of tritium into the environment is maintained. CECE is one of the most efficient process to remove tritium from water so that the CNL (Canadian Nuclear Laboratories, formerly the Atomic Energy of Canada) has studied, developed for many years and successfully demonstrated its effectiveness for several heavy water production and tritium removal applications [52]. CECE process has been deeply studied and tested in TLK (Germany). The TRENTA 4 Facility at TLK, consisting of CECE process together with a cryogenic distillation (CD) process, will demonstrate the feasibility of returning the ISS protium stream into the WDS. The facility will simulate the behaviour of both WDS/ISS with protium and deuterium, as well as HTO with approximately 5 GBq kg^{-1} of activity concentration [53]. A side effect of CECE is the accumulation of deuterium in the electrolysis system that cannot be avoided even in ITER WDS.

Figure 10 shows the combination of WGS and ISS in ITER. CECE is represented by the combination of a thermal isolated Liquid Phase Catalytic Exchange (LPCE) column, which is 8 m length in the TRENTA facility [54], and the electrolyser which is comprehensive of the Pd-Ag permeator [55]. LPCE column consists in structured mesh metal packing and a hydrophobic catalyst.

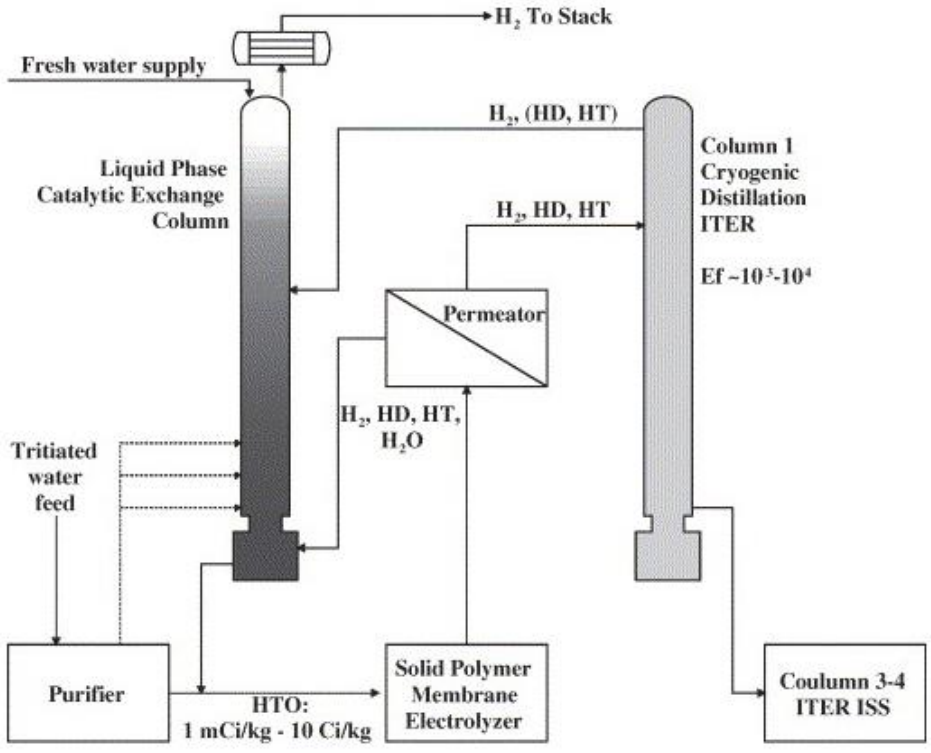

Figure 10. Direct combination of ISS and the WDS of ITER [44].

The tritiated water HTO is initially treated and sent to a solid Polymer membrane Electrolyser. In order to better control the process, the tritiated water Q_2O will be in the holding tanks of WDS, from where the water is constantly fed to the exchange columns or to the electrolysis unit [54]. The tritium in the gas phase (mostly HT) generated is routed in a Pd-Ag permeator which separates most of the Q_2. The permeate returns to the ISS for tritium recovery while the retentate is transferred to the bottom of the LPCE column in which the gas mixed to the tritium-enriched water is heated up. Along the LPCE column, on one side of the generated hydrogen stream is decontaminated and discharged into the environment, while on the other side tritiated vapour and water is enriched in tritium. In particular, along the catalyst surface the isotope transfer of tritium from the gas phase (HT_g) to the water vapour ($H2O_v$) takes place as:

$$HT_g + H_2O_v \rightarrow H_{2g} + HTO_v \qquad (11)$$

The packing material is responsible for the exchange of the HTO_v in the vapour phase with $H2O_l$ molecules in the liquid phase[56] as shown:

$$HTO_v + H_2O_l \rightarrow HTO_l + H_2O_v \qquad (12)$$

The tritium-enriched water stream in the boiler of the LPCE column is sent to an electrolyser and the gaseous tritium is sent back to the ISS for tritium recovery.

However, the performance of the LPCE process with all three hydrogen isotopes present need to be well known and properly taken into account even though in the corresponding experimental program at TLK on WDS development a direct combination with the ISS appears feasible [44].

1.3.1.5 Vent and Atmosphere Detritiation System (VDS/ADS)

In future fusion power plants, a WDS system and atmosphere and vent detritiation system (ADS/VDS) will represent the final barrier for tritium release into environment. In the TEP, impurities are separated from hydrogen isotopes, which are sent to the ISS, while the remaining low-tritiated waste gas goes to a Vent Detritiation System (VDS) for decontamination purposes before release into the environment [57].

Moreover, Decontamination Systems (DS) are mandatory to minimize the maximum exposure dose of workers. In ITER, for example, both airborne emission and water

effluent releases have been established during normal plasma operation and maintenance, about 0.1 g/year and 1 g/year for HTO and HT respectively [57].

Multiple barriers are essential for both the confinement of tritium within its respective processing components and for the environment release minimization. Therefore, ADS and VDS are crucial elements in the concept.

All detritiation systems of fusion devices consist in the oxidation of molecular tritium or tritiated compounds to water on precious metal catalysts, followed by trapping of the produced tritiated water in molecular sieve beds. Molecular Sieves Beds (MSBs) require regeneration; the tritiated water product is sent back to the WDS for decontamination and the recovery of tritium occurs in the ISS [34] as already explained.

Figure 11 shows the detritiation systems dislocated in fusion device buildings. The ventilation and confinement criteria follow the experience and practice of other tritium facilities while the confinement guidelines follow conventional nuclear facilities, which implement primary and secondary confinement. Depending on the specific area, different detritiation system could be adopted (one or more in the same building). In general, within the tritium plant, there are only three systems through which the tritium plant building is connected to the environment. These systems are:

- The Heating Ventilation and Air Condition (HVAC) systems
- The VDS
- The ADS

The technologies adopted by this sub-system are essentially:

- Room temperature oxidiser (RT CAT)
- High temperature oxidiser (HT CAT)
- Wet Scrubber Columns (WSC)
- MSBs

Figure 11 shows the classification of a generic fusion plant.

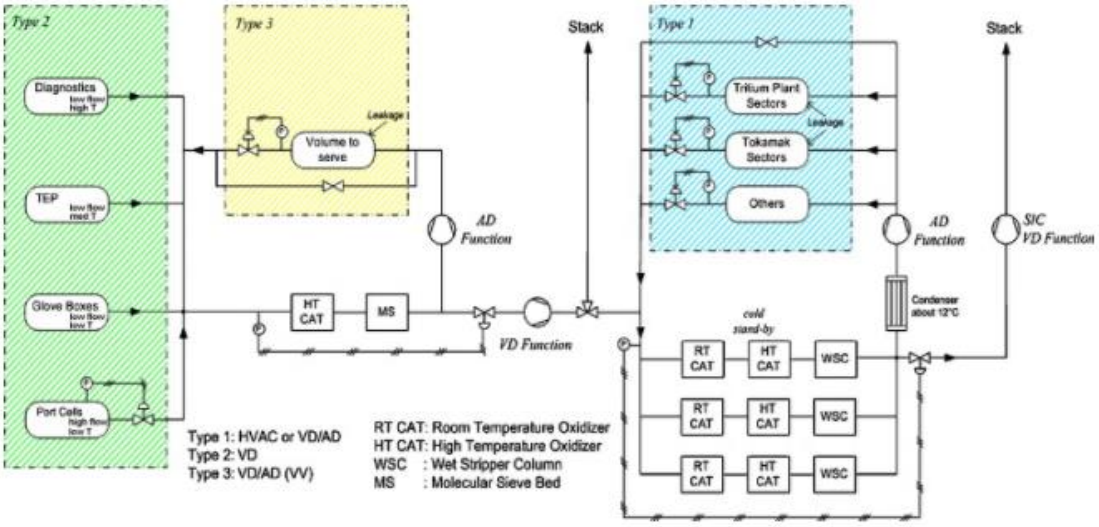

Figure 11. Block diagram of VDS and ADS in nuclear fusion devices [58]

Tritium Plant is divided into three HVAC zones served by three independent systems. These systems maintain different levels of depression in the areas where the level of contamination with tritium allow discharge into the environment but they do not serve any contaminated area. Every area is classified depending on the risk of tritium release.

The type 1 zone is defined non-nuclear zone ("white zone") providing main personal access to the Tritium Plant building. Systems, which handle tritiated water or gaseous tritium, are separated in two different "green zones", which are contamination-controlled zones. Type 3 is the nuclear zone in which there are the ISS and SDS [34]. Detritiation of solid waste and recovery of tritium will be done in the Hot Cells, which will also be processed by the DS.

Many of the processes in the DS are modular and is exchangeable each other for redundancy. In ITER the entire system will process all the effluent from the ITER facility both in normal and off-normal operations to maintain the tritium emission to the environment to 10^{-8} [50] or less. In the last decade, counter-current water scrubber was considered for this process in order to improve the reliability in case of off-normal events [58].

Figure 12 shows the multi-barrier concept in ITER. It can be distinguished primary and secondary confinement. The primary systems parts need to be protected against over-pressure, over-temperature and tritium permeation through structural materials, therefore a physical barrier (pipe work, components) which can be enclosed in a

surrounding containment is required. Typically, glove boxes have surrounding containment served by a Glove Box Detritiation System (GDS).

During normal operation the VDS (700 $Nm^3 h^{-1}$ in ITER) processes tritiated streams from tritium plant, vacuum pumping, GDS and it operates as the only barrier to the environment. During an off-normal event, the HVAC systems are isolated and ADS starts its operation in closed loop (throughput of 4500 $Nm^3 h^{-1}$ in ITER) until the tritium content decreases down to opportune threshold which allow discharge through the VDS. The VDS ensures the negative pressure inside the buildings even in case of accident while the ADS assures that the tritium concentration is rapidly decreased in the rooms. Extracted air and all the Tritium Plant airborne area, with the exception of the WDS, is treated in the VDS. In the case of WDS, the conversion of the LPCE column exhaust gas to water-like species would create additional tritiated liquid wastes [57].

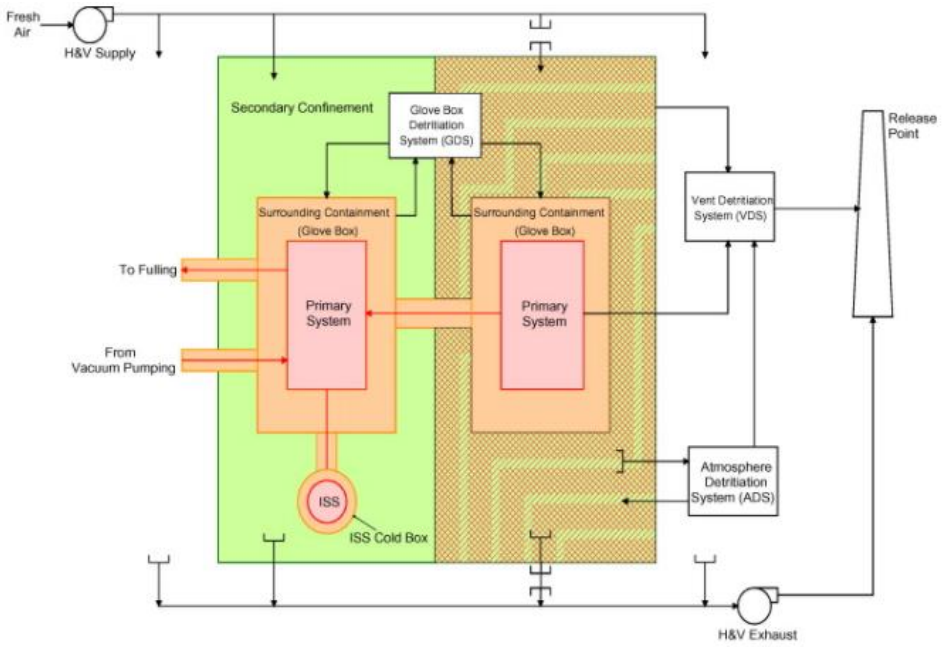

Figure 12. Simplified multiple barrier concept of ITER [34]

The complexity of the ITER ventilation (HVAC) and ADS/VDS has grown over the years, closely following the development of generic confinement strategy. It consists in firstly compile a coherent set of requirements and specifications for the different nuclear buildings of ITER in France. Second an overall concept for HVAC, ADS/VDS, depression systems and safety tritium monitoring which satisfies all the key requirements shall be developed [34].

1.3.2 Outer Fuel Cycle

The duty of the outer fuel cycle is to recover and purify the tritium produced inside the blanket. Currently, there are several blanket concepts under investigation therefore the structure and technologies of the outer fuel cycle depend on the specific blanket.

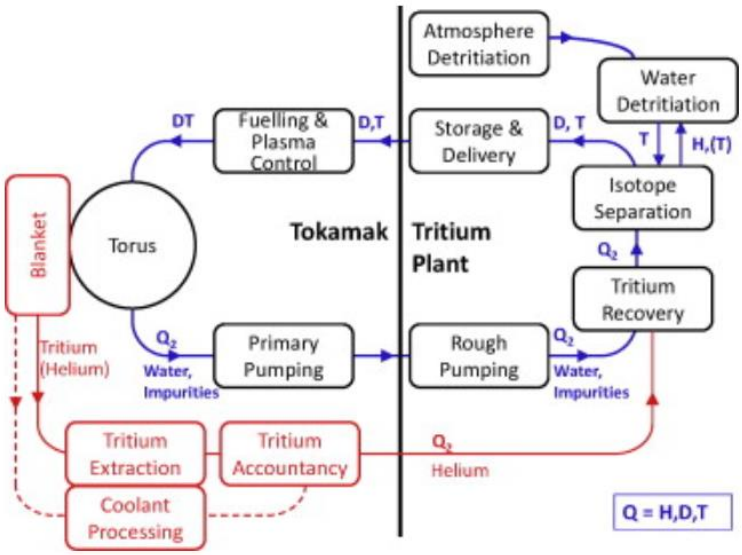

Figure 13. Fusion fuel cycle block design distinguished by outer fuel cycle (in red) and inner fuel cycle(in blue)[41].

As shown in Figure 13, the outer part consists of the Tritium Extraction and Recovery Systems (TERS), the Coolant Purification System (CPS) and the Tritium Accountancy System (TAS). The TERS has to recover the tritium produced inside the blanket, the CPS removes the tritium that permeates from the blanket in the primary coolant system while the TAS measures all the extracted tritium and send it to the inner fuel cycle.

The TAS is an unavoidable system because it is deputed to tritium inventory control. In TAS, tritium is temporary stored and accurately measured. In this configuration, it is possible to perform a real-time control of the tritium released in coolant, through measuring the tritium extracted from CPS, and the one extracted from the BB. Additionally, the tritium recovered should be easily reusable, in order to minimize the impact and additional load for the ISS in the inner fuel cycle.

In order to fulfil these requirements, the outer cycle has to overcome to main aspects: firstly, it has to recover the tritium extracted from the BB, which will be present only

as traces (ppm); secondly, it has to separate tritium from different forms as Q_2 and Q_2O. Ideally, it will be convenient to recover tritium in Q_2 form with the minimum protium diluition [41].

1.3.2.1 Main features of the breeding blanket concepts

The outer fuel cycle has a key role in fusion success. The challenges, aimed to a self-sufficient blanket technology are huge especially for DEMO. For now, ITER will test six different lithium-based mock-ups of blankets also called Test Blanket Modules (TBMs) [59]..

DEMO BBs will occupy about 90% of the surface area surrounding the Vacuum Vessel (VV) and, then, plasma. Consequently, it will capture the large majority of the high-energy neutrons that are produced in the D-T reactions.

The main functions, which the BB should simultaneously accomplish, are:

- *Tritium breeding and heat production* obtained by breeding tritium and converting neutron energy to heat. This region is exposed to high neutron flux, especially in the first ~20 cm closest to the plasma [39]. The nuclear reactions that occur inside the blanket, attributed to Lithium (Li) isotopes with neutron interactions, are

$$n + {}^{7}Li \rightarrow T + {}^{4}He + n' \qquad (13)$$

$$n' + {}^{6}Li \rightarrow T + {}^{4}He \qquad (14)$$

  where n' is a thermal (slow) neutron. It is the case in which n is thermalized with a heat generation. The reaction (13) occurs when the fast neutrons coming from the reaction (4) reach the blanket surface. Reaction (13)produces slow neutrons, which react with ^{6}Li producing more tritium, according to Figure 3 and (14).

- *Tritium and heat extraction*, which is performed after neutron interaction with the consequence of a high-grade heat, suitable for electricity conversion cycle, and tritium formation, which is extracted from the BB and send to TERS.

- *Neutrons and radiation shielding* in which the BB contributes together with the divertor to the shielding of the vacuum vessel, magnets and other equipment outside the reactor from nuclear radiation

In order to fulfil the entire requirements for DEMO operations, nuclear, thermo-hydraulic and structural-mechanical strategies have to be taken into account in the design. The complete set of requirements on which the blanket system should be designed is still under completion and evolves in parallel with the design.

In the European Power Plant Physics and Technology (PPPT) programme and, in particular, in the PPPT-DEMO program, two different blankets has been considered: the first blanket set has to be designed in order to sustain 20 dpa (displacement per atom) neutron damages. A second set should be designed for 50 dpa; this means that one scheduled replacement of the whole blanket system is necessary in the life of the reactor. The architecture of each segment of the BB follows the principle of the Multi-Module-Segment (MMS) concept, which consist of a robust Back Supporting Structure (BSS), including the manifold system, that supports the breeder zone (BZ) and the First Wall (FW) [60]. The segments have still to protect, together with the shield, the VV against damages limiting the dpa to 2.75 [60] and reducing the heat load the activation of the VV structures[61].

Concerning the heat load, EUROFER steel which will be the main structural material must be kept under ~550 °C, solid breeders under 920 °C, beryllium under 650 °C and PbLi under ~550 °C[60].

The T self-sufficiency can be achieved only with an accurate nuclear design of the BBs. In particular, the amount of steel that is used as structural material has to be reduced to 12–15% or less in order to maintain the Tritium Breeding Ratio (TBR) to acceptable levels. The structural stability should be carefully implemented to sustain the EM forces, constitute another typical load challenge, and avoid an excessive increasing of the steel amount in the Breeding Zone. During the operation, the breeder materials at low pressure, between 0.2 MPa and 1 MPa depending on the specific breeder, should remain fully separated from the high pressure cooling system (8 MPa for helium and 15.5 MPa for water).

One conclusion could be that the tritium extraction technologies used in ITER are far to be considered the baseline for DEMO outer fuel cycle. In fact, the required tritium production and the coolant flow rate will be about three orders of magnitude

higher than those for ITER. Therefore ITER will focus on testing the BBs technology in tritium production, while the methods and processes for a DEMO outer cycle and, in general, tritium processes and components, require new R&D efforts [41]. Even if the TBM programs will be successful, large gaps would still exist because the DEMO blanket development cannot be fully explored in ITER. For this issue, further R&D and design activities are being implemented.

The breeding blanket can be classified depending on the nature of the materials in solid (Li-ceramics) and liquid (Li and Pb-Li alloy) breeders. Otherwise, an alternative classification could be done referring to the coolant; in this case can be distinguished helium-cooled or water-cooled blankets with the only exception of the dual-coolant blanket.

The official EU DEMO BBs under investigation are [69] [70]:

- Helium-Cooled Pebble Bed (HCPB) a ceramic pebble-bed blanket made of Be-multiplier and Li orthosilicate (43.6% Be, 9.7% Li4SiO4, 36.9% He, 9.8% EUROFER by volume) and cooled with helium at 8 Mpa
- Helium-Cooled Lithium Lead (HCLL) a liquid LiPb blanket (85% LiPb, 7% He, 8% EUROFER) cooled with helium at 8 Mpa
- Water-Cooled Lithium Lead (WCLL) a liquid LiPb blanket (85% LiPb, 5% water, 10% EUROFER) cooled with pressurized water (15.5 Mpa)
- Dual-Coolant Lithium Lead (DCLL) a self-cooling liquid LiPb blanket and helium cooling elsewhere (85% LiPb, 3% He, 4% SiC, 8% EUROFER)[39]

Solid blanket concepts, the HCPBs, include a combination of a ceramic breeder both in form of pebble beds (Ø 0.25÷0.63 mm for Li_4SiO_4), a beryllium-based multiplier such as Be or Be-Ti alloys and Ø1 mm Be [64]. The ceramic breeder and Be multiplier can be in the form of pebble beds of lithium orthosilicate (Li_4SiO_4) and lithium metatitanate (Li_2TiO_3) which currently are the best candidate. Li is enriched 30% in ^6Li in case of Li_4SiO_4 breeder and 60% in case of Li_2TiO_3 breeder. Maximum allowable temperatures are 920 °C in ceramic, 650 °C in Be, and 550 °C in steel [59].

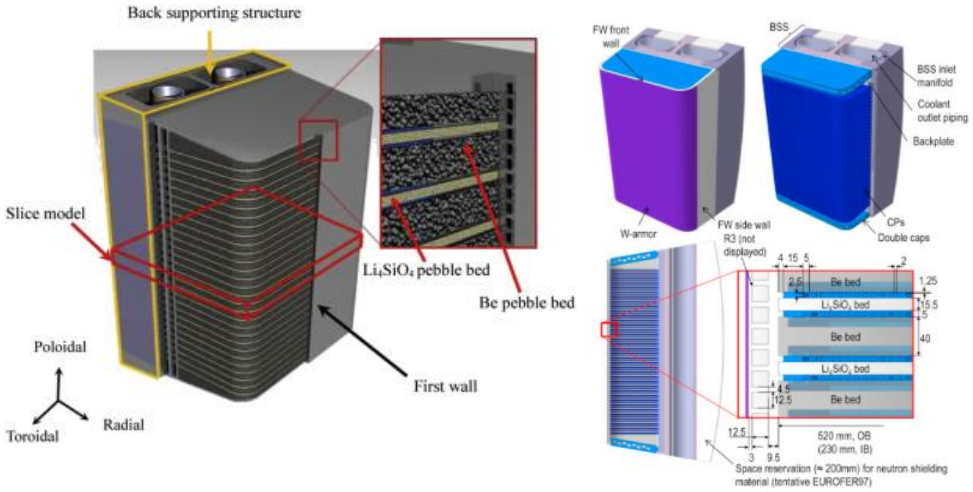

Figure 14. HCPB BB based on a "sandwich" architecture - detailed pictures [65]

The blanket is characterized by a 8 MPa helium gas with a temperature of 300–500 °C as coolant, EUROFER as structural material, helium (+0.1% vol. H_2) with a pressure of about 0.2 MPa as purge gas, and tungsten as FW armour material. The blanket has a "sandwich" shaped (Figure 14) arrangement of flat cooling plates and alternating Li_4SiO_4 and Be pebble beds (refer to [66] and [65] for more details).

In general solid breeders (with Be multiplier) have many advantages:

- smaller radial thickness and ^6Li enrichment (40% in case of Li_4SiO_4) to achieve a sufficient tritium breeding ratio (TBR ~ 1.14) [39]
- rely on a simple and efficient mechanism of tritium extraction with a low pressure He purge flow;
- better control of the undesired permeation of tritium to the coolant and (possibility of avoiding the permeation barriers);
- Higher energy multiplication in the breeder zone that would help increase the total plant efficiency.

On the other hand the critical aspects are:

- chemical compatibility between Be-based material and water/air (coolant) or, in case of accident scenario, with air or water (case of the WCPB) with hydrogen production due to the Be-Q_2O reaction;
- Tritium permeation to the coolant
- thermo-mechanical interactions between the pebbles and the structure(neutron irradiation effects, thermal-mechanical property degradation) which imposing limits on both the power density (low thermal

conductivity of the ceramic breeder) and on the blanket lifetime (irradiation damages in PB and Be);

- Li burn-up in the ceramic;
- High cost of fabrication and re-processing of the PB and Be-multiplier, since the lithium must be reprocessed and enriched to 30–60% ^{6}Li (above the natural level of 7.5%)[67] (Supply of enriched lithium could be a potential critical point for the entire fusion program) [62];
- Compatibility of Be with structural material;
- Availability of Be material to be used in future reactors (hundreds of tons per device).

As declared in [39] and [60], currently, the most promising ceramic blanket concept in Europe is the solid blanket, with most of the attention on the HCPB.

Conversely, liquid blankets demonstrate higher breeding performances than the solid one, while the Pb-Li alloy is preferred to pure Li because of lower hydrogen solubility.

Concerning the liquid BBs, theoretically, the eutectic Pb-15.8Li enriched to 90% in ^{6}Li alloy [60] could be the most attractive breeder due to its highest intrinsically achievable TBR, its large thermal conductivity and its immunity to irradiation damage. It can lead to tritium self-sufficiency without employing additional neutron multipliers and allows for tritium extraction outside the vacuum vessel. LiPb has an additional advantage of being inert in air and of having a controlled reaction with water. In substitution to this last one, LiPb can also be used as a coolant in advanced blanket concept[39]

On the contrary, the drawbacks are related to Li burn-up, transmutation and activation and requiring methods for chemical control/purification.

The liquid blankets are:

- HCLL in which the LiPb alloy has the breeding role while He is the coolant. Each HCLL blanket module consists of a Eurofer steel box formed by a U-shaped (Figure 15. EU HCLL blanket: (a) general view, (b) PbLi flow path [68] [69] plate composing the first and side walls (coated with a 2 mm tungsten layer) closed by two caps on the top and bottom and on the back by a set of Back Plates (BP) and tie rods[68]

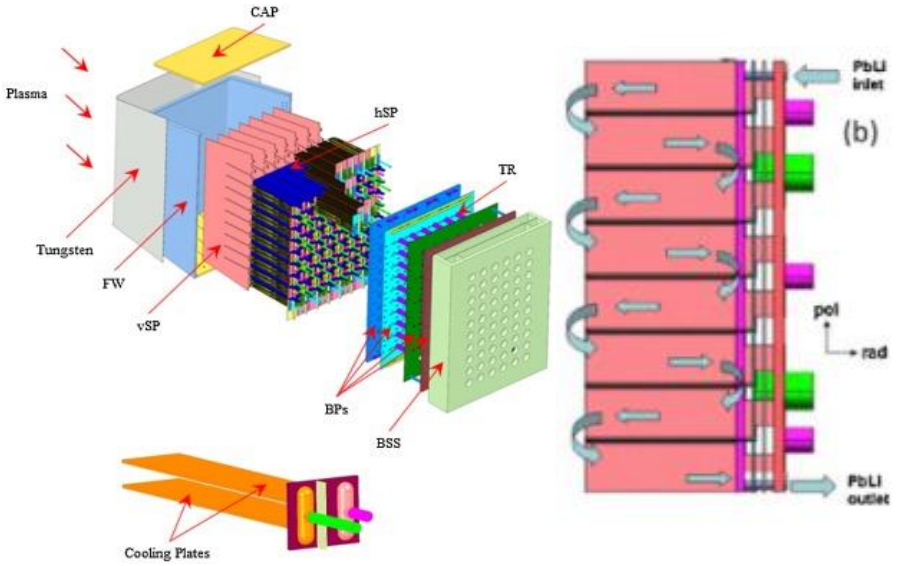

Figure 15. EU HCLL blanket: (a) general view, (b) PbLi flow path [68] [69]

- WCLL, which is similar to HCCL except for the coolant that, in this case, is the water. The concept is characterizes by the use of water at PWR conditions (285-325 °C at 15.5 MPa) [60]. The water coolant flows through double wall tubes (DWT) with a C-shape (Figure 16) and placed on a radial-toroidal plane. The computed velocity in the tubes is less than 2 m/s [70]. The coolant, even though is preferable to He because its higher heat capacity, interact with PbLi in case of failure, and with tritium which permeate from LiPb to water with the risk of embrittlement of the structural material. These issues can be minimised by dimensioning the LiPb container using double-wall tubes as coolant pipes applying tritium permeation barriers in order to avoid the tritium permeation[71].

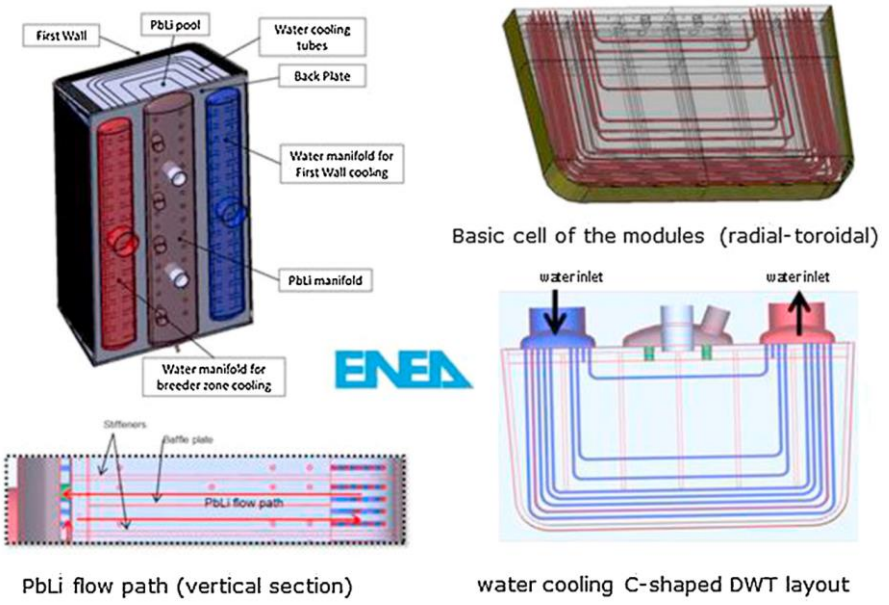

Figure 16. New WCLL design 2015

- DCLL in which LiPb operate as both breeder and coolant (60% of the blanket heat transport) by increasing sufficiently the flow rate. An auxiliary helium coolant is used to cool the FW. The concept is interesting for the potentiality to operate at high PbLi temperatures (up to 700 °C) with consequently a high efficiency of the power conversion system [60]. One of the mayor issue in DCLL is the MagnetoHydroDinamic (MHD) pressure drop which can be minimised by using SiC inserts which, however, rapidly degraded because neutron irradiation and helium transmutation in SiC. This last effect has to be better understood. One more issue is the limitation is the temperature of the structural material with LiPb that do not have to exceed 550 °C [72].

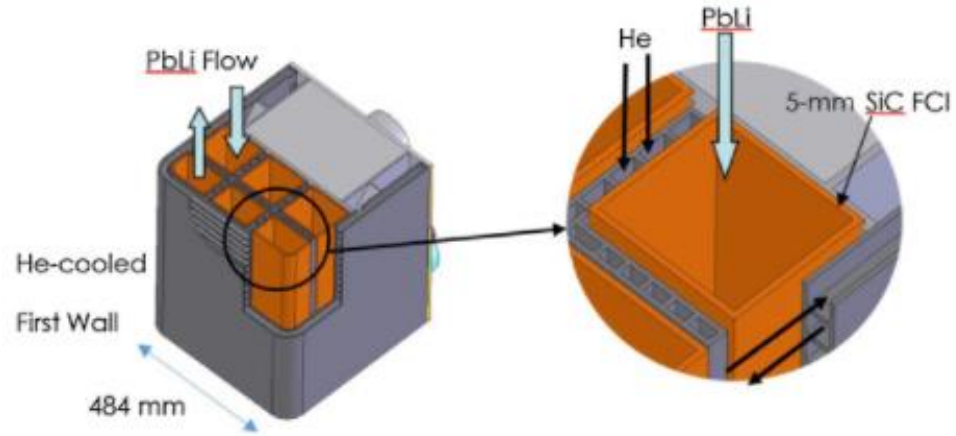

Figure 17. Sketch of a DCLL blanket design, including a poloidal duct with SiC FCI and He and PbLi flows [73].

Main other limitation of the liquid metal blanket concepts are:

- Corrosion of the pipes and blanket structures by circulating LiPb;
- Efficient extraction and purification of tritium from LiPb at high temperature;
- Control of tritium leakage and minimisation of permeation to coolants;
- Control of Polonium and other transmutation products in irradiated LiPb;
- Cost of ^{6}Li enrichment, as LiPb concepts rely on up to 90% of ^{6}Li enrichment to minimise the radial thickness of the breeder zone.

The choice of the breeding blanket coolant in DEMO has a substantial impact on the design and materials selection, operation, maintenance, safety and economics of the plant. Heat fluxes higher than 1 MW m^{-2} are at the limit of the present technology (materials, performance, etc.) especially for helium as coolant, and, by using water-cooled FW protection, the power handling is marginally higher. Additionally, with the cooling system it is necessary to handle and control the tritium contamination in order to avoid recovering tritium from large quantity of coolant. For this reason, the BB outer cycle and the coolant are completely isolated but permeation effects remain, enhanced by the high temperature and the huge surface of the blanket module and structural materials.

Those technical issues influence the choice of:

- thermal power conversion efficiency
- pumping power requirements;

- power handling requirements of the FW;
- achievable tritium breeding ratio;
- breeder tritium extraction;
- tritium permeation and primary coolant tritium purification and control;
- chemical reactivity of coolant and breeder / coolant leakage [39] .

Concerning the TERS, for the HCPB there will be a dedicated paragraph in the next chapter, while in case of liquid blankets, the TERS is placed on a bypass line. The PbLi alloy can be heated up to 450 °C before entering into it. Downstream the TERS, the Pb-Li flow is cooled down to 300 °C (HCLL), or 326 °C (WCLL) through heat exchanger.

The TERS have been carefully assessed considering safety, integration, operation and performances, synergy with the inner fuel cycle, technology readiness level, costs, etc. As outcome Permeator Against Vacuum (PAV) have been pre-selected as baseline methods for the liquid BBs because of the technology readiness. Nevertheless, two conceptual designs of lithium-lead loops for testing PAV at high velocity flows [74] and Vacuum Sieve Tray (VST) [75]using tritium have been completed.

2. Tritium Extraction and Recover Systems (TERS) of the HCPB blanket: the membrane-based concept

The design at the conceptual level of the Tritium Extraction and Recovery Systems (TERS, also called TES or Tritium Extraction System) of the four BBs will be tested in ITER in view of the final conceptual design of DEMO TERS. However, a simple scaled-up of ITER TERS to DEMO throughput seems to be very hard, since DEMO will continuously breed tritium (0.5 kg per day). For this reason, the design of DEMO Blankets and of the related TERS represent one of the major topic in the EUROfusion activities [76]. In this work is reported the DEMO HCPB blanket status and the main DEMO-HCPB TERS.

2.1 Description of the HCPB blanket

The HCPB-2015 BB concept has been designed and developed for the latest release of the DEMO 1 tokamak (April 2015). Different version of the HCPB has been developed during the last 5 years, therefore, in this paragraph, only the last reference HCPB blanket architecture (HCPB-2015 v3) will be presented [77].

As introduced in Section 1.3.2.1 Main features of the breeding blanket concepts, in the solid blanket the Be is in form of a pebble bed with sizes of 1 mm and it used as a neutron multiplier in order to promote the tritium production in the ceramic breeder (Li_4SiO_4) pebbles according to (13) and (14).

Various kinds of lithium-containing ceramics have been studied as potential candidate breeders [78,79] for DEMO. Because of high burn-up of the lithium, a change in chemical composition of pebble beds are under evaluation in advanced breeder materials development program between Japan and EU. DEMO blankets having higher nuclear heat density usually require larger volume fraction of coolant.

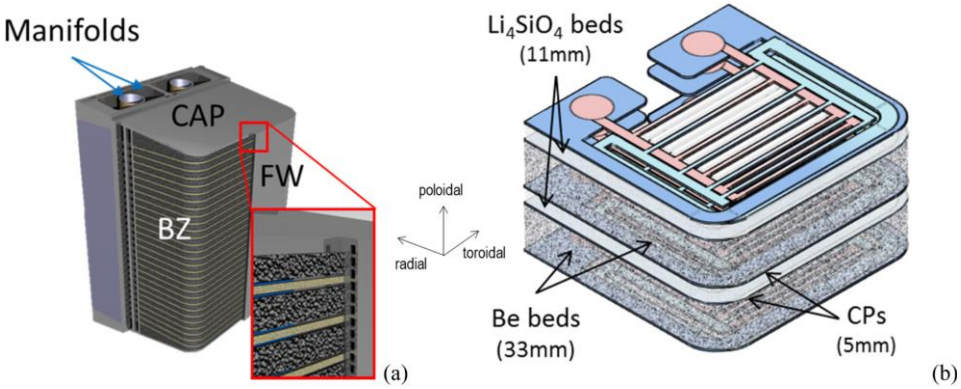

Figure 18. CAD design of HCPB TBM in ITER [80]

Lithium containing ternary oxides ($LiAlO_2$, Li_4SiO_4, Li_2ZrO_3, and Li_2TiO_3) have been proposed as breeder blanket materials. Among them, lithium titanate (Li_2TiO_3) has been recognized as a prominent candidate material because of its chemical stability, good tritium release and low-activation characteristics. However, the mass of Li_2TiO_3 strongly decreases with time because of evaporation of lithium in a H_2 atmosphere and lithium burn-up [81]. To prevent this mass decrease at high temperatures, Li_2TiO_3 with excess lithium (Li_2+xTiO_3+y) has been developed as an advanced tritium breeder [82].

While Li_2+xTiO_3+y pebbles have some good properties, the TBR is smaller than that of the most interesting Li_2O because of its low lithium density. Therefore, research and development of new lithium-containing ceramic composites with not only high stability but also high lithium density materials is of great importance. Super advanced materials are investigating the possibility of a new-concept solid solution of a Li2O–TiO2–ZrO2 (LTZO) material, since the atomic radii of Ti and Zr are similar [83]. Furthermore, grain size control is simpler for LTZO pebbles than for Li2+xTiO3+y pebbles. In accordance with the tritium release characteristics, it has been determined that the optimum grain size is <5 μm. Li2+xTiO3+y pebbles were sintered under vacuum and subsequent 1% H_2–He atmospheric conditions to obtain the target values, LTZO pebbles with grain size <5 μm were easily sintered in air. Thus, LTZO solid solution has great potential for use in super advanced tritium breeders [62].

The HCPB-2015 v3 (Figure 14) is based on an internal arrangement of parallel Cooling Plates (CP) joined at the front and the sidewalls of the First Wall (FW) and at the back plate. The parallel CPs create volume layers where the breeder ceramic pebble bed and the Neutron Multiplier Material (NMM) pebble beds are emplaced

in alternate sequence (Figure 19). The thickness of the breeder ceramic pebble bed is 15.5 mm while for the Be pebble bed layer is 40 mm.

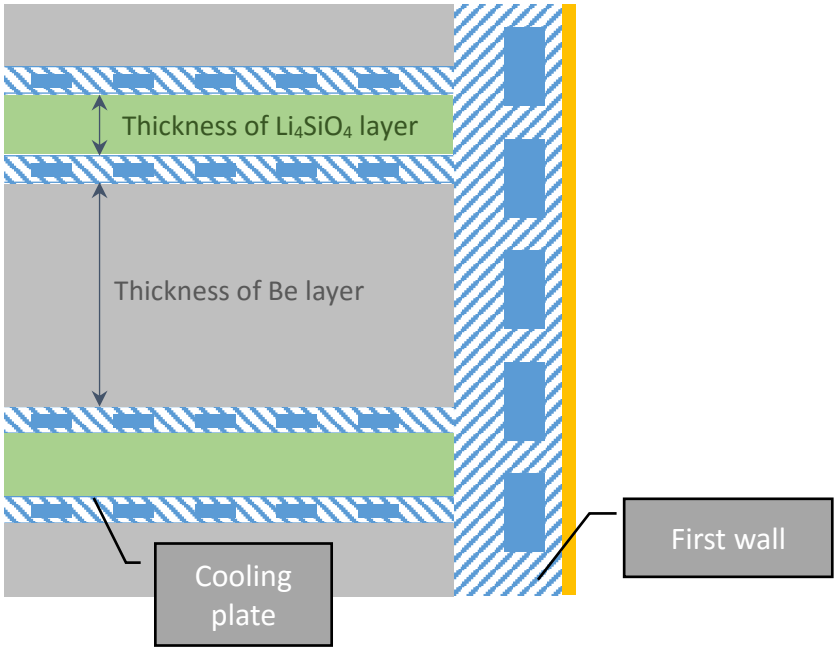

Figure 19. Basic layout of the HCPB-2015 BB concept[84]

The joint of FW, CP and back-plates encloses the breeding zone region forms a BB module, which is fixed at the BSS through bridge plugs that act both as a connecting structure and as a channel guiding the purge gas. In every module, there are two different circuits: He used as a coolant and He doped with hydrogen used as a purge gas aimed to tritium extraction. The materials involved in the HCPB blanket modules, comprehensive of both the Out-Board (OB) and In-Board (IB) units, are summarized in Table 4.

Table 4 HCPB-2015 material composition[84]

HCPB						
Material Composition						
Vol. (%)	**Armour (2mm)**	**FW (t=25mm)**	**Breeding Module**	**Caps**	**Backplates /Internal Manifolds**	**BSS**
Eurofer	0	64.91	9.85	67.2	41.39	60.61
Be	0	0	36.63	0	0	0
Li_4SiO_4 (60% ^6Li)	0	0	14.91	0	0	0
Tungsten	100	0	0	0	0	0
Void (helium /vacuum)	0	35.09	38.61	32.8	58.61	39.39

Currently, three basic strategies can be envisaged for the architecture of the HCPB BB. These are reported in Figure 20.

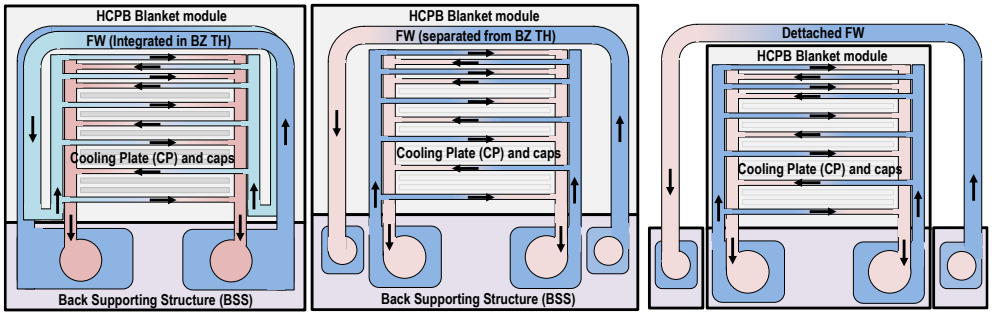

Figure 20 Three basic possible architectures of the HCPB BB, depending on the uncertainty level on the FW heat flux. Left: HCPB-I. Middle: HCPB-S. Right: HCPB-D [84]

The different architecture has been developed depending on the uncertainties level on the Fist Wall (FW) heat load of DEMO. Figure 20 left shows the HCPB with Integrated FW with the breeder zone thermos-hydraulics (the helium coolant in the FW and the BZ is coupled in series) for the tokamak regions where the FW heat flux is predictable with a reasonable uncertainty (e.g. ±10% from the nominal heat flux) and to a maximum of ≈0.5 MW/m². Figure 20 middle shows the HCPB with Separated FW from the breeder zone thermos-hydraulics (helium coolant in the FW and BZ decoupled helium loop for the FW and BZ in parallel) for the regions where the FW heat flux is not predictable (i.e. uncertainties higher than ±10%), but with peak heat fluxes bounded to ≈1 MW/m². The last concept, Figure 20 right, is the HCPB with detached FW from the breeding blanket for all those regions of the BB plasma-facing surface where the FW heat flux is not predictable, i.e. uncertainties higher than ±10% from the nominal heat flux and where the heat flux is higher than 1 MW/m². Here a mechanical detachment of the FW is needed, with a possible need to a coolant medium change such as water and/or FW architecture change in the case that the heat fluxes are considerably larger than 1 MW/m².

In those different architectures, the purge gas and coolant must achieve their specific requirements. In particular, concerning the purge gas, which is helium with an addition of 0.1% wt. H2, the inlet temperature at the BB segments, is ≈300°C. This temperature is set due to the lower design limit temperature of EUROFER97. The purge gas temperature outlet of the BB is <550°C, as the purge gas will flow out of the BB modules through the different EUROFER97 structures. It will exit the BSS most probably at about ≈400°C.

The purge gas pressure is set to 0.2 MPa at the BZ of the BB modules. The pressure choice is a good trade-off value between the minimization of the T partial pressure in the purge gas finalised to decrease the T permeation through the CPs [85] and the maximization of the pressure to avoid the Smoluchowski effect. It predicts that, differently from the kinetic theory of gases which is related to unconfined gases, the thermal conductivity of a confined gas, which is this the case (confinement in-between pebbles), decreases as the pressure of the gas decreases. This is due to the increasing mean free path λ of the confined gas molecules as the pressure is reduced having a negligible contribution to the heat transfer, in particular below 0.15 MPa [86].

The purge gas flow scheme has been as well revised in the "sandwich" concept, which is a back-to-front scheme, with independent purge gas flows in the Be and the Li_4SiO_4 bed. This scheme, differently from the previous versions, facilitates the T-release and transport in the region with lower T-concentration because of the flow of a cleaner purge gas, and also might reduce the T-permeation into the coolant and avoids the contamination of the purge gas by elements of the Be bed.

Due to the independent fluxes of purge gas in the different pebble beds, three different configurations (options) have been identified:

- common inlet/independent outlet scheme
- the independent inlet/independent outlet
- the semi-independent inlet/independent outlet

In the common inlet/independent outlet scheme (Figure 21 top) a single piping for the inlet purge gas is available and connected to all the pebble beds. Sub-lines purge the Li_4SiO_4 and Be beds, separately. After purging the BZ, the gas is collected into the gas chambers at the backplate. Depending on the precedence of the purge gas (Be or Li_4SiO_4 bed), it is diverted into an outlet line dedicated to Be or to Li_4SiO_4, in order to help to the tritium accountancy. This scheme uses He + 0.1%wt. H_2.

In independent inlet/outlet (Figure 21 bottom left), two types of purge gas are used: He+0.1%wt H_2 and He+0.1%wt H_2O. The addition of a small percentage of H_2O steam to the purge gas will result in a drastic reduction of the T-permeation to the coolant. However, the purge with steam doping is not desired in the Be pebble bed due to the hydrolisation of Be at high temperatures. Therefore the purging with steam

content is performed in this option only through the Li_4SiO_4 bed, and the Be bed is purged with He+0.1%wt H_2 as usual.

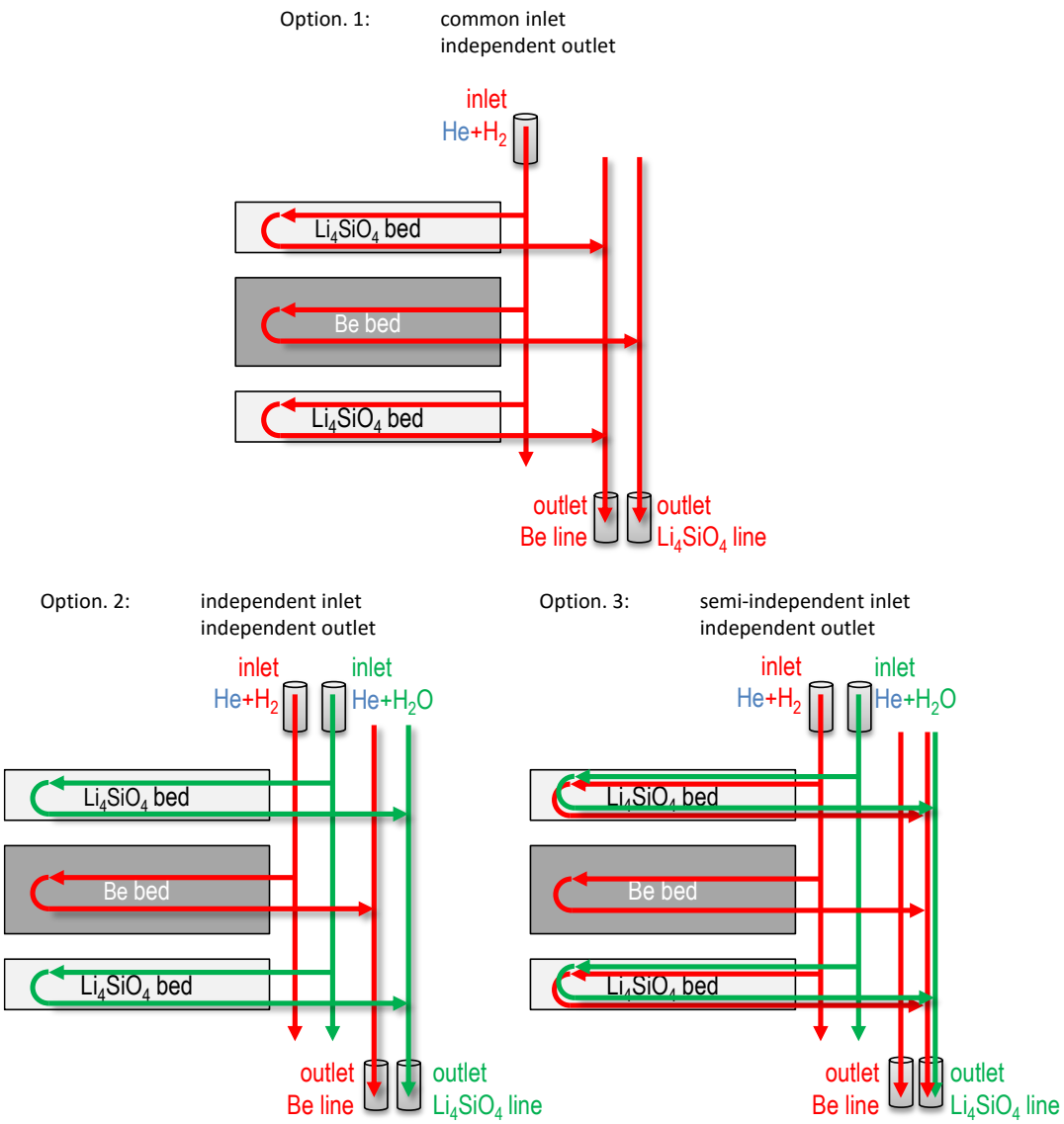

Figure 21. HCPB-2015 "sandwich" purge gas scheme.

The main drawback of this option is the impossibility to pressurize all beds, as they are physically separated, meaning that only either the Be beds or the Li_4SiO_4 will be pressurized during an in-box Loss Of Coolant Accident (LOCA). On the other side, the main advantage is the use of H_2O for the Li_4SiO_4 bed, which promotes the isotopic exchange reaction on the surface of the breeding material between the H_2O and the gas. Given the doping amount into the purge gas, practically 99% of the released T can be in form of HTO and the T permeation to the coolant would be negligibly small compared to that when having H_2 as doping agent.

Option 3, in the figure, is a hybrid between the two above. In this case the line with He+0.1%wt H_2O purges the Li_4SiO_4 pebble beds and the He+0.1%wt H_2 purges both the Be and Li_4SiO_4 beds (Figure 21 bottom right). By doing so, the line of He+0.1%wt H_2 is common for all the pebble beds and it allows their pressurization during an in-box LOCA event. Additionally, the purge of the Li_4SiO_4 beds with He+0.1%wt H_2O would reduce the T permeation to a minimum.

Helium is also the default fluid used as a coolant for the HCPB. This coolant is particularly suitable because it offers nearly nuclear inertness on neutron flux to the BB, molecular stability under fast neutron flux irradiation at high temperature, the highest thermal conductivity among gases and a high heat capacity.

A coolant pressure of 8 MPa is found to be a good trade-off value between the following aspects:

- BB pressure drop: a maximization of the coolant pressure leads to lower pressure drops
- Piping dimensions: a maximization of the coolant pressure leads to smaller piping dimensions
- BB primary stresses: a minimization of the coolant pressure leads to lower primary stresses
- Expansion tank volume: a minimization of the coolant pressure leads to lower compression ratios, leading to a smaller size of the expansion tank

The coolant inlet temperature is set to 300 °C, which is a value set by the lower temperature design limit imposed by the EUROFER97 in order to avoid a working temperature close to the shifted ductile to brittle transition temperature due to the neutron irradiation. The coolant outlet temperature is set to 500 °C, as the EUROFER97 creep strength is greatly reduced at temperatures above ≈550 °C. Table 5 reports and summarize the main design parameters mentioned above both for the coolant and the Tritium Removal circuit.

Table 5. Main operating parameters of HCPB-2015 BB [84]

DEMO HCPB 2015	
Fusion Power [MW]	2037
Total Power to the BB [MW]	2796.4
Coolant	
T_{in} [°C] - T_{out} [°C]	300 - 500

Mass Flow Rate [kg/s]	OB segment: 35.1 IB segment: 22.1
Overall Coolant/s Mass Flow Rate [kg/s]	2690.4
Maximum Coolant/s Speed [m/s]	52.1
Operational Pressure [MPa]	8
Overall Coolant/s Pressure Drop [MPa]	<0.26
Tritium Removal TR	
Neutron Multiplier	Be
Breeder	Li_4SiO_4
T_{in} [°C] - T_{out} [°C]	450 - 450
TR Mass Flow Rate [kg/s]	OB segment: 0.331 IB segment: 0.165
Overall TR Mass Flow Rate [kg/s]	0.497
Maximum TR Speed [m/s]	62.5
Operational TR Pressure [MPa]	0.2
Tritium	
TBR	1.205

2.2 Tritium Extraction and Recovery Systems (TERS) of the HCPB blanket

In the last paragraph, it has been explained how the tritium is extracted from Li-pebble beds. Once the tritium has been extracted, the purge gas is sent to the TERS for tritium removal from helium. The gas stream, outward the blanket, contains few ppm of tritium in form of Q_2 and Q_2O and other impurities.

Different candidate technologies have been carefully assessed taking into account safety, integration, operation aspects and performances, synergy with the inner fuel cycle, technology readiness level and costs [60]. Candidate processes include cryogenic trap, cryogenic adsorption, pressure and/or temperature swing adsorption, getters, permeators, and catalytic membrane reactors [87]. The different techniques have been reviewed in the EUROfusion BB project to identify the baseline process and the back-up solution(s) at conceptual level for DEMO-HCPB TERS. In general, TERS have to satisfy several requirements among which:

- High flow rates as well as high tritium amounts handling in the blanket system;

- Tritium inventory minimization;
- high tritium extraction efficiency from the blanket;
- Low tritium permeation into the coolant;
- Accurate, fast and reliable tritium analytics.

To cope with the requirements for DEMO, one needs is to find improved and maybe even new processes for the tritium extraction system and the coolant purification system.

Currently, regarding the DEMO-HCPB TERS, the European baseline process comprised a cold trap followed by a cryogenic molecular sieve bed proposed by Cristescu (see Section 2.2.1) while a membrane-based continuous process proposed by TLK has been chosen as a backup solution (see Section 2.2.2)[76].

Tritium processes relying on Cryogenic Traps (CT) and Molecular Sieve Bed (MSB) are well-proven technologies able to achieve the required tritium extraction efficiency even though redundant components (usually two) operate in parallel for each stage: while one is removing tritium from helium, the other is regenerated to recover the tritium accumulated in the component. This mode can ensure a continuous tritium removal from blanket but implies two main drawbacks: the first is a cyclic operation of the components with regeneration sequences; the second is the huge increase of the tritium inventory and also the start-up inventory (maybe several hundred grams in a getter bed) [41]. A further drawback of such approach is that the regeneration phase generates transients in tritium flow rates and concentrations routed to the tritium plants and that it implies tritium dilution with a carrier gas [87].

On the other hand, membrane separation are of great advantage because they are simple, reliable, compact, and ensures the smallest achievable inventory due to the continuous operation. However, the membranes considered for tritium processing are not a ready technology for operation in the blanket. Preliminary tests are undergoing on inorganic membranes, in particular Zeolite Membranes (ZM) [88] while dense Pd-based membranes used in TEP are exclusively permeable to Q_2 but not really performing for tritium extraction at so low partial pressures. The next paragraphs are dedicated to describe both systems giving more attention, in this work, to the membrane process.

2.2.1 HCPB TERS based on cryogenic trapping

In the EUROfusion report [89], Cristescu proposes a design at DEMO scale of the HCPB TERS based on cryogenic trapping. The report includes the design of the main parts (molecular sieves, cold traps, exchanger, compressors) over simulations for a more precise estimation of the Molecular Sieve Bed (MSB) desorption behaviour and cost estimation analysis.

The design of the HCPB TER on the preliminary conceptual stage is based on the trapping/adsorption of Q_2O on the RMSB (Reactive Molecular Sieve Bed) and the adsorption of Q_2 on the CMSB (Cryogenic Molecular Sieve Bed) at cryogenic temperatures. Tritium is recovered from the RMSB via catalytic isotope exchange between purge gas (D_2) and Q_2O and in the CMSB during regeneration of the bed.

In the TERS, about 10,000 $Nm^3\ h^{-1}$ of He (0.4 $kg\ s^{-1}$), doped with 1 % of D_2 (10 $Nm^3\ h^{-1}$) for better extraction of T, is circulated through the HCPB BB. Downstream the BB, the amount of Q_2 will be 10 $Nm^3\ h^{-1}$ (composition: H_2 = 95.8 %; Q_2 = 0.73 %; H_2O = 3.47 %; Q_2O = 0.03 %) that yields a T production rate of about 15 $g_T\ h^{-1}$ (assumption of T production rate of 360 $g\ d^{-1}$ [90]) in gaseous and liquid form. Due to the composition, a moisture content of 6.1 $kg\ d^{-1}$ is accumulated.

Figure 22 shows the conceptual design of the HCPB TERS based on cryogenic trapping. Downstream of the HCPB BBs, the temperature of the He-loop is cooled down to 35 °C via heat exchanger HX-01 and heat exchanger HX-02. In order to maintain a system pressure of 3 bar (abs), a He compressor (PC-01) is implemented upstream of HX-02. The Q_2O content of the He-loop will be fully retained in the RMSB. The dried gas stream is then cooled down inside HX-03 via N_2 vent gas and CMSB He off-gas down to - 184.65 °C (88.7 K). Cryogenic temperatures of -196 °C (77 K) are attained by the use of Liquid Nitrogen (LN2) inside the CMSB. Here, approx. 10 Nm^3/h of Q_2 are trapped inside the CMSB by cryogenic adsorption. The remaining He carrier gas is reheated in HX-03 and afterwards used in HX-01 for cooling the BB off-gas. Before entering the BBs again, 10 Nm^3/h of D_2 are supplied in the He Make-up Unit together with He-compensation due to minor losses throughout the system.

For regeneration of the RMSB, the respective vessel will be isolated from the process and is heated up to 150 °C via electrical heater HTR 01/02 while it will be flushed with D_2 in counter-current direction. The main purpose of this D_2 purge is to promote

the isotopic exchange inside the bed. The D_2 gas stream is then directed to condenser CS-01 and demister DS-01 where the moisture content will be separated and collected in vessel TA-01 while the dried D_2 is sent back to the Tritium Plant (TP). After that, a separate He-loop will be applied on the RMSB. Here, the RMSB will be heated up to 250 °C and the He will be circulated via blower PB-01 until the adsorbent is fully regenerated.

The regeneration of the CMSB is realized by isolation from the process and applying sub-atmospheric pressure of 0.9 bar (abs) while the respective vessel is heated up via electrical heater HTR 03/04. For the case of an incidental pressure increase inside the CMSB during regeneration, relieving tank TA-02 is foreseen in the off-gas line directed to the TP.

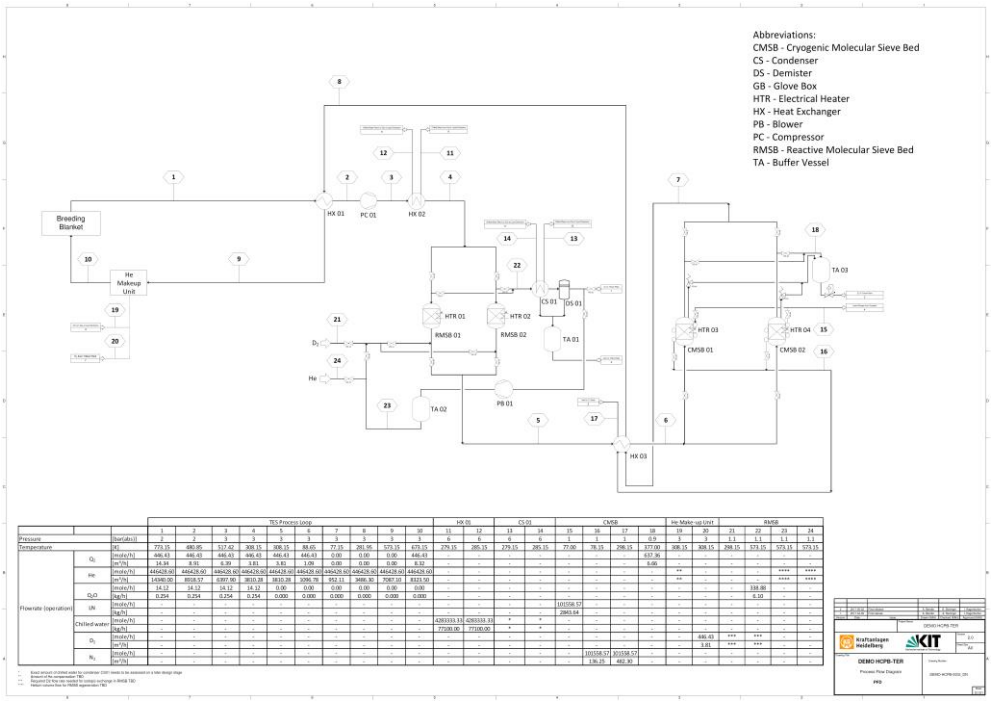

Figure 22. Conceptual Design of the DEMO HCPB-TER [89]

Start-up, design and off-design operation modes has been also defined. Additionally a preliminary design of the heat exchanger, compressors and the design of the RMSB and CMSB has been assessed.

A large amount of cooling power is needed to cool the He carrier gas stream together with the yielded Q_2 from 773.15 K down to 77 K. The cooling is realised by a series of heat exchangers and the usage of Liquid Nitrogen. Here, a chilled water consumption of 94.8 m³/h and a Nitrogen consumption of 545.12 kg h^{-1} during

normal operation of CMSB and a peak consumption during start-up of 9203.12 kg h^{-1} for a short time was estimated. The main driver for the electrical power consumption is the He-compressor, where 325 kW were estimated. In order to increase the availability of the HCPB-TERS, it is recommended to add a third RMSB and CMSB vessel to the design as well as a redundant He-compressor. By implementing these additional redundancies, it would be possible to run the plant even if one of the main components is unavailable. In the first estimation of main equipment costs, it was reached a price of 4 MLN €. However, due to uncertainties the price for the whole system could sum up to 12 MLN €.

2.2.2 HCPB TERS based on membrane separation

A different concept has been proposed by TLK [38] for DEMO 2015. The main idea is to take benefit of the PERMCAT [45], combining it with zeolite membrane cascades, which use has been encouraged during the recent R&D results [91] finalised to obtain a fully continuous process. In this process (Figure 23), it is possible to treat few quantities of either Q_2 and/or Q_2O in purge gas (He) or treat only Q_2 by pre-treating the stream via drying or oxidation processes to separate the Q_2O. Both the option are currently under investigation.

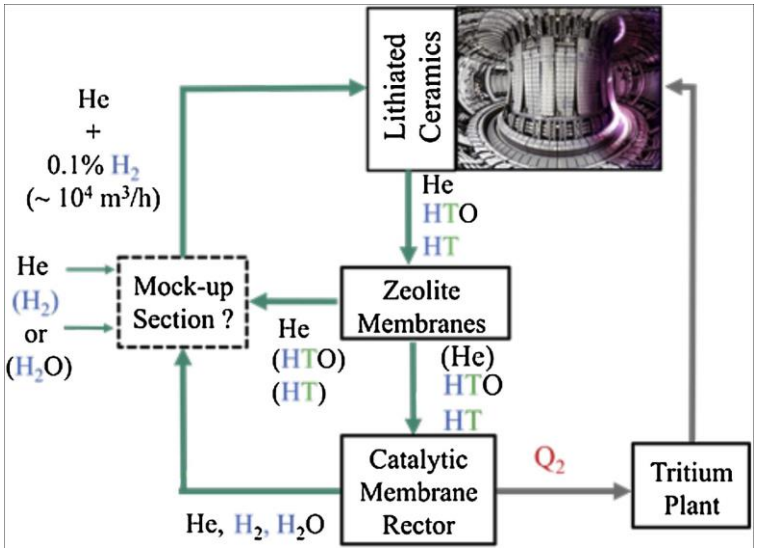

Figure 23. Schematic diagram of the advanced TES concept of the solid Breeding Blanket of DEMO. The curly brackets evidence the species depleted in the corresponding streams [76]

Figure 23 shows the combination of the Zeolite Membrane (ZM) and the Catalytic Membrane Reactor (CMR) finalised to tritium separation in the HCPB blanket. The

tritiated gas, outward the blanket, is sent to the pre-concentration unit, which consist in zeolite membranes cascade. This last, allows to separate the gas in two streams: He depleted in tritium which returns to the Mock-up section in order to restore the purge gas and route it back to the BB; the enriched stream containing tritiated water and gaseous tritium which is sent to the CMR (or permeator in absence of HTO in this stage). The CMR provide a selective separation of hydrogen isotopes, which are successively routed into the accountancy system and in the inner-fuel cycle afterwards.

2.2.2.1 Zeolite membranes

Zeolite membranes have been identified as the most promising material to consistently pre-concentrate the Q_2 and Q_2O species. In zeolite membranes, hydrogen isotopes separation from helium is achieved via Knudsen diffusion mechanisms, surface diffusion, preferential chemical affinity (e.g. hydrophilic), or molecular sieving depending on the specific material and/or geometry. A major difficulty for molecular sieving comes from the very small difference between molecular diameters for He/Q_2O/Q_2. Different promising membranes and process options have been identified in [38]. The only uncertainties on zeolite membranes are the relatively low maturity level and insufficient experimental data on separation performances of Q_2 or Q_2O, especially tritium, from He. Several experiments with He, H_2, and H_2O, feeding different zeolite membranes prototypes as single gases or as mixtures have been performed [92,93]. The results evidenced relatively high single gas permeances but limited separation factors (around 1.7 towards H_2 at 25 °C), regardless of the feed composition (in the range 0.1% - 10% H_2/He) [94]. While more considerably higher separation performances for H_2O/He experiments for MFI-ZSM5 and NaA zeolite membranes between 10 and 500 nm were obtained. The separation factor greatly increases with the decrease of the membrane temperature for the MFI-ZSM5 at 1% H_2O/He. The higher separation factors towards H_2O suggests that the purge gas could be doped with this species instead of H_2. Hydroxy-sodalite membranes (H-SOD) have extremely small pores (0.27 nm) not accessible for Q_2, so that very high selectivity can be expected with respect to He for defect free membranes [95]. In the study [96] different membrane material were tested and results shown that MFI and NaA membranes are good candidate for further investigation. The pre-concentration stage is necessary to permit an efficient separation and consequently to contain the size of the CMR tritium recovery stage.

2.2.2.2 Pd-based membrane and Membrane Reactor

Dense metallic Pd-based membranes are used to perform a ultra-pure hydrogen isotopes separation. In TERS, such membranes are not directly suitable for blanket application due to the very low tritium concentration. Permeation performances of molecular tritium decrease at low tritium partial pressure [97]. In fact, in the backup solution, ZM permeation allows to achieve a tritium-enriched stream, which is routed to the Pd-based membranes unit in order to efficiently separate tritium from helium. With regard of the tritium extraction from He purge, tritium is present in both molecular (Q_2) and oxidized forms (Q_2O). This issue brings to two main uses of Pd-Ag membrane in fusion field: the first is just as a permeator (or separator) for hydrogen isotopes separation; the latter is as a CMR (Catalytic Membrane Reactor) obtained by adding a specific catalyst for reaction and permeation.

The Pd-based membrane and membrane reactor consist of thin-walled tubes, which can be manufactured obtaining a thickness of about 50 and 150 μm. Tubes of lower thickness could not work under the operating conditions typical for hydrogen separation processes (about 1.7 MPa at 400°C for and in hydrogen separation processes up to 0.2–0.3 MPa [98]). The main fabrication methods are cold-rolling, diffusion welding of metal foils [99] or extrusion [100]. Thin-walled membranes of 100-150 μm can reach rupture pressure of about 1-1.5 MPa on hydrogen separation. In order to reduce the costs and increase the hydrogen permeance, Pd-based supported membranes has been studied. Thin Pd-based layers are deposited over porous supports made of glass, ceramic, or metal. Both physical and chemical (reactive) techniques are adopted for preparing the Pd coatings.

The Pd-composite membranes with ceramic supports are usually composed of three parts, a Pd-based layer, the ceramic porous support, and an intermediate ceramic layer of small porosity, which reduce the thermal mismatching between the support and the Pd-alloy film. For instance, ceramic layers have been positioned in between stainless steel porous supports and Pd-Ag and Pd films. These membranes were successfully tested up to 500°C. Their effectiveness as diffusion barriers for Pd membrane deposited over porous stainless steel supports at 400°C was demonstrated by the presence of a zirconia layer [18]. Further thickness reduction could be beneficial for increasing the permeance and reducing costs.

Up to now, only preliminary experiments on a small-scale reactor have been performed to identify the most suitable operative conditions and catalyst materials. An experimental campaign was carried out on a Pd-based membrane aimed at measuring the capability of this device in separating hydrogen from the helium. Many operative conditions have been investigated by considering different He/H_2 feed ratios, several lumen pressures, and reactor temperatures. The results are reported in [88] and will be reported in the next chapters of the present work together with the design and commissioning of a medium scale CMR device at ENEA Frascati.

Since the Pd-based membrane is the main topic of this dissertation, the next paragraph is dedicated to the description of this technology.

2.3 Pd-based membrane and Catalytic Membrane Reactor (CMR)

Recent reviews presented in work [101] and [102] report several membrane and membrane reactors (including Pd-based concepts). Among them, the metal-supported tube-shaped membranes, with particular focus to the self-supported membranes, have also been produced at ENEA Frascati laboratories [103].

A membrane can be described as a structure having lateral dimensions much greater than its thickness through which mass transfer may occur under a variety of driving forces such as gradient of concentration, pressure, temperature, electric potential [104]. The membranes are classified on the base of their nature, geometry and separation regime. Depending on the material, Pd-based membranes are classified as synthetic, inorganic and metallic (supported and self-supported) membranes. On geometry point of view, they are tubular or flat sheet shaped. Depending on the separation regime, they can be classified in dense or porous membranes.
Self-supported dense Pd-based membranes are able to perform a ultra-pure separation of hydrogen isotopes because of the high affinity (solubility and diffusivity) between the hydrogen isotopes and the metallic lattice [105]. In general, the Pd/H system is of interest for several applications such as hydrogen purification, catalysts for hydrogenation/dehydrogenation reactions and materials for hydrogen storage. Pure palladium exhibits inadequate properties for membrane applications. Pd lattice can absorb large amounts of hydrogen with consequent embrittlement of the metal. At pressure lower than 2 MPa and below 300°C (Figure 24), hydrogen in Pd co-exists under two hydride forms, phases α and β [106]. Transition between

these two phases produces cyclic lattice strains that, at macroscopic level, are responsible for the embrittlement of the metal [107].

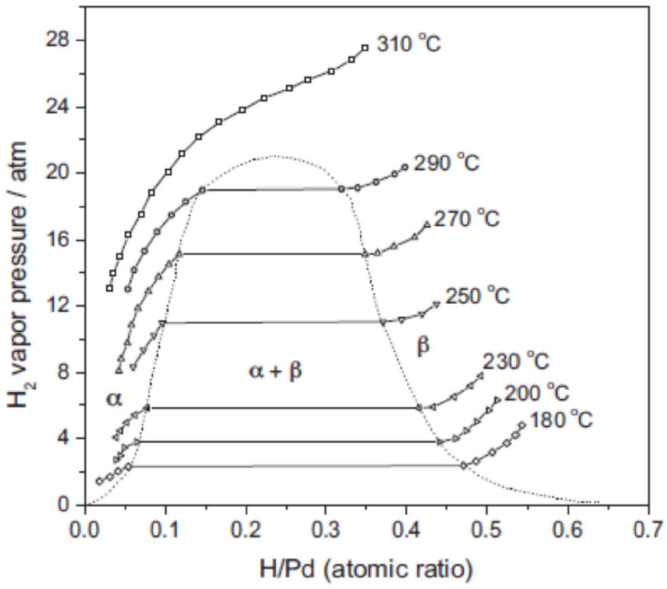

Figure 24. P-C-T phase diagram of the Pd-H system [108]

The effect of Ag addition results in a decrease of the critical temperature and pressure for the phase transition and in an increase of the hydrogen solubility. However, the diffusion coefficient of hydrogen significantly decrease in this alloy. The simultaneous variation of solubility and diffusion coefficient affects the hydrogen permeability values. In particular at 350 °C and 2.2 MPa, the maximum permeability value is reached for the 23% Ag alloy [109] together with the mechanical strength, and electrical resistivity. The silver addition also makes feasible the joining through diffusion welding of the Pd-Ag foils or tubes.

Excluding Pd-Y, which are rarely used because of their modest workability, Pd-Ag has also the highest permeability among the Pd alloys. The diffusion of hydrogen through palladium, iron, and platinum was observed since 1860s by the French group of Deville and Troost and in Britain by Graham [99]. The first commercial application of a metal membrane, concerning the hydrogen purification using a 23 %wt Pd-Ag membrane, dates back to 1964 [105].

2.3.1 Hydrogen permeability in Pd-Ag membranes

As already introduced, hydrogen can permeate selectively dense metal layers, and, accordingly, this phenomenon is exploited when metal membranes are applied for separating ultra-pure hydrogen from gas mixtures. The hydrogen mass transfer

through dense metal membranes includes several transport mechanisms which can be reassumed in three main parameters:

- Solubility

The hydrogen solubility is a measure of the amount of hydrogen present in the metal lattice; it is controlled by the kinetics of the reactions that occur over the metal surface. Two hydrogen fluxes are established through the metal surfaces when hydrogen gas comes in contact with a metal as shown in Figure 25 in which a piece of metal is put in a container under a hydrogen atmosphere at constant temperature and pressure.

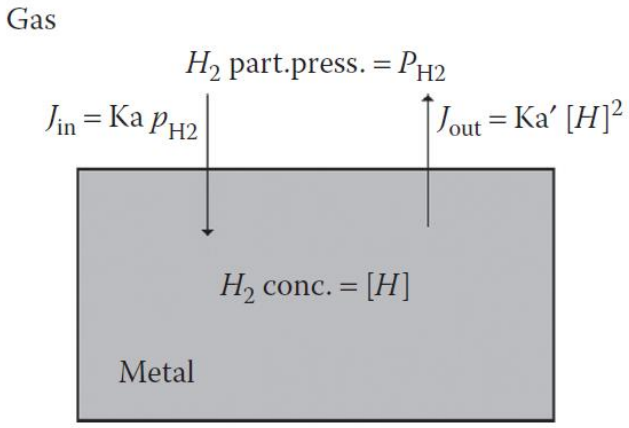

Figure 25. Hydrogen solubility into metals with hydrogen fluxes entering and leaving the metal surface[18].

The hydrogen flux entering the metal surface is proportional to the hydrogen partial pressure in the gas phase

The term $1/K_a$ (and $1/K_a$' in Figure 25) can be defined as a mass transfer resistance due to the surface reactions. The well-known Sieverts' law establishes at a given temperature the relationship between the concentration of hydrogen (protons) into the metal lattice in equilibrium with the hydrogen (molecules) in the gas phase. In fact, the solubility coefficient S (mol m^{-1} $Pa^{-0.5}$) is related to the constant Ke (constant Ke = K_a'/K_a, m^6 Pa mol^{-2}) through the following equation:

$$S = \frac{1}{Ke^{0.5}} \qquad (15)$$

An Arrhenius-based law expresses its dependence on the temperature as follows:

$$S = S_0 e^{-\frac{E_a}{RT}} \qquad (16)$$

Where S_0 (m^2 s^{-1}) is the solubility pre-exponential factor, E_a (J mol^{-1}) is the activation energy of the solubility, R (8.314 J mol^{-1} K^{-1}) is the gas constant.

- Diffusion

A gradient of hydrogen concentration in the metal lattice produces a flux. Under equilibrium (t = > ∞) and other general hypotheses (i.e., D = constant), the integration of the Fick's second law for a metal layer of thickness th (m) leads to Fick's first law:

$$J = D\,\frac{[H_{up}] - [H_{down}]}{th} \qquad (17)$$

Where D (m^2 s^{-1}) is the diffusion coefficient, t is the time (s), *up* and *down* represent the upstream and downstream hydrogen concentration, respectively. An Arrhenius law is also applied to the diffusion coefficient to account for its dependence on temperature:

$$D = D_0 e^{-\frac{E_D}{RT}} \qquad (18)$$

Where D_0 (m^2 s^{-1}) is the diffusivity pre-exponential factor, E_D (J mol^{-1}) is the activation energy of the diffusion.

- Hydrogen Permeation

When the surfaces of a dense metal layer are exposed to hydrogen at different partial pressures, a mass transfer of hydrogen (permeation) occurs from the side at higher pressure (upstream) to that at lower one (downstream). Five main transport mechanisms have been recognized for the permeation:

- Adsorption of the molecular hydrogen on the first metal surface (upstream surface)
- Dissociation of the hydrogen into two protons at the first metal surface (upstream surface)
- Diffusion of the protons through the metal lattice

- Recombination of the two protons at the opposite side of the metal wall (downstream surface)
- Desorption of the molecular hydrogen from the metal surface (downstream surface)

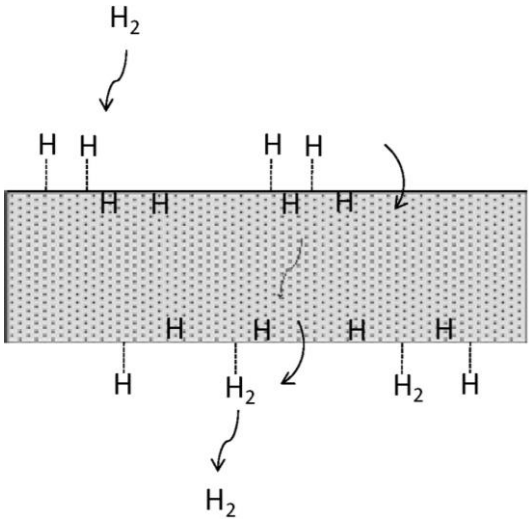

Figure 26. Solution diffusion mechanism of hydrogen permeation through a palladium membrane [108]

The product of the solubility and the diffusivity is defined as the permeability coefficient Pe (mol s^{-1} m^{-1} $Pa^{-0.5}$). According to Equations (16) and (18), its dependence from the temperature follows the Arrhenius behaviour:

$$Pe = Pe_0 e^{-\frac{E_P}{RT}} \qquad (19)$$

Where Pe_0 (mol m^{-1} s^{-1} $Pa^{-0.5}$) is the permeability pre-exponential factor, E_P (J mol^{-1}) is the activation energy of permeability. It results that $Pe_0 = D_0 \times S_0$ and $E_P = E_D + E_S$.

Many authors report a Sieverts' law obtained for the case of a dense metal layer including other mass transfer resistances modified by introducing a generic pressure exponent n, which is in the range 0.5 and 1, as follows:

$$J = \frac{Pe}{th}\left(p_{H_2up}^n - p_{H_2down}^n\right) \qquad (20)$$

For a membrane made of several layers of different materials, such as the case of a composite membrane, just one permeability coefficient cannot be used. The deviations from the Sieverts' law, which correspond greater exponent values, can be attributed to a variety of factors (i.e. the presents of

porous support for thick Pd layer, low thickness of the Pd-based membrane, low hydrogen partial pressure, presence of impurities, etc.) and usually n is assumed 0.5 because referred to a metal Pd-Ag membrane ideal behaviour [18].

Because of the large mass differences among the hydrogen isotopes, isotope effects are appreciable in properties relating to the velocities of ions, atoms and molecules, and vibration and rotation of atoms and molecules. Among various properties of hydrogen in materials, solubility, diffusivity, and permeability are quite important not only for T safety but also for T fuel self-sufficiency.

Since hydrogen solution and permeation are likely proportional to incident flux, the isotopic effects in solubility (S) and diffusivity (D) would be proportional to the square root of mass ratio as follows:

$$S_H/S_D = \sqrt{2} \quad (21) \qquad S_H/S_T = \sqrt{3} \quad (22)$$

$$D_H/D_D = \sqrt{2} \quad (23) \qquad D_H/D_T = \sqrt{3} \quad (24)$$

Similar isotope effects are often observed in hydrogen permeability. Large mass differences among hydrogen isotopes result in large difference in their quantized rotational and vibrational states. Actually significantly large isotope effects originating from quantum effects are observed in diffusion coefficients. The diffusion coefficients do not follow single Arrhenius relationship in their temperature dependence, and the upper shift at lower temperatures is attributed to the quantum tunneling effect. Above the room temperature, the difference becomes less and the differences in not only diffusivity but also solubility and permeability of H, D, and T are within the factor of the square root mass ratio, which is in most case near the experimental error [12].

2.3.2 Pd-Ag membrane reactors

A Catalytic Membrane Reactor (CMR) is a device in which a catalysed reaction and selective permeation are simultaneously carried out [110] by combining a Pd-Ag membrane permeator with a catalyst. In this way, it is possible to perform simultaneously the chemical reaction and product separation in a single operation. Therefore, CMRs are capable to provide a selective removal of one or more products

with the reaction, so that the reaction equilibrium is continuously shifted to increase the product formation, obtaining values of reaction conversion beyond the thermodynamic equilibrium. These effect is the so called “shift effect” of the membrane [111].

The design of the membrane module has to take into consideration the significant hydrogenation strain of the Pd-Ag alloy. The membrane module has to be tightly connected to the Pd-Ag membrane in order to ensure its selectivity, and at the same time has to permit its elongation/contraction due to the thermal and hydrogenation cycles. In the case of a single-tube membrane module, both ends of the Pd-Ag permeator should be tightly fixed to the module (Figure 27 left).

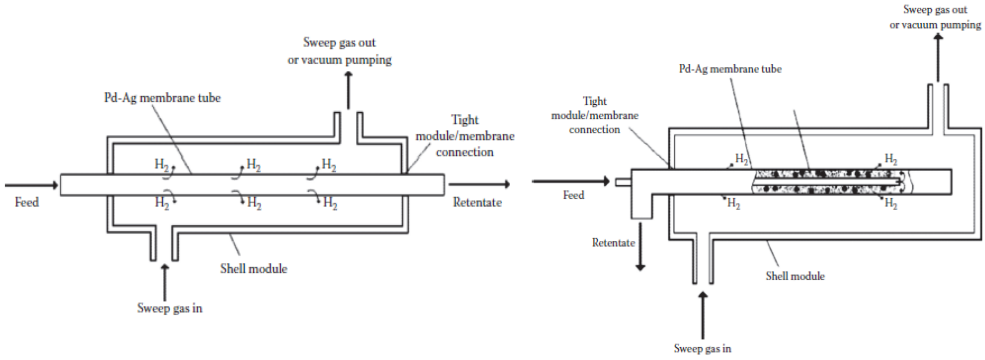

Figure 27. on the left a both-end membrane module; on the right a dead-end (or finger-like) membrane module[112]

When hydrogenated, the Pd-Ag permeator expands much more than the module, this results in a compressive force over the thin-walled tube when hydrogenated at low temperature (i.e. by considering a tube of wall thickness of 50 µm and diameter of 10 mm, the compressive force is about 2600 N). The finger-like (or dead-end) configuration shown in Figure 27 (right) permits the free elongation/contraction of a Pd-Ag tube that is tightly fixed to the membrane module at one of its end. In this way, no stress is applied to the permeator tube, thus increasing its stability in presence of hydrogenation [105]. Hydrogenated Pd-Ag elongation ($\varepsilon_{H/Pd\text{-}Ag}$) is about 1.5% whereas the hydrogenated Pd ($\varepsilon_{H/Pd}$) elongates by about 0.3%. It results that the $\varepsilon_{H/Pd\text{-}Ag} \approx 5 \times \varepsilon_{H/Pd}$ [18].

At TLK, a both-ended membrane reactor (called PERMCAT), shown in Figure 28, has been deeply studied and tested in different operating condition [29,113]. In PERMCAT, the tritiated gases are sent into the reactor shell where a catalyst bed

promotes, through the Isotopic Swamping (IS), the exchange of tritium with hydrogen, which is fed in a counter-current mode in the membrane lumen.

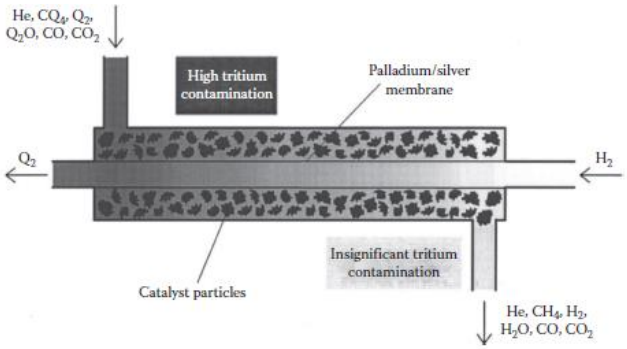

Figure 28. representation of a PERMCAT reactor (catalyst in shell side)[114]

Only the hydrogen isotopes can permeate through the dense Pd-Ag tube, the tritium is transferred from the shell side to the lumen, thanks to the isotopic exchange over the catalyst. The decontamination factors required (up to 100) can be attained using long and thin-walled permeator tubes.

Several other design configurations of Pd-Ag membrane tubes of about 100 μm wall thickness were proposed by TLK [115] and ENEA Frascati [112,116], as reported in Figure 29. In Figure 29 left, the first reactor (a) uses a typical finger-like configuration;; the tritiated gases are fed in the shell side whereas the hydrogen is sent inside the membrane lumen. In the second reactor (b), a preloaded bellows is joined to the Pd-Ag membrane tube in order to compensate for expansion/contraction. In a third reactor (c), the permeator is a corrugated Pd-Ag tube working as a bellow-type membrane. The membrane reactor was designed for water detritiation of the Joint European Torus (JET) housekeeping waste. In this device, the direct ohmic heating of the membrane was achieved by inserting a bimetallic Cu and Inconel spring, which gave electrical continuity, and pre-tensioning of the membrane, respectively.

In laboratory applications, the scale-up of membrane devices consist in multi-tube modules. At ENEA Frascati laboratories, a bundle of 19 Pd-Ag tubes in finger-like configuration was realized for separating up to 6 NL min^{-1} of ultra-pure hydrogen. The design of the multi-tube reactor, aimed to steam and oxidative reforming of ethanol and methane, is well described in [114]. Recently at TLK, a new technical scale, multi tube, single bed PERMCAT was designed, manufactured and commissioned [117]. It is noteworthy, as already highlighted that, even though the

both laboratories adopt the same technology, the engineering design follows different approaches. On the contrary, of TLK, in the ENEA CMRs, the feed is routed inside the membrane while the permeated gas is recovered in the shell. One further difference in the operation is the catalyst location. In TLK, it is located in the shell while in ENEA it is placed inside the membrane.

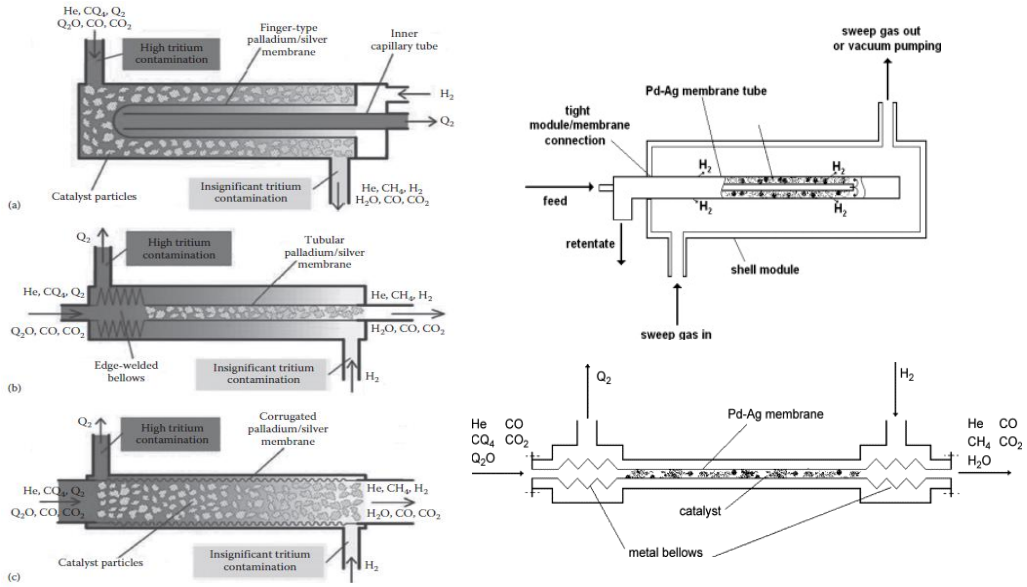

Figure 29. Simplified diagrams of three different PERMCAT reactors developed at TLK(left side) [113] and in ENEA (right side) [112,116]

Scale-up studies, tests, and optimization design of multi-tube membrane reactors, aimed to reduce the size of membrane devices, are under investigation in many fields, fusion included. Other membrane configurations similar to the design of flat-and-frame heat exchangers was developed [18] [118,119].

Single and multitube Pd-membrane reactors adopting the finger-like configuration were developed at ENEA Frascati laboratories [120] and they will be presented in the next chapter.

3.Permeation and reaction tests with a single Pd-Ag membrane reactor

As descrived in last chapter, the reference scenario for a DEMO HCPB TERS is based on the use of a cold trap followed by a cryogenic molecular sieve bed while a back-up solution is based on the use of zeolite membranes (developed by KIT-TLK) followed by a Pd-Ag permeator module and a catalytic membrane reactor (both developed by ENEA Frascati), as shown in Figure 30. According with the data provided in [121], the HT/HTO ratio in the He purge stream leaving the blanket, is about 97/3 meaning that most of the generated T will be found as HT. The preconcentration stage (made of a zeolite membrane cascade) has the scope to remove part of the helium and thus to enrich in tritium the gas stream to be treated in the Pd-Ag membrane modules and in the catalytic membrane reactor (CMR).

In particular the Pd-Ag membrane modules will separate the tritium in the gas phase (HT), while the CMR will recover and separate the tritium present in the oxidized phase (HTO). The precise composition of the gas stream to be treated in the three membrane modules (i.e. zeolite, Pd-Ag and CMR) is still unknown, but it is clear that it will be characterized by a very low tritium (few ppm) concentration in a large He flow and by the presence of tritium in both molecular (Q_2) and oxidised form (Q_2O).

In this view, the experimental activity carried out in this work has the dual scope to 1) evaluate the Pd-Ag permeator separation performance at the different He/H_2 feed flow rates and 2) assess the efficiency of the CMR in performing the tritium removal from water via two reactions: the Isotopic Swmaping (IS) and the Water Gas Shift (WGS). To do this, a dedicated facility, called HyFraMe (Hydrogen Frascati Membrane), has been build and several experiments were carried out as described in this Chapter.

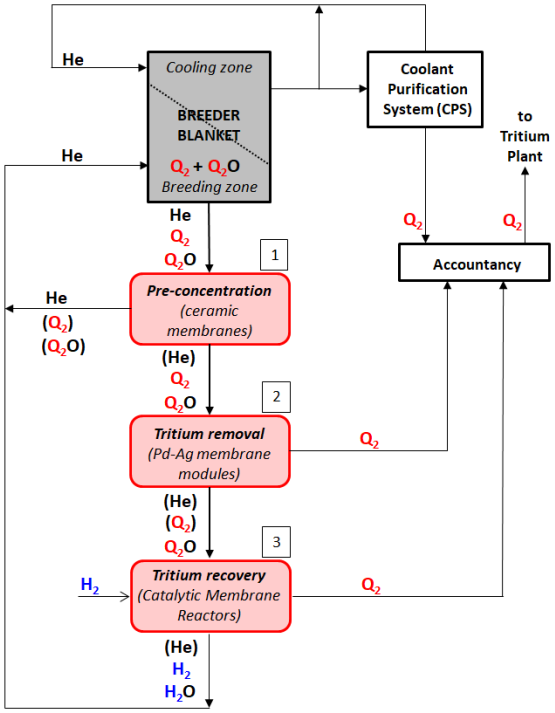

Figure 30. TERS concept with: 1) ceramic membranes as pre-concentration stage, 2) Pd-Ag membrane for hydrogen isotopes separation and 3) CMR for tritium recovery for water[91].

3.1 Description of the HyFrame Facility

The scope of the facility is to define the performances of a sigle Pd-Ag permeator in separating hydrogen isotopes separation starting from a He-H_2 gas stream and the abilit of a CMR in water decontamination in view of DEMO operations.

Several tests have been performed in the dedicated experimental apparatus, particularly permeation and reaction tests have been performed separately because of two reasons: i) it was interesting to understand the influence of the operating conditions on the permeation and on the reaction, ii) due to the very low water content expected in the He purge, it was not possible to experimentally reproduce and control the composition of the feeding stream scaled down to a single tube (this constraint will be overcome in the experiments with the multi-tube where higher feeding flow rate are allowed).

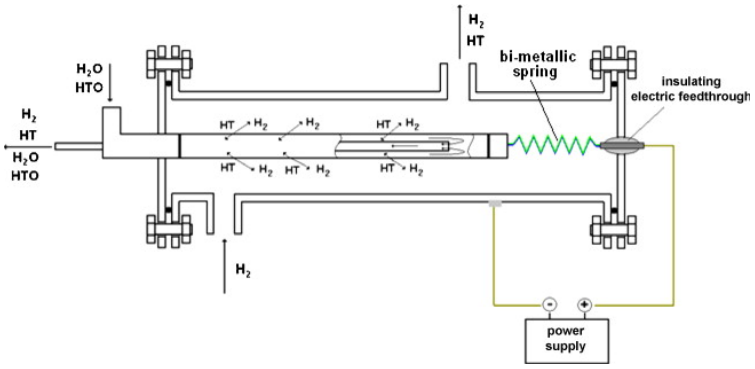

Figure 31. Scheme of the membrane reactor [122].

In the experiments, a single Pd-Ag (25% wt.) tube in a having wall thickness of 113 µm, length of 500 mm and diameter of 10 mm has been used(Figure 31). The membrane tube is assembled in a finger-like configuration: one end of the membrane tube is brazed on one of the flanges of the reactor shell while the other end of the membrane tube is closed and linked to the other flange of the shell by a metal spring. Such an extension spring has an outside diameter of 15.2 mm and consists of Inconel coils of diameter 2 mm. The shell input/output use two ¼" VCR connections while the membrane lumen inlet/outlet are ½" VCR connections. The reactor is heated up via Joule heating operated by inducing a direct current in the membrane itself.

The HyFraMe setup is showed in Figure 32 and the results have been published in [123].

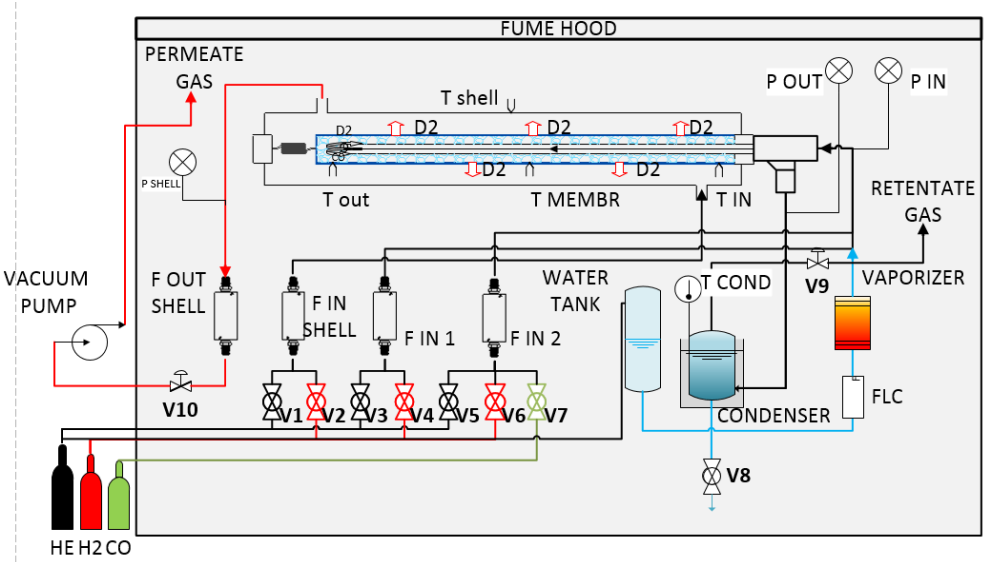

Figure 32. Simplified HyfraMe facility layout

The reactor is equipped with 4 K-type thermocouples three of which measure the temperature in equidistant points on the membrane surface, in particular: T_{in} at the inlet/outlet side, T_{membr} in the middle and T_{out} in the far end, while the thermocouple T_{shell} measures the shell temperature.

In the plant there are other 3 thermocouples dedicated to the vaporizer system setting and control that are useful for: temperature set point in PID control (T_{vap}); water/steam temperature monitoring downwards the heating system (T_{vap2}); flow temperature measuring before reactor inlet (T_{vap3}). One more thermocouple measures the condenser temperature (T_{cond}). The shell side of the membrane reactor is connected to a vacuum pump (Adixen ACP15 with ultimate pressure of 0.03 mbar). Through Mass flow MKS controllers (F_{IN}, F_{OUT} and F_{SHELL_IN}) it is possible to set a specific flow for each gas fed in the membrane in the way that the gas composition can be set and controlled. On the contrary, $F_{SHELL\ OUT}$, is totally opened in order to measure the gas flow leaving the shell side. Additionally equipments are MKS pressure gauges (P) and the electric steam generator.

Other external equipments are a Gas Chromatograph (GC) and a Fourier Transform Infrared Spectroscopy (FTIR), which have been introduced in order to measure the gas and water composition during the WGS and IS reaction tests, respectively. This measurements allow to calculate the decontamination performances during each test.

In ENEA laboratory, both GC and micro-GC (µGC) can be used to estimate the gas composition. The GC is an analytic instrument that measures the content of various components in the gas stream. The sample injected into the instrument is routed in a separation column via an inert gas (Helium in the GC and Argon in the µGC). The various components are separated inside the columns. Successively, the detectors identify and quantify the components leaving the columns. In order to well estimate the sample composition a dedicated calibration is necessary The calibration is performed by using certified gas tank containing a known amount of a certain gas mixture (in our case H_2, CH_4, CO, CO_2 and N_2). IN this way it is possible to assess the standard sample peak retention-time (appearance time) of the specific gases and, identifying the specific peak area for different pre-calibrated concentrations. Successively, by comparing the area of the test sample with the calibration straight line calculated, it is possible to calculate the concentration.

Currently different gas chromatography analysis methods exist. GC and µGC works in two different ways. Nevertheless, in this work only the µGC will be described,

because it have been used in HyFraMe experiments. The reason is due to the purge gas adopted by the μGC which is Ar instead of He (this last is also present in the samples therefore cannot be identified by using He purge gas in the GC).

The μGC is a Varian CP-2002/2003 and it is equipped with two-channel column:

- Channel 1, equipped with a CP-Molsieve column, separates and analyses the permanent gases except for carbon dioxide;
- Channel 2, equipped with a PoraPLOT Q column that analyze a broad range of polar and apolar volatile compounds.

The Thermal Conductivity Detector measures the different thermal conductivity between the sample gas and the carrier gas (Ar in this case)

Regarding the FTIR, it have been used a SHIMATZU IRAffinity-1S. The FTIR spectrometer consists of a source, interferometer, sample compartment, detector, amplifier, A/D convertor, and a computer. The source generates radiation, which passes the sample through the interferometer and reaches the detector. Then the signal is amplified and converted to digital signal by the amplifier and analog-to-digital converter, respectively. Eventually, the signal is transferred to a computer in which Fourier transform is carried out. The Michelson interferometer, which differentiate FTIR spectrometers from an FTIR spectrometer and a dispersive IR spectrometer, is used to split one beam of light into two beams in different directions. Then the Michelson interferometer recombines the two beams and conducts them into the detector where the difference of the intensity of these two beams are measured as a function of the difference of the paths.

This instrument is used to identify the heavy water concentration in light water by investigating the water absorption spectra. It have been used in the IS experiments to evaluate the water decontamination starting from pure heavy water.

Concerning the data acquisition, a National Instruments Data acquisition (DAQ) analogic measurement hardware have been used together with a LABVIEW interface which provide a real time monitoring and control (via computer) of the facility as shown in Figure 33.

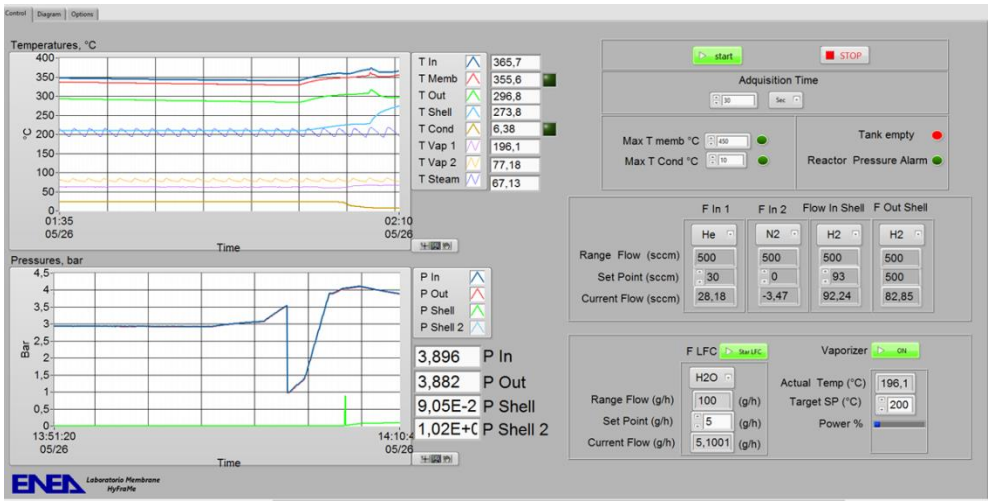

Figure 33. LABVIEW Interface

The DAQ is directly connected to the sensors (thermocouples, mass flow meter, pressure gauges, etc.) and to a computer (Figure 34) in which the data are saved and stored.

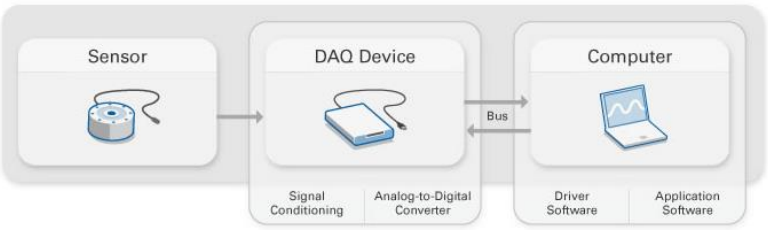

Figure 34. semplified scheme of Hyframe Data Acquisition.

3.2 Experimental procedure

Figure 35 shows the the HyFraMe facility installed in a new ENEA Membrane Laboratory.

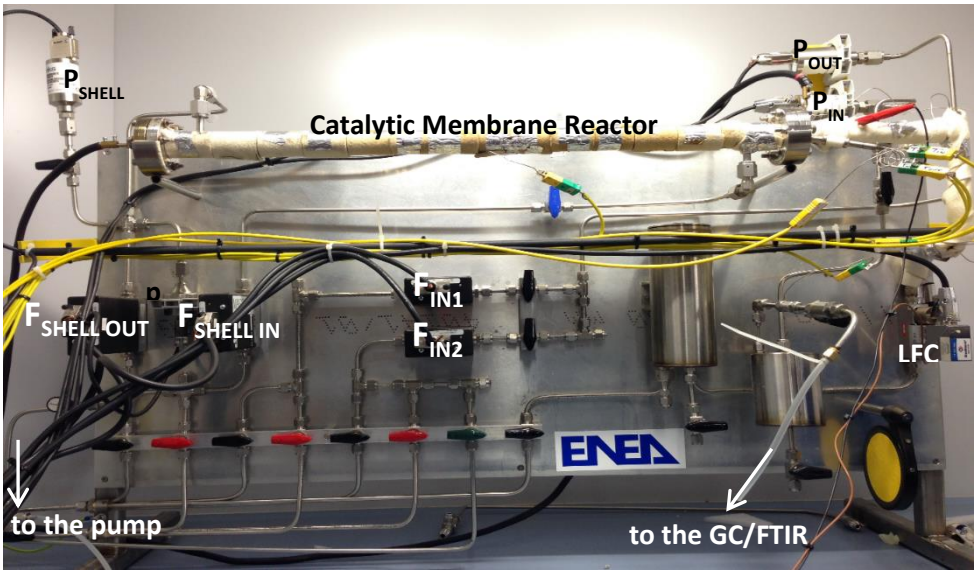

Figure 35. HyFraMe facility

The facility has been designed to operate in two different configurations in order to perform:

- Permeation Tests
- Reaction tests

Each procedure will be described in section 5.2.1 and 5.2.2.

In order to ensure the correctness of the performances measured in the reactor, at the end of every daily experimental session, a night leakage test is performed to verify the leak tightness of the membrane and the set-up (i.e.weldings, fittings and connections). In order to do so, a specific procedure has been developed. It consists in pressurizing the lumen side of the membrane with an inert gas, usually helium, and reducing the pressure in the shell side through the vacuum pump. This operation allows to identify the leakage either in the lumen circuit, or in the membrane or in the shell circuit. In fact, if a pressure drop is measured in the lumen and an appreciable increasing in the shell is not detected, it means that the leakage belongs to the lumen circuit (the gas leaks outside). In case of a lumen pressure drop and an increasing of the shell pressure, the leak is belonging to the membrane itself or membrane brazings/weldings (the inert gas leaks from lumen to shell). For last, in case of pressure increase in the shell without any variation in the lumen pressure, the leakage can be attributed to the shell circuit (the gas leaks outside). In all of these cases, the leakage should be found through a leak detector and repaired.

3.2.1 Permeation procedure

In case of permeation operations, the gas composition and flow to send to the membrane is set by the flowmeters F_{IN1} and F_{IN2}. The gaseous stream is routed inside the Pd-Ag membrane via a small (2mm) stainless steel tube (see Figure 31). The He-H_2 gas stream is routed in the membrane and the hydrogen permeates selectively the membrane and is collected in the shell side by vacuum pump, while the non-permeated gases (retentate stream) leaves the membrane without mixing the feed stream. The amount of hydrogen fed in the membrane is known and well controlled while $F_{SHELL\ OUT}$ measures the permeated gas. In this configuration, the hydrogen yield can be directly measured and the permeation efficiency could be easily calculated.

All the tests can be performed by varying temperature (regulating the current of the power supply), flows (by LABVIEW interface), pressure (by needle valves V9 and V10 in Figure 32).

In these operations, some components as the vaporizer and the condenser are useless therefore can be isolated. The operating condition investigated during the experiments are summarised in Table 6.

Table 6. List of the HyFraMe permeation tests (P_shell ~ few mbar)

Temperature [K]	**Lumen Pressure [kPa]**	**He/H_2 feed flow ratio [a.u.]**	**He flow rate [Ncm^3/min]**	**H_2 flow rate [Ncm^3/min]**
573 - 623 - 673 - 723	100 - 200 - 300 - 500 - 700	5	450	90
		10	500	50
		15	450	30
		20	500	25

The test duration is about 30 minutes each. A total of 80 permeation tests have been performed.

3.2.2 Reaction Procedure

Two different reactions were investigated under different operating conditions (i.e. reactor temperature, lumen pressure, feeding molar ratio and isotopic swamping): Water Gas Shift (WGS) and Isotopic Swamping (IS) [123]. Both WGS and IS have been studied because are suitable for tritium extraction from water in the HCPB blanket.

In the follow sections, the WGS and IS operation will be described together with the list of the experiments performed. The tests have been carried out by using heavy water instead of tritiated water. In all the experiments, pure heavy water (*Cambridge isotopes laboratory Inc*, purity 99.9%) has been fed in the membrane lumen.

3.2.2.1 WGS Experiments

During WGS reaction tests, a gas stream of CO and D_2O (steam) is sent in the feed side of the reactor. The water flow is regulated through the liquid flowmeter controller (LFC) and the vaporizer is operative at the set point temperature of 200°C. The CO flow is regulated through on of the F_{IN} flowmeter controller while the vacuum pump allows to reach a rough vacuum in the shell. The WGS reaction occurs with a resulting molecular deuterium production, see formula (25).

$$D_2O + CO \leftrightarrow CO_2 + D_2 \qquad (25)$$

According to the semplified block diagram in Figure 36, the retentate (the non-permeated steam coming out the reactor) is driven into a condenser to collect the un-reacted water. Then, the dried gas composition is investigated via batch Gas Chromatographic (GC) analysis carried out at the end of each test once steady-state conditions are reached. A needle valve downwards the condenser allows to regulate the pressure in the lumen side. The dried gas stream mainly consists of CO_2, small amount of D_2O vapour, un-reacted CO, un-permeated D_2 and methane impurities.

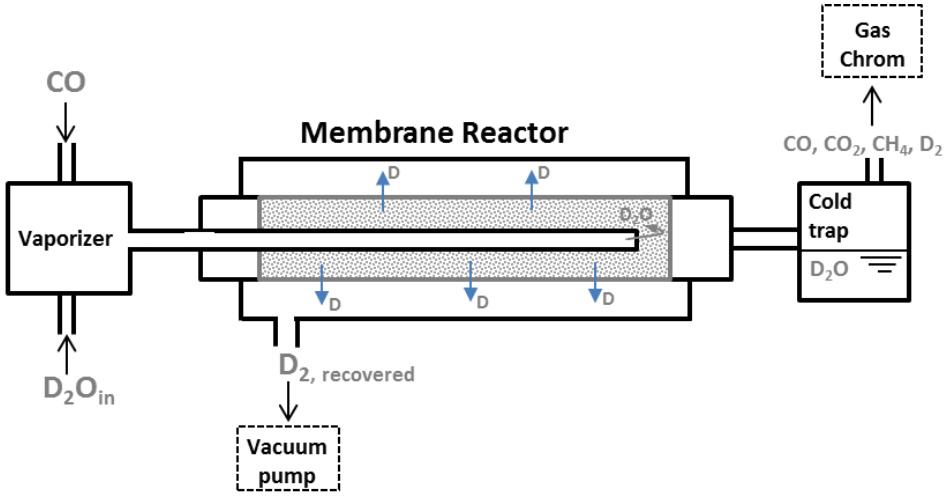

Figure 36. Block diagram of the WGS operation in CMR

In particular, the presence of methane should be as low as possible because, otherwise, additional efforts are required in tritium treatment due to the good stability of CQ_4 molecule. On the shell side, the vacuum pump guarantees a low pressure. The flowmeter $F_{SHELL\ OUT}$ measures the permeated hydrogen flux.

A previous calibration of the Variant CP-2002 µGC has been performed using mixed gas tanks. The main gases such as H_2, N_2, O_2, CO, CO_2 has been calibrated for different molar concentration values (Table 7).

Table 7. Certified tanks used for GC calibration

Tank	**Composition**
Mix 1	70% H_2, 30% N_2
Mix 2	4% CH_4, 4% CO, 4% CO_2, 88% N_2
Mix 3	1% CH_4, 1% CO, 1% CO_2, 97% N_2
Mix 4	20% H_2, 80% N_2
Mix 5	19.94% CH_4, 20.01% CO, 20.00% CO_2, 40.05% N_2

The calibration curves is reported in

Figure 37.

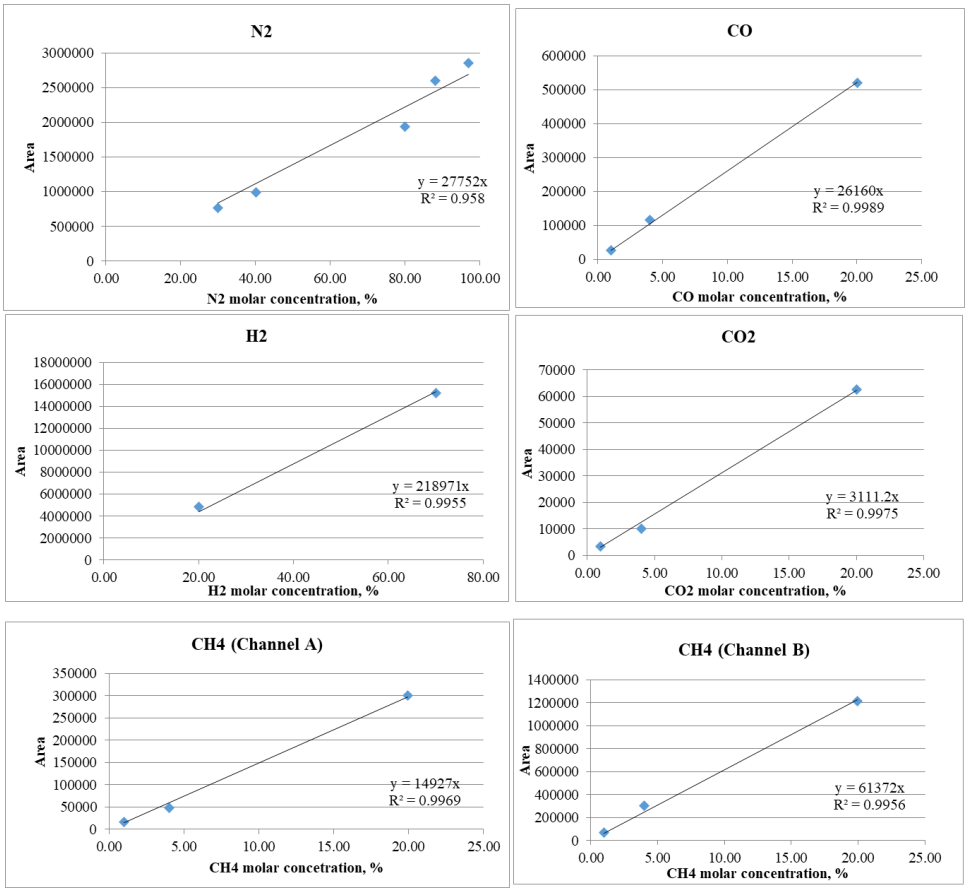

Figure 37. Calibration straight lines of the µGC gases

During both WGS and IS tests, the reactor temperature has been varied between 573 and 673 K, the lumen pressure between 100 and 500 kPa and the reactor shell has been connected to a vacuum pump ensuring a shell pressure between 2-3 kPa. After this campaign, a second set of experiments has been carried out with the aim to investigate the influence of the D_2O/CO feed molar ratio (Table 8. List of WGS experiments (Pshell ~3-10 kPa)).

Table 8. List of WGS experiments (Pshell ~3-10 kPa)

D_2O/CO feed ratio	**D_2O, mol h^{-1} (g h^{-1})**	**CO, mol h^{-1} (sccm)**	**$T_{reactor}$, K**	**P_{lumen}, kPa**
~1	0.25 (5)	0.25 (93)	573-623-673	100-200-300-400-500

~ 1.5	0.25 (5)	0.16 (62)	623	300
~ 0.75	0.25 (5)	0.33 (125)	623	300

The information of the permeated gas, extracted in the shell, together with the information of the gas composition, allow to calculate the decontamination efficiency of this reaction

3.2.2.2 IS Experiments

In the IS reaction tests the heavy water vapour is fed in the reactor lumen together with a carrier gas (He) while the shell side is flushed with hydrogen whose pressure (about 3-6 kPa) is regulated by means of a needle valve upstream the vacuum pump. The reaction, enhanced by the catalyst, is an isotopic exchange between the deuterium and the hydrogen as shown in the formula (26).

$$D_2O + H_2 \leftrightarrow H_2O + D_2 \qquad (26)$$

On the retentate side, the condenser separates the water from the He carrier; water is gathered at the end of each test through the V8 valve in a phial, for Infrared analysis.

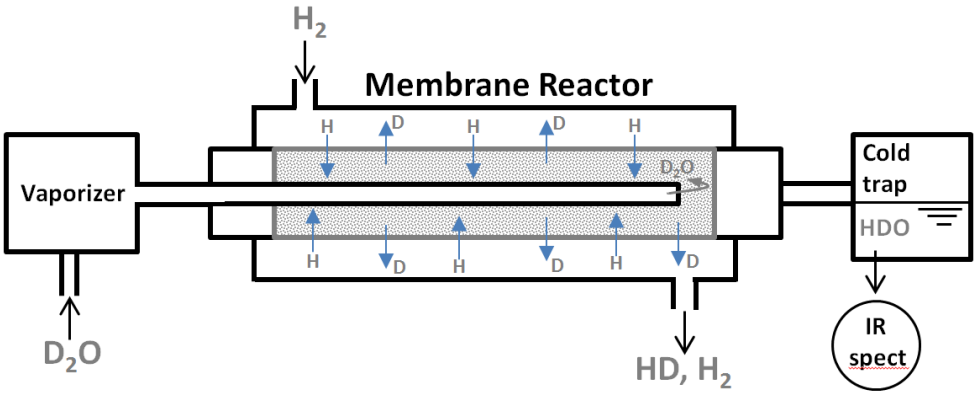

Figure 38 Scheme of the IS operation in thee CMR

In case of IS reactions, a small amount of He has been also send as carrier gas (0.08 mol h^{-1} equivalent to 30 sccm), while in WGS reaction tests, the CO itself worked as a carrier.

Table 9. List of IS experiments (Pshell ~10 kPa)

H_2/D_2O swamping ratio	D_2O, mol h^{-1} (g h^{-1})	H_{2shell}, mol h^{-1} (sccm)	$T_{reactor}$, K	P_{lumen}, kPa
~1	0.25 (5)	0.25 (93)	573-623-673	100-200-300-400-500
~2	0.25 (5)	0.50 (186)	673	200
~4	0.25 (5)	1 (372)	673	200

At the end of each experiment, a sample of the retentate stream is collected for post-analysis. In case of IS tests, the condensed water of the retentate consisting of a mixture of heavy and light water is analyzed to assess the D_2O/H_2O composition, through the FTIR analysis that measures the bending and stretching signal of the OD bond. A calibration of the Infrared spectrometer SHIMADZU IRAffinity-1S has been performed by testing the O-D stretching (at about 2500 cm^{-1} wavenumber frequency) and bending signal (at about 1200 cm^{-1}wavnumberfrequency) in different mixture of H_2O / D_2O. The calibration has been performed by preparing several vials with a known H_2O/D_2O concentration as shown in Table 10.

Table 10. Calibration Sample of the FTIR spectrometer

FTIR Calibration Samples			
#	D_2O concentration [%]	H_20 [g]	D_20 [g]
1	0.00%	1.032	-
2	10.00%	0.900	0.100
3	30.01%	0.702	0.301
4	50.00%	0.504	0.504
5	75.12%	0.250	0.755
6	90.09%	0.100	0.909
7	99.99%	-	1.024

As reported in [124–126] the FTIR calibration has been done considering the O-D bond (O-D stretching mode) quantified according to the intensity of the peak at 2490 cm^{-1}. Figure 39 reports the calibration results of the SHIMADZU IRAffinity-1S.

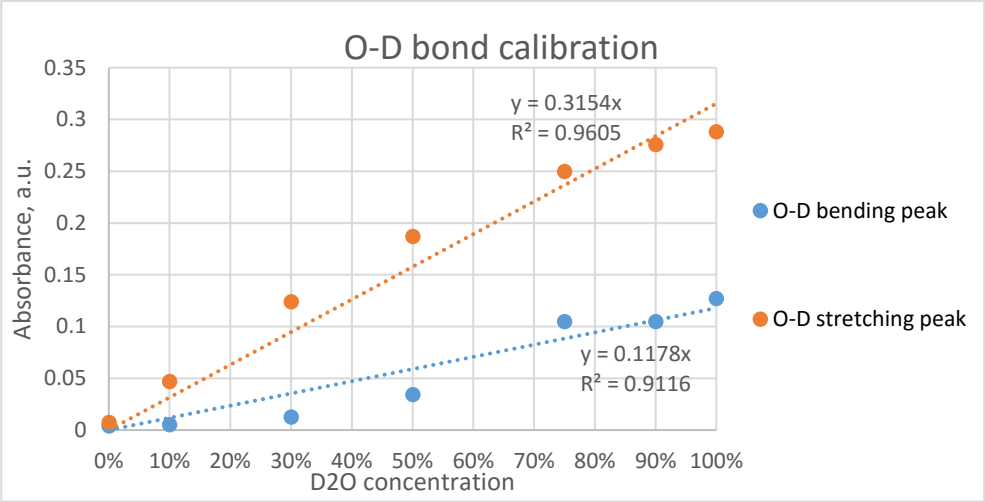

Figure 39. Calibration straight lines of the O-D bond in FTIR spectrometer

In particular, the bending and stretching peaks have been taken into account for the calibration. Due to the higher value in the regression coefficient, the O-D stretching straight line has been selected for the calibration and evaluation of the decontamination factor in IS tests.

3.2.2.3 Catalysts

The performance of the WGS and IS, as well as the formation of undesired by-products, mainly depends on the catalyst used inside the CMR.

Focusing on the experiments of this work, two different catalysts have been tested for the WGS and IS reactions. In both cases, 16 g of catalyst have been filled inside the Pd-Ag membrane lumen. The first catalyst (CAT1) has been synthesized by the Instituto de Investigaciones en Catálisis y Petroquímica (FIQ, UNL-CONICET), Santa Fe, Argentina. It is in form of pellets with irregular dimensions (from 1x1x1 mm to 4x2x1mm). Its composition has been checked by using X-Ray Fluorescence analysis (XRF) (model Shimadzu-720): Pt (0.62 wt.%), SiO_2 (56.32 wt.%) and La_2O_3 (43.06 wt.%). The activation of this catalyst has been done in two steps: the first consisted in a thermal activation at 673 K (heating ramp of 1.5 K min^{-1}) in Ar atmosphere for 30 minutes; the second has been performed inside the membrane reactor in H_2 atmosphere at 673 K for 2 h.

CATALYSTS	
NAME	**CATALYSTS DESCRIPTION**
CAT1	➢ Non-commercial catalyst (synthesized by Instituto de Investigaciones en Catálisis y Petroquímica, Argentina) ➢ Pt (0.62 wt.%), SiO_2 (56.32 wt.%) and La_2O_3 (43.06 wt.%) ➢ pellets (from 1x1x1 mm to 4x2x1 mm) 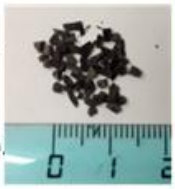
CAT2	➢ Commercial catalyst (produced by BASF) ➢ Pt-based dry unreduced catalyst (Pt 1 wt.% on alumina support, SP-01 T) ➢ pellet of 1.5 mm x 1.5 mm cylindrical shape 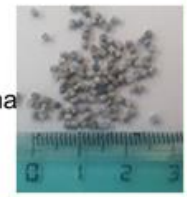

Figure 40. Catalysts used for the WGS and IS reactions

The second catalyst (CAT2) tested is a commercial one produced by BASF. It consists of a Pt-based dry unreduced catalyst (Pt 1 wt.% on alumina support, SP-01 T) in regular small pellets cylindrically shaped 1.5 mm x 1.5 mm. The activation has been performed by reducing it in the membrane reactor through flowing H_2 at 573K for about 2 h.

3.3 Experimental results

In this section, the results of the HyFraMe facility will be presented together with the main parameters for performances evaluation. In particular, permeation and reaction tests will be discussed separately.

3.3.1 Permeation results

Permeation tests aimed at measuring the ability of a Pd-Ag membrane in removing hydrogen from a He/H_2 gas stream have been carried out.

As already described in section 2.3.1 Hydrogen permeability in Pd-Ag membranes, the permeability of dense metal membrane is described by the Sieverts' law and the dependence of the permeability coefficient from the temperature is ruled by an Arrhenius-type behaviour:

$$Pe = \frac{J \times t}{\left(\sqrt{p_{lumen}} - \sqrt{p_{shell}}\right)} \qquad (27)$$

$$Pe = Pe_0 e^{-(E_a/RT)} \qquad (28)$$

Where:

- P_e is the hydrogen permeability (mol m^{-1} s^{-1} $Pa^{-0.5}$), t is the metal wall thickness (m)
- p_{lumen} and p_{shell} are the hydrogen partial pressure inside (upstream) and outside (downstream) the membrane
- Pe_0 the pre-exponential factor (mol m^{-1} s^{-1} $Pa^{-0.5}$, E_a the activation energy (J mol^{-1})
- R the gas constant (8.314 J mol^{-1} K^{-1}) and T the absolute temperature (K)

The permeability is calculated during the permeation experiments by knowing the membrane geometry, the hydrogen fed and recovered flows, the p_{lumen} and p_{shell}, according to (27).

Then by the linearization of (28), it is possible to assess the activation energy (E_a) and the pre-exponentional factor (P_{e0}) at different temperatures.

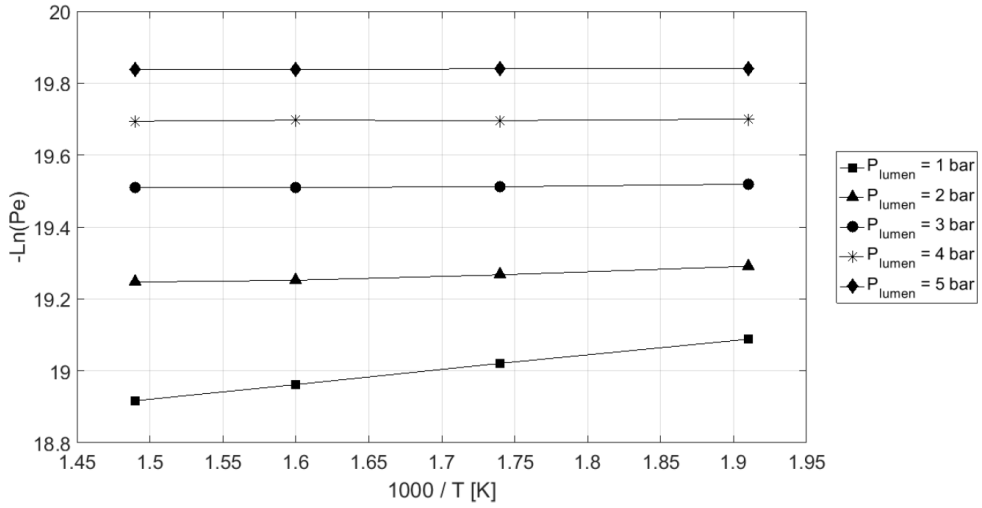

Figure 41. Measured permeability at different pressure conditions for He/H2=1

Figure 41 shows the dependence of the logarithm of permeability by the inverse of the temperature. The results are in agreement with the literature as shown in Table 11.

Table 11. Comparison of the permeability coefficient calculated in the HyFraMe membrane with the literature coefficient

Lumen pressure [bar**]**	**Thickness [µm]**	**E_a [kJ/mol]**	**Pe_0 [mol/(m*s*$Pa^{0.5}$)]**	**Feed flow**	**Reference**
1	113	3.365	1.11×10^{-8}	He/H_2=1 mix	This work
1	200	8.086	8.78×10^{-8}	Pure hydrogen	Literature
2	150	2.566	1.09×10^{-8}	Pure hydrogen	Literature
2	84	3.610	3.33×10^{-8}	Pure hydrogen	Literature

The literature presents a thorough dissertation of the effect of the membrane thickness and the surface effects on hydrogen permeability in Pd-Ag membranes [127, 128]. Accordingly, the influence of the pressure on the permeability observed in the tests can be explained by the surface effects which control the hydrogen mass transfer for thin-walled membranes (wall thickness < 200 µm). Furthermore, since the permeation test have been carried out with a H_2/He mixture instead of pure H_2, deviations from the Sieverts' law could be due to the mass transfer resistance through the gas film.

The results of the permeation tests are presented in term of:

- Hydrogen permeated in the shell, measured by $F_{SHELL\ OUT}$;
- Separation efficiency expressed as the ratio between the hydrogen separated in the shell and the one fed in the lumen:

$$\eta = \frac{F_{IN,H2}}{F_{SHELL\ OUT,H2}} \times 100 \qquad (29)$$

Both the parameters are important to identify the quantity of hydrogen that could be recovered and the efficiency of the process at different temperature, pressure and He/H_2 ratio.

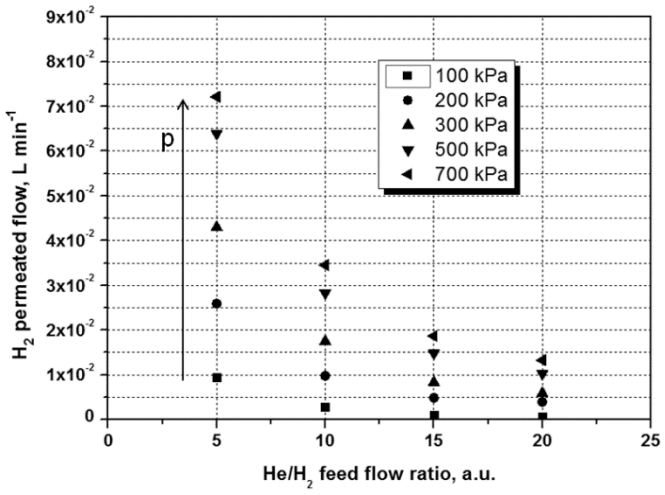

Figure 42. Hydrogen permeated flow for tests at 623 K (lumen pressure few kPa)

Figure 42 shows the results of the H_2 permeated in the permeation tests, at different pressure and feed molar ratio. The results show that by increasing the feed molar ratio the hydrogen permeated decrease significantly. This behaviour is expected in agreement with the literature. In fact, by increasing the feed ratio, the hydrogen partial pressure decreases, therefore decrease the pressure gradient between lumen and shell with a consequent performance drop. On the other hand, by increasing the lumen pressure, the permeated hydrogen is higher even though, moving on high feed ratios this gap become less appreciable.

Figure 43 reports the separation efficiency calculated in function of the feed flow ratio. Congruently with Figure 42, the separation efficiency rapidly decreases as the feed flow ratio increases (Figure 44)

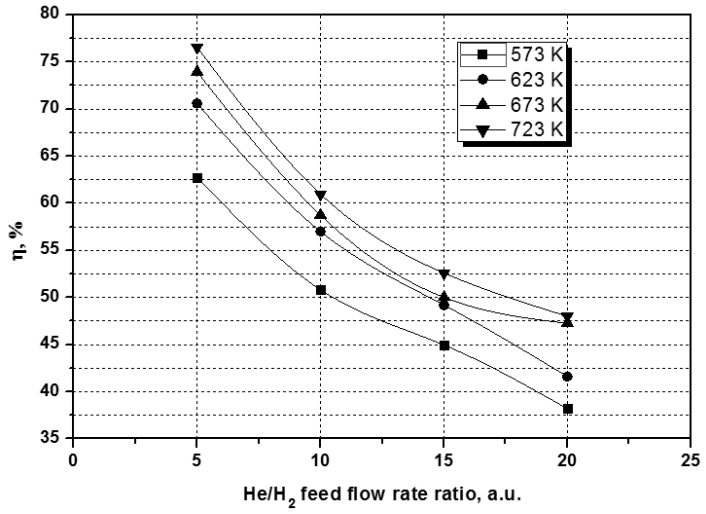

Figure 43. Efficiency (η) of hydrogen removal tests along He/H2 feed flow ratios for several reactor temperature at lumen pressure of 500 kPa (lumen pressure at about few kPa).

Figure 44 shows that the temperature does not significantly influence the efficiency at higher pressure (> 400kPa) while an appreciable influence is detected at lower pressure. In particular, according to the literature, the efficiency increases as well as the temperature increases.

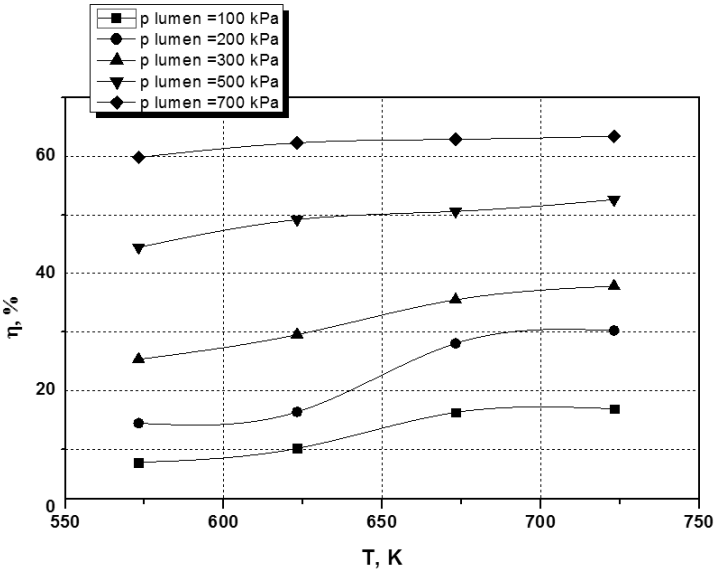

Figure 44. Efficiency (η) of hydrogen removal tests for the He/H2 feed flow rate ratio of 15 (lumen pressure at about few kPa).

3.3.2 Reaction results

The results of the reaction tests are expressed in terms of Decontamination Factor (DF). For the WGS tests, the DF_{WGS} has been calculated as the percentage molar ratio between the D_2 recovered in the shell side and the D_2O fed (30).

$$DF_{WGS} = \frac{D_{2\,Fshellout}}{D_{D2O}} \times 100 \qquad (30)$$

Where DF_{WGS} is the decontamination factor in WGS experiments (%), $D_{2Fshellout}$ is the flow rate of deuterium collected in the shell side (mol h^{-1}) and D_{D2O} is the heavy water feed flow rate (mol h^{-1}).

In the IS experiments, the decontamination factor has been assessed by performing IR spectroscopy of the water fed into the reactor and collected in the retentate side (4).

$$DF_{IS} = 1 - \frac{O - D_{retentate}}{O - D_{in}} \times 100 \qquad (31)$$

Where O-D is the intensity of the IR spectrum at 2490 cm^{-1} (O-D stretching mode) of the water collected in the retentate side ($O\text{-}D_{retentate}$) and of the water fed in the reactor ($O\text{-}D_{in}$).

3.3.2.1 WGS results

Figure 45 shows the results of the WGS tests carried out with the catalysts CAT1 (on the left) and CAT2 (on the right). All the results are reported in terms of DF vs. pressure and temperature. Looking at CAT 1 results, by increasing the temperature of the reactor from 573 to 623 K, the DF_{WGS} factor considerably increases (more than 10 percentage points) while, at higher temperature (from 623 K to 673 K) there is not an appreciable difference in term of decontamination capability. Otherwise, the temperature does not affect significantly the CAT2 performance.

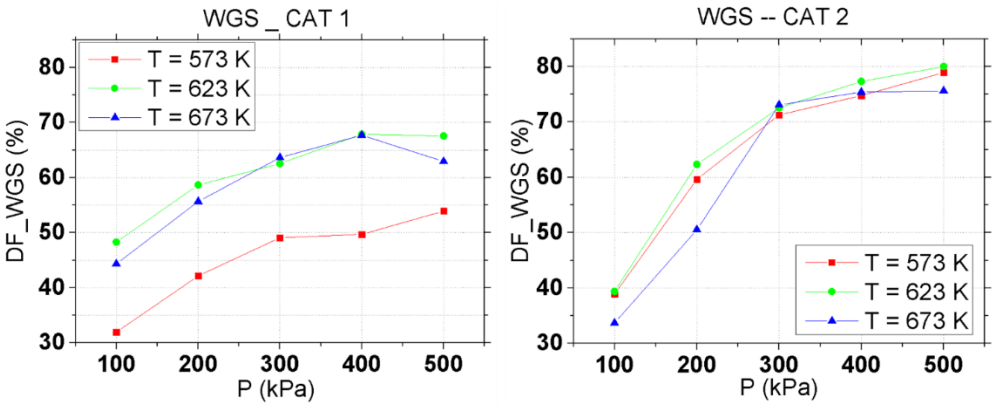

Figure 45. WGS results for CAT1 (on the left) and CAT2 (on the right) at different lumen pressure (100-500 kPa) and reactor temperature (573-673K), constant CO/D2O feeding molar ratio equal to 1.

This result is reasonably coherent with literature because the DF_{WGS} is influenced by both the hydrogen formation and its permeation through the membrane. The permeation is enhanced at high temperature while the WGS reaction, and then the hydrogen production, is promoted at lower temperature. Then it is reasonable that at 623 K there is the best balance between the membrane permeation and WGS reaction yield. In general, the DF factor increases by raising the lumen pressure.

Concerning the CAT2, the performances are a little bit lower at low pressure (between 33% and 39% at 100 kPa), while they are higher between 300 kPa and 500 kPa (between 71%-73% at 300 kPa and 75%-80% at 500 kPa) compared to CAT1 performances. Otherwise, the temperature affects very modestly the DF_{WGS} when using the CAT2.

As known by literature, the most critical drawback of the WGS is the methane formation. Especially in the fusion fuel cycle processes, the methane production must be seriously avoided. This could be done by adopting specialized catalysts that are methane hinder and by operating in particular conditions of pressure and temperature. The Figure 46 (left side) collects all simulations performed with AsTher; these give indication about the operational field in which operate in order to reach low methane formation. The simulations suggest operating at low pressure and temperature. It is mandatory to clarify that AsTher calculates the methane production under thermodynamic equilibrium; these simulations are therefore far from the test conditions because the membrane reactor operates in a non- equilibrium conditions because of the continuous hydrogen removal through the membrane.

Figure 46 qualitatively compares the performance, in terms of methane formation, calculated for a traditional reactor under thermodynamic equilibrium (left) and the

experimental results of the CMR (right). The thermodynamic analysis can provide some guidance concerning the feasibility of secondary reactions, in particular those which lead to the methane formation from CO and CO_2:

$$CO + 3H_2 \leftrightarrow CH_4 + H_2O \qquad (32)$$

$$CO_2 + 4H_2 \leftrightarrow CH_4 + 2H_2O \qquad (33)$$

In traditional reactors, thermodynamically the methane yield increases vs. the pressure (see reactions $CO+3H2\leftrightarrow CH_4 + H_2O$ (32) and $CO_2 + 4H_2 \leftrightarrow CH_4 + 2H_2O$ (33)). Differently, in a membrane reactor with the increase of the pressure more hydrogen permeates thus extracting one of the reactants: this induces a right-shifting effect in the methanation reactions ($CO+3H2\leftrightarrow CH_4 + H_2O$ (32) and $CO_2 + 4H_2 \leftrightarrow CH_4 + 2H_2O$ (33)).

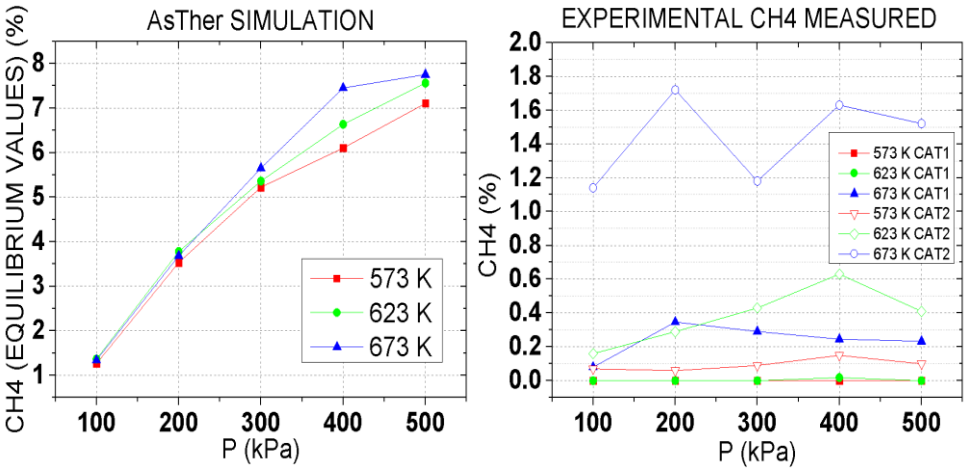

Figure 46. On the left: results (CH4, mol.%) of AsTher simulation at different pressures and temperatures. On the right: CH4 (mol.%) amount in the retentate stream of the WGS experiment for both catalysts at different temperatures and pressures.

In fact, according to (25), the membrane provides a selective removal of one of the products (deuterium in this case), so that the reaction equilibrium is continually shifted to increase the product formation. In previous works [129], the feed gas stream has been assumed to be continuously at equilibrium throughout the membrane reactor which means that the WGS reaction is not limited by chemical kinetics and the experiments demonstrates that the reaction conversion closely approaches the theoretical maximum values. In particular, such an assumption can be validated in the present work for the catalyst CAT1, which has been previously tested in a similar Pd-membrane tube [130].

Anyway, both catalysts demonstrate very good performances in term of methane production (Figure 46 right). In particular, it is important to underline that using the non-commercial catalyst (CAT1) the methane production at 573 K and 623 K is below the GC detection limit, while by increasing the temperature to 673 K, the methane production reaches its maximum value at 200 kPa (0.35%). Regarding the CAT2, a higher methane production has been measured but always less than 1% at 573 K and 623 K while it reaches the maximum value of 1.72% at 673 K and 200 kPa.

Lastly, the influence of the feeding molar ratio (D_2O/CO) on the decontamination factor has been investigated. It was evident that the CAT2 DF_{WGS} was always higher.

3.3.2.2 IS results

Differently from the WGS experiments, the IS performances (Figure 47) seem to be not considerably influenced by the lumen pressure, especially in the CAT2 tests. Otherwise, the temperature is clearly one of the crucial parameter for the DF_{IS} that increases at the higher temperatures when the hydrogen isotopes permeability is maximum. For CAT2, by increasing the temperature from 573 K to 673 K, the DF_{IS} raise of 8-10 percentage points, while, in the CAT1 tests at 100 kPa, the performances are rather similar. Considering the same increasing of temperature from 573 K to 673 K at 300 kPa, the values of the DF_{IS} vary between 38% and 43% for the CAT1 and between 28% and 42% for the CAT2. This demonstrates that the CAT1 is more suitable for IS reaction than the CAT2 especially at low temperatures and pressures. Several tests at different H_2/D_2O swamping ratio have been carried out as shown in the Figure 48.Both catalysts show the same trend even though the CAT1 has the best performances in all cases. As expected, the DF increases by working with an excess of swamping hydrogen.

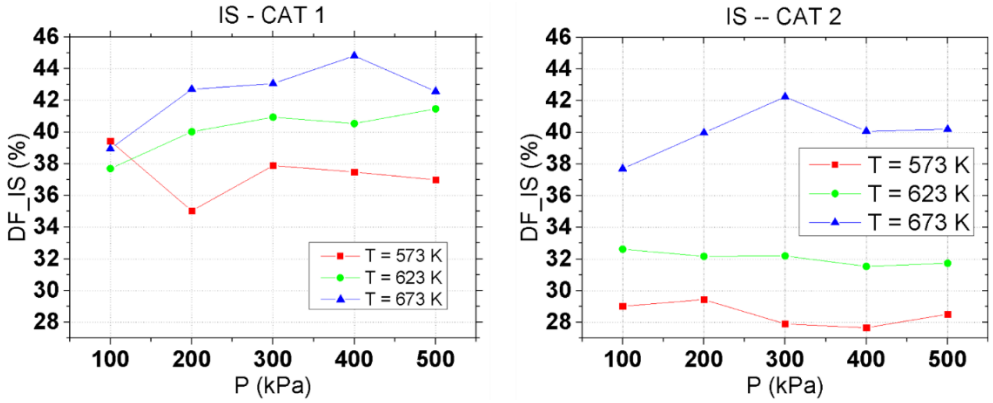

Figure 47. IS results for CAT1 (on the left) and CAT2 (on the right) at different pressure (100-500 kPa) and temperature (573-673K), at constant H2/D2O swamping ratio of 1 and shell pressure of 10 kPa.

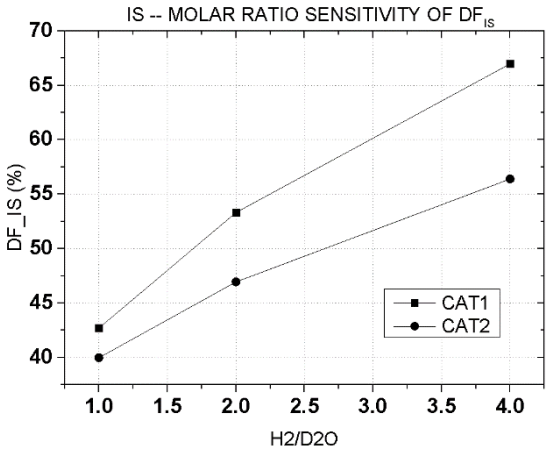

Figure 48. Experimental result and comparison of IS reaction for both catalyst at T = 673 K, P = 200 kPa at different H2/D2O swamping ratios.

In general, in both the tested catalysts there is an increasing of the decontamination factor of 8-percentage points, at least, by doubling the hydrogen swamping molar flow rate and 16-percentage points, by increasing by four times the hydrogen-swamping ratio.

3.4 Discussion results

The permeation tests in Hyframe facility confirm that, at high He/H_2 feed flow ratio, the separation capability dramatically decreases. Therefore, in case of the HCPB in which the feed flow ratio is high, a pre-concentration stage is necessary to reduce the He/H_2 feed flow ratio. The reaction results clearly show that both the catalysts tested reach good performances in WGS and, especially, low methane formation.

In fact, the WGS is characterized by a higher reaction rate and it is easier to set up. In a membrane reactor it allows to directly separates hydrogen isotopes from water. Nevertheless the most affecting drawback is the by-products formation, in particular tritiated methane, which should be completely avoided because of safety reasons and the difficulty to separate tritium from methane. In this view, the WGS is not a "clean" reaction even though, in this work, it is esperimentally proved that by adopting specific catalysts, the by-product formation may be minimised and perhaps avoided. The presence of methane between the products of the WGS reaction indicates that a catalyst with higher selectivity is required.

Regarding the methane formation in WGS, by using CAT1 in all the experiments performed, the measured methane was always under the 0.40 mol.%. At 573 K and 623 K, the methane production is under the detection limit of the micro-GC analyser. Anyway, with CAT2 the amount of methane produced is barely appreciable (at maximum 1.72 mol.% of methane was measured at 673 K and 400 kPa). On the other hand, the DF_{WGS} using CAT1 is lower than CAT2 experiments. The DF_{WGS} reaches values above 80% at 623 K, 500 kPa.

On the other hand the IS is a "cleaner" reaction because no by-products occur. Nevertheless, operations with IS in membrane reactors have, as output, a current of hydrogen isotopes extracted from water diluited in a huge amount of hydrogen. This ouput may significantly overload the ISS in which the tritium should be separated afterwards. Additionally the ISS has lower decontamination perfomances than WGS, therefore, in order to reach high recover efficiency, membrane multi-stages could be necessary.

In the IS experiments, the DF_{IS} (CAT1) is about 67% and 43% with a swamping ratio $H_2/D_2O=4$ and $H_2/D_2O=1$, respectively. The best value for CAT2 is 56% ($H_2/D_2O=4$) against 39.98% ($H_2/D_2O=1$). These values were measured at 673 K at 200 kPa.

In practice, although the operation at higher pressure increases the promotion of decontamination capability, feasibility and safety reasons suggest to work at low pressure (around 100-200 kPa). It is noteworthy that increasing the H_2/D_2O swamping ratio, better decontamination performances can be achieved but a deeper and more expensive isotopic separation of T_2 from H_2 will be needed.
Focusing on the application of this technology in the HCPB breeding blanket, one of the issue is to understand if, by adopting the WGS reaction, the methane produced

is tolerable for the further processing. In such a case, the WGS can be preferred because of its higher DF values.
In conclusion, in view of a DEMO HCPB breeding blanket, the HyFraMe facility have demonstrated that a preconcentration stage is necessary in order to operate an efficient separation of molecular hydrogen isotopes. Regarding the water decontamination the CAT1 could be suitable to perform the WGS because of the almost absence of methane formation. In general both reactions have demonstrated their efficient applicability in water decontamination. The single-tube membrane reactor tested in this work (diameter 10 mm and length 500 mm) could be suitable to recover the tritium from the DEMO HCPB by considering a DF of 40% at ambient pressure and 623 K.

A further step is to test a middle-scale multi-tube membrane reactor in order to assess the scalability of those results in view of DEMO operation. The next chapter is dedicated to the design and commissioning of a middle scale multi-tube membrane reactor.

4. Mechanical design and commissioning of a middle-scale multi-tube membrane reactor

The main purpose of the work is to test the ability of a membrane reactor in hydrogen isotopes (both Q_2 and Q_2O) recovery from a He flow. The tests with the single-tube reactor have been performed only on binary gas mixture containing or He-Q_2 or He-Q_2O as described in Chapter 5, however, as already described in the chapter 4, one of the expected scenario foresees the treatment of the ternary gas mixture containing He-Q_2-Q_2O. To perform experiments with this real scenario, it is necessary to manufacture a multi-tube reactor because the amount of water contained in the gas mixture is too small to be accurately measured and controlled by using a single tube reactor. Moreover, the scale-up of the reactor represents a useful opportunity to assess the scalability of membrane performances in hydrogen separation and reaction.

The following paragraphs provide the description of the multi-tube mechanical design, the layout of the new experimental facility, so called Middle-Scale Membrane Reactor (MeSMeR), the commissioning of the facility and the foreseen experimental plan.

4.1 Preliminary design of the multi-tube membrane reactor

The membrane diffuser has been studied by a simplified model based on the mass transfer mechanisms (solubilization, diffusion and permeation) of the hydrogen into the Pd-alloy metal lattice. The temperature influences the permeation coefficient Pe following an Arrhenius-like trend. The hydrogen permeability values of Pd-Ag membranes at different temperatures have been taken from literature [98].

The expression (20) shows that, by increasing the partial pressure of the hydrogen isotopes, the permeation flow rate increases thus involving a higher separation efficiency and minimizing the membrane area. Accordingly, the pre-concentration stage of the He stream coming from the blanket allows the design of the Pd-Ag separator to be optimized through a significant reduction of the membrane module dimensions.

In order to take in account the pressure depletion due to hydrogen permeation, a code developed by ENEA has been used[131]. That model simulates both Pd-membrane and membrane reactors for tritium recovery in the applications of the fusion fuel cycle. The membrane device (both Pd-Ag tube and shell module) is divided in finite elements in each of them the mass balances are performed taking into account the permeation and reaction kinetics. In particular, the permeation of the hydrogen isotopes considers surface reactions together with the diffusion through the metal bulk. The presence of surface reactions reduces the driving force of the permeation by reducing the hydrogen pressure upstream and increasing the hydrogen partial pressure downstream .

$$J = P_e \frac{\left[\left(-\frac{J}{K_{af}}+p_{hf}\right)^{\frac{1}{2}} - \left(\frac{J}{K_{as}}+p_{hs}\right)^{\frac{1}{2}}\right]}{d} \qquad (34)$$

Such equation is in implicit form and, thus, it is numerically solved by the simulation code. The model takes in account also the effect of the isotopic competition.

The model requires, as input data, the feed gas properties (flow rate, pressure and composition), the geometry of the tubes (diameter, length and thickness) and the operating temperature.

Based on the mass balances of the TES system, the flow rate and the composition of the stream feeding the membrane diffuser have been calculated.

Through the simulation, the influence of the operating parameters on the design of the membrane unit has been assessed. Particularly, the required membrane surface, under several operating conditions, has been evaluated, for different tubes geometries. The membrane area required vs. the tube thickness is reported in Table 12 where a linear relationship between these parameters is showed. Once defined the overall permeation area the diameter and the length of the tubes can be fixed.

Table 12 Permeation area required for different thicknesses of the membrane tubes at 623 K.

Thickness [m]	Area [m^2]
5.00×10^{-5}	1.43
1.00×10^{-5}	2.85
1.50×10^{-5}	4.28

The Figures 49, 50 and 51 show the behaviour of the membrane surface area vs. the lumen pressure, the He*/He ratio and the shell (permeate) pressure, respectively. This analysis demonstrates that operating at 1 MPa there is no significant difference in the membrane area by changing the temperature in the range 623-673 K (Figure 49). All the simulations has been performed considering a feed flow rate of 10000 $Nm^3\ h^{-1}$. Based on these considerations, the membrane unit design has been figured out at 1 MPa and 623 K with a membrane area of about 3 m^2.

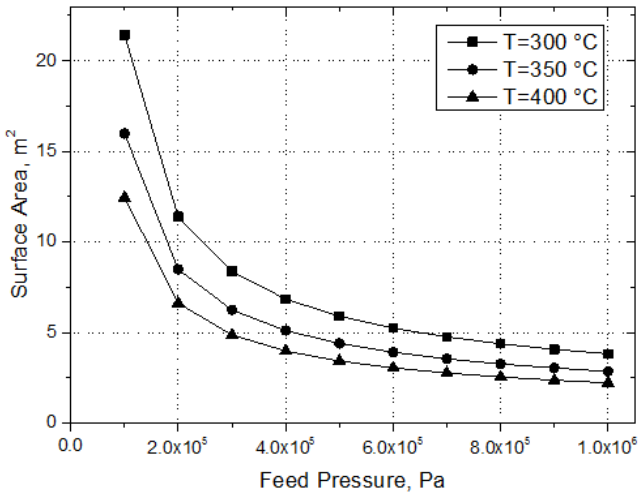

Figure 49 Membrane surface area vs. the lumen pressure at different temperatures with a shell (permeate) pressure of 5 kPa.

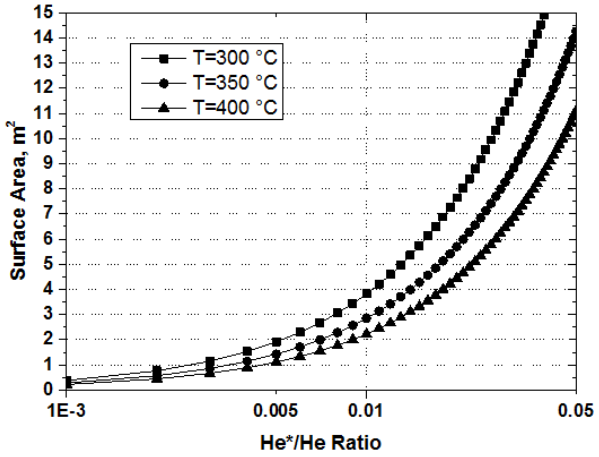

Figure 50 Membrane surface area vs. the He/T feed ratio at different temperatures and 1 MPa of lumen pressure and 5 kPa of shell pressure.

Figure 50 shows that the surface area is dramatically affected by the He*/He ratio. In particular, moving over value of 0.01, the one adopted in the design, small increases of He*/He significantly increases the permeation area.

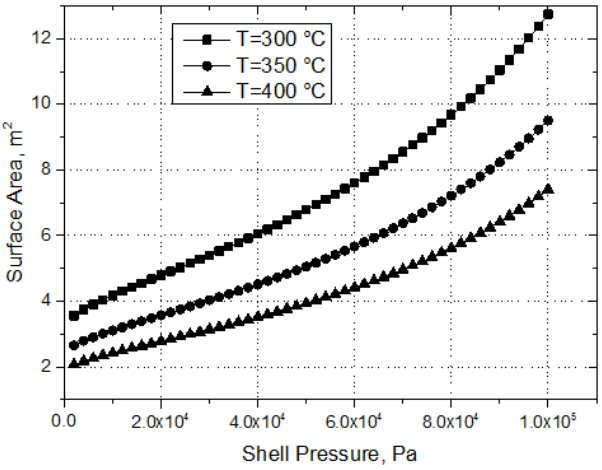

Figure 51 Membrane surface area vs. the shell (permeate) pressure at different temperatures and 1 MPa of lumen pressure.

To investigate the influence of p_{shell} on the surface area, a sensitivity analysis has been reported in Figure 51. It shows that by decreasing the shell pressure, the surface area significantly decreases, keeping constant all other parameters, until to 4000 Pa. Successively, under 4000 Pa, the decrease of the membrane surface is less appreciable. In this analysis, p_{shell} was assumed to be 5000 Pa.

The wall thickness has been fixed by verifying that the mechanical stress would be acceptable for the mechanical resistance of the membrane material. Figure 6 shows the mechanical stress vs. the membrane tube thickness for different diameters: the value of the maximum stress achievable (max tensile stress) is also reported in

the graph for comparison. Such a value has been calculated by applying a safety factor 5 to the ultimate tensile strength of the Pd alloy (380 MPa at 673 K) [132]. Under the operating conditions above established, the Figure 52 reports that a membrane tube of thickness of 0.100 mm and diameter of 10 mm complies with the stress criteria.

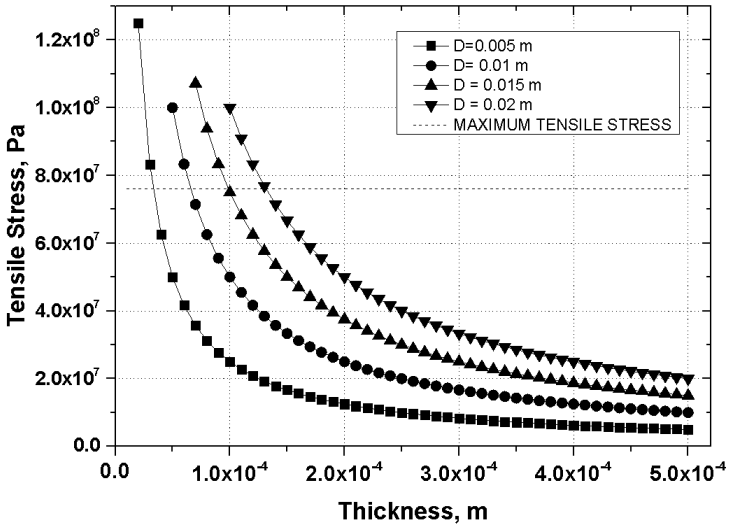

Figure 52 Tensile stress values vs. the membrane thickness for different tube diameter at 623 K and 1 MPa lumen pressure

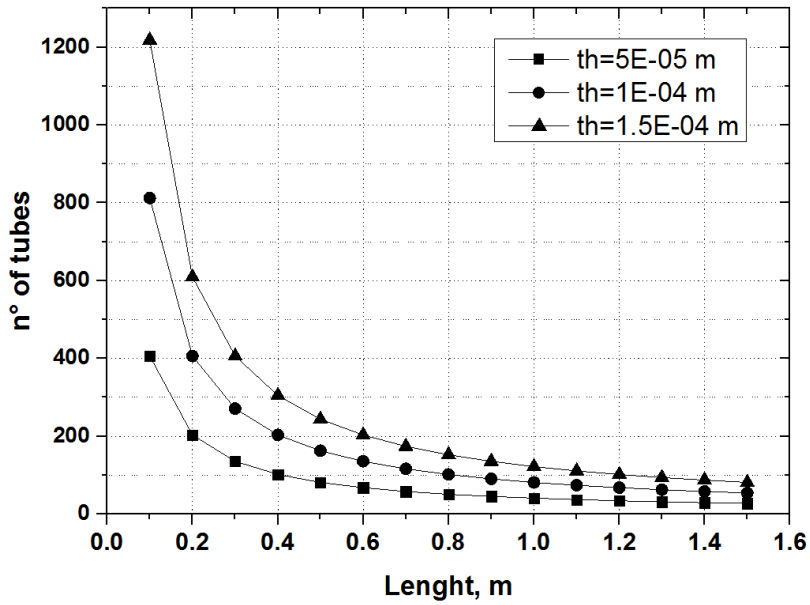

Figure 53 Number of tubes vs. the length for different thickness values at 623 K, 1 MPa pressure and tube of 10 mm diameter.

Once calculated the surface area, the number of tubes can be assessed by considering the effects of the geometric parameters (i.e. tube length) as reported by

the Figure 53. By optimizing the membrane tubes geometry through the criterion of the mechanical resistance, each membrane tube should have a diameter of 10 mm, a length of 500 mm and a thickness of 0.1 mm. This means that 180 Pd-Ag tubes will be required for the membrane module therefore, the new middle-scale multi-tube membrane reactor has been equipped with 10 tubes in order to assess the configuration technologies and test the performances in hydrogen separation and reaction.

4.2 Description of the multi-tube reactor module

The multi-tube reactor which is composed of 10 Pd-Ag (23 wt.%) tubes (lumen side), a cylinder (shell side), several Swagelok/VCR connections, CF flange and valves. It consists in 2 membrane modules which are equipped with 5 membranes each, as shown in Figure 54 right, inserted in the Cylinder (the shell). Every membrane module is equipped with

- 5 Swagelok Short weld gland ¼”
- 1 CF100 fixed tapped Flange
- 5 DN 10 VCR welding connectors
- 5 Female nuts VCR ¼”
- 5 manufactured Tee-VCR 1/4
- 5 M7 Grab screws
- 5 Vespel cones
- 5 DN10 Swagelok cups

The geometrical characteristics of the Pd-Ag tubes inside the reactor are reported in Table 13 with a total permeating area of about 0.16 m^2 (exact value 160131.5534 mm^2).

Table 13. Geometry of the Pd-Ag membranes assembled in the multi-tube.

Membrane #	**Geometry**		
	L (mm)	**ID (mm)**	**Th (µm)**
1	510	9.99	120
2	507	10.13	110
3	507	10.01	110
4	509	10.00	120
5	512	10.05	113
6	508	9.95	115
7	505	9.97	105

8	508	9.95	115
9	510	10.10	118
10	513	10.06	130

The 10 Pd-Ag tubes are assembled according with a finger-like configuration to avoid the membranes damage during the thermal and hydrogenation cycles.

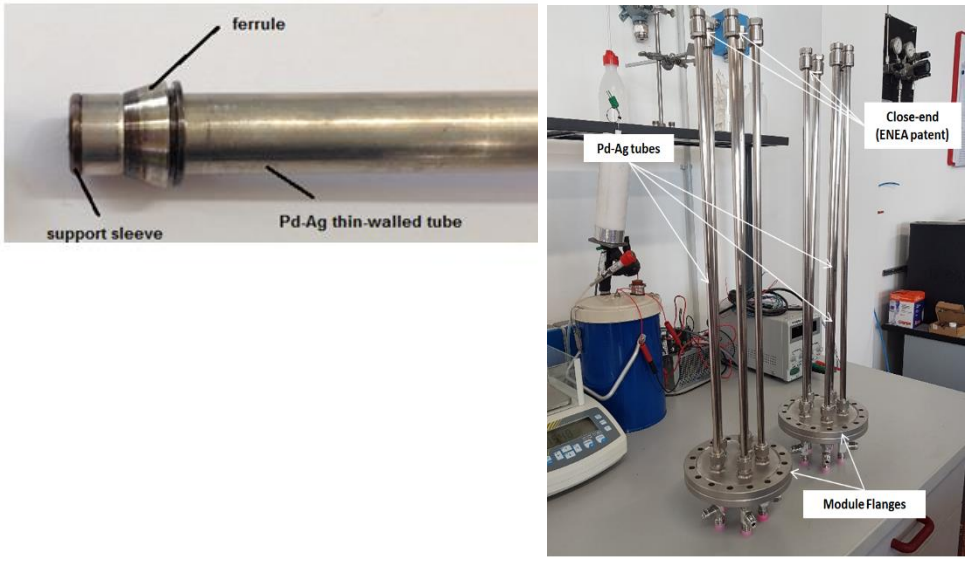

Figure 54. Detail of the Pd-Ag tube connections (left side), picture of the 10 Pd-Ag membranes connected at the two flanges.

The Pd-Ag tubes connections have been realized by commercial compression tube fittings adapted by using special inserts or support sleeves that avoid the collapse of the thin-walled tube. Figure 54 left provides a detail of the Pd-Ag tube connection while, at the right side, shows all the Pd-Ag tubes connected at the two flanges.

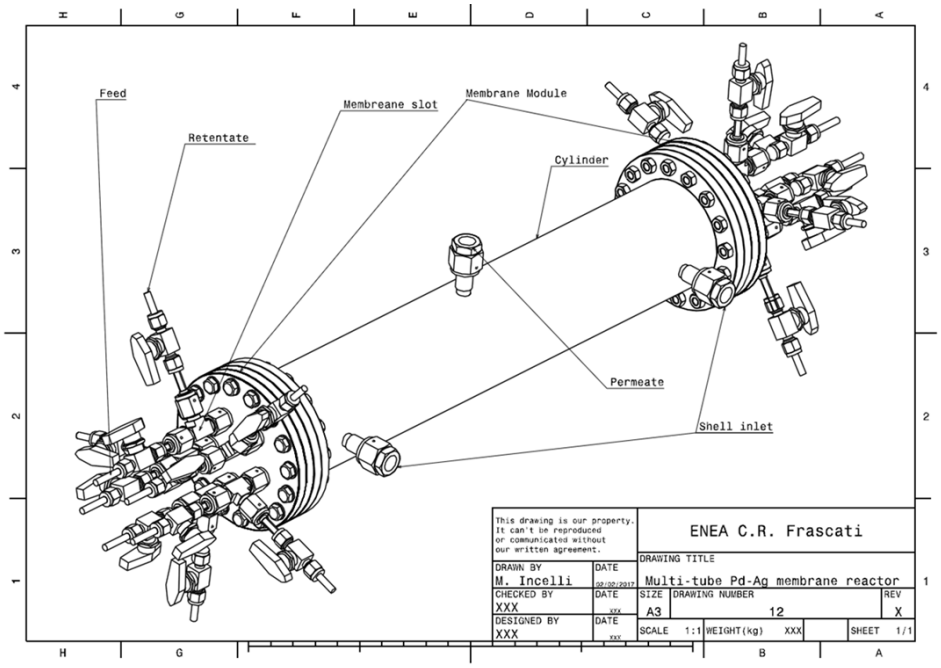

Figure 55. Technical drawing of the multi-tube membrane module.

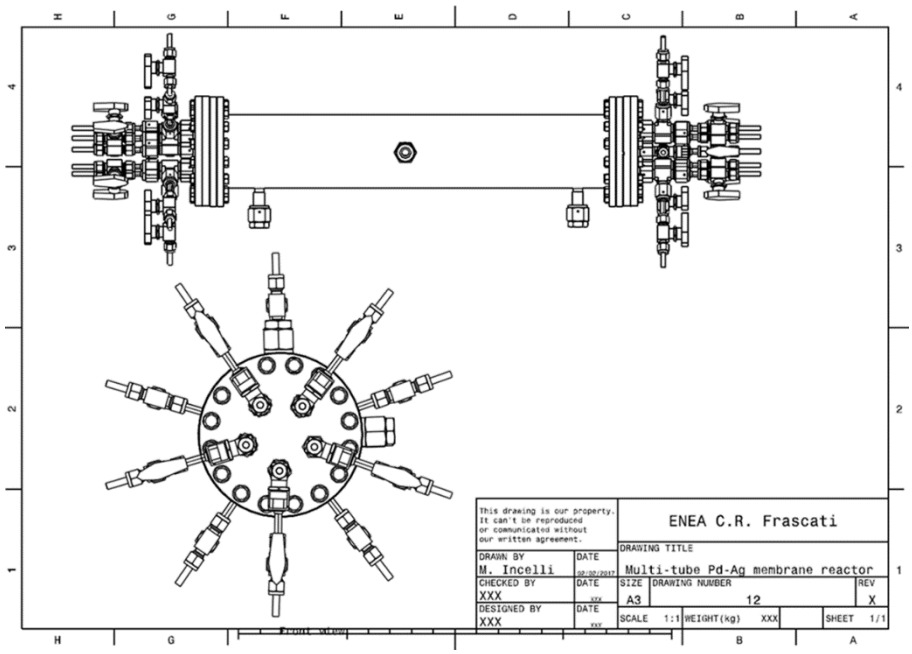

Figure 56. Technical drawing of the multi-tube membrane module: particular of one flange with the 5 Pd-Ag tubes.

Figure 55 and Figure 56 shows the Catia Drawings of the multi-tube membrane reactor. The modules are assembled in the cilynder in a very compact configuration. The cylinder has an internal diameter of 98 mm and a length of 574 mm. An electric heating resistance is installed on the shell surface and the insulation is filled between the resistance and the external cover. Figure 57 shows the assembled membrane module integrated with the heating and insulation system.

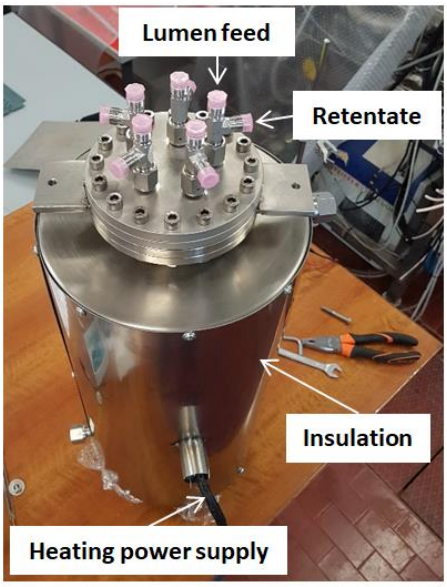

Figure 57. Picture of the assembled multi-tube membrane module.

In the outer part of the flanges each membrane is attached to custom Tee-connection which allows the gas feed and the retentate removal (see Figure 58). Obviously, the Tee-connections have been opportunely modified to avoid the mixing between the feed and the retentate gas stream. In the feed and in the retentate side of each Tee there is an on/off valve: the first allows to isolate the membrane in case of failure while, the second, avoids the mixing between retentate and permeate streams in case of membrane failure.

Figure 58. Picture of the Tee-connection attached to each membrane tube.

In general, welding have been performed following the GTAW (TIG) technique considering tolerances of 0.1 mm. The reactor is equipped with 4 K-type thermocouples three of which measure the temperature in equidistant points in the

central axes of the reactor at different height, in particular: T_{in} on the top side, T_{membr} in the middle and T_{out} in the far end, while the thermocouple T_{shell} measures the shell temperature (in the middle).

4.3 Layout of the new experimental facility Medium-Scaled Membrane Reactor (MeSMeR)

The multi-tube membrane reactor is integrated inside a dedicated facility called MeSMeR (Medium-Scale Membrane Reactor). The facility allows to control the gas and liquid flows rate by using mass flow controllers (MKS series), the lumen and shell pressure and the temperature of several components (i.e. reactor, evaporator, condenser, etc.). Table 14 provides the list and the technical specifications of the instrumentation installed in the facility.

Table 14. List of the instrumentation installed in MeSMeR.

Type of instrument	**Name**	**Model**	**Range**
Mass flow controller	F_IN1	MKS GE50A Elastomer-sealed Mass Flow Controller	0-5000 sccm
	F_IN2		0-5000 sccm
	F_IN3		0-1000 sccm
	F_CARRIER	MKS 1179B Elastomer-sealed Mass Flow Controller	0-20000 sccm
	F_SHELL OUT		0-20000 sccm
Baratron pressure sensor	P IN	722B Baratron®Compact Absolute Capacitance Manometer	0-10000 mbar
	P OUT		
	P SHELL		
Vacuum Pump	VACUUM PUMP	Adixen ACP15	n.a.

Figure 59 provides a simplified view of the MeSMeR facility while Figure 60 illustrates the CATIA drawing of the facility. A 3D layout has been realised in order to assess the volume of such facility (total dimension of about 630mm x 600mm x 1300mm).

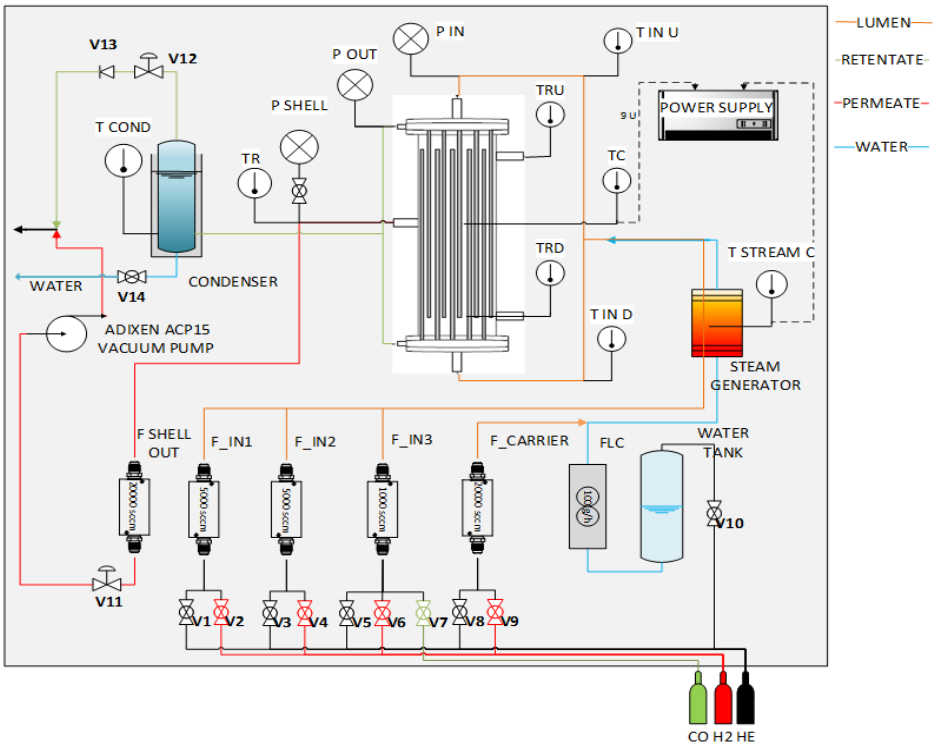

Figure 59. Simplified view of the MesMeR facility.

During the tests with the ternary mixture CO, H_2, He and D_2O (steam) are sent to the reactor by means of F_IN1, F_IN2, F_IN3 and FLC flowmeters at the desired flowrates. When the gas mixture reaches the multi-tube reactor, the hydrogen isotopes will be separated from He and water and collected in the shell side. By measuring the hydrogen flow rate leaving the shell ($F_{SHELL\ OUT}$), it will be possible to assess the decontamination factor of the membrane module. The retentate (i.e. not permeate) stream will be collected from each membranes and driven into a condenser for water removal. The composition of the dry retentate will be analysed by a GC; in fact the shell side is connected to a vacuum pump and the gas analysis will be performed by using a gas chromatographer (Agilent 7820A GC).

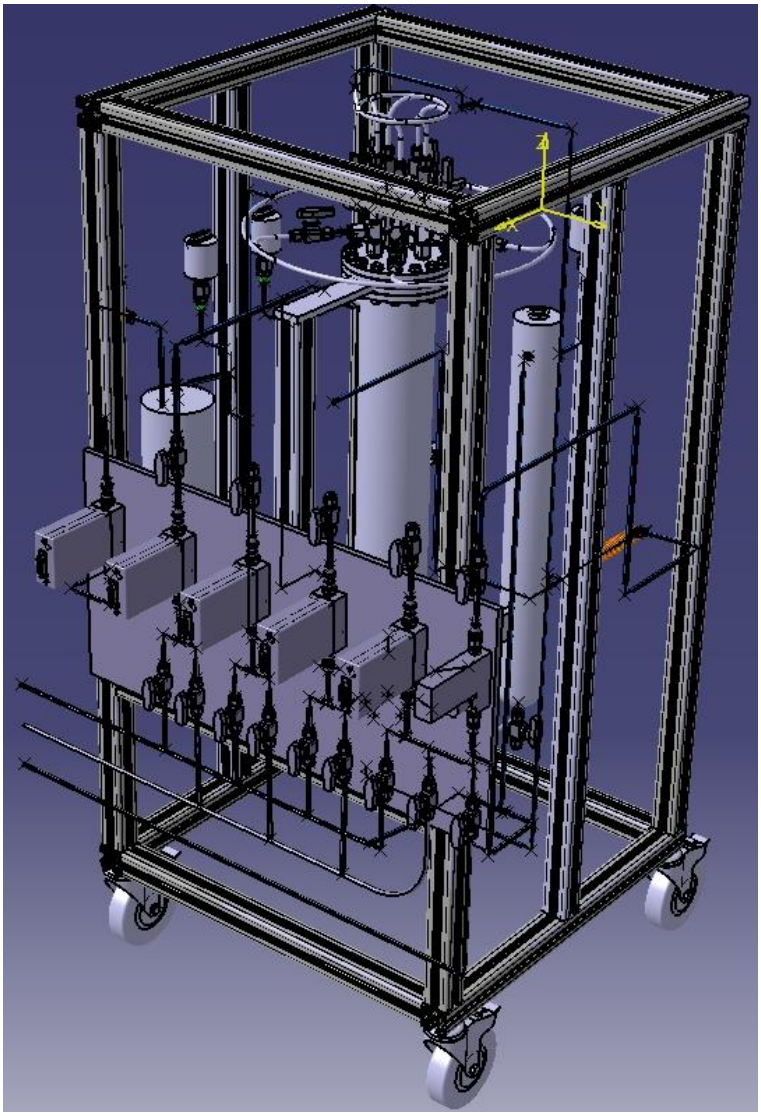

Figure 60. CATIA drawing of the MeSMeR facility.

The multi-tube membrane reactor and the instrumentations have been assembled on a structure made of Bosch profiles. Figure 61 illustrates a picture of the different components before their assembly: the leak tester (left side), the multi-tube reactor (middle) and the Bosch profiles (right side) with some instrumentation already installed.

Figure 61. Picture of the MeSMeR facility before assembly.

For its operation, the MeSMeR facility has to be served with dedicated gas lines, which are visible in Figure 62. The picture shows the assembled MeSMeR facility. The lower panel hosts the gas and liquid mass flow controllers and the water condenser. Each membrane is equipped with two valves: one in the feed side and one in the retentate side, for a total of 20 valves. In this way, several operations are possible: i) check the leak tightness of each membrane, ii) operate with different numbers of membranes, iii) isolate one membrane in case of failure. The three barometers allow to measure the gas pressure before entering the membrane, inside the lumen side and in the shell side. Several thermocouples (yellow cables) are placed in different parts of the facility, in particular in the two flanges and in the middle of the shell. The black box is the temperature controller unit, while the red one contains the National Instruments DAQ.

Figure 62. Picture of the MeSMeR facility.

4.4 Leak test of the multitube reactor

Before assembly the membranes modules inside the cylinder (shell side) it is very important to check the tightness of the membrane tubes. Therefore, a leak test has been performed by using a leak detector in sniffing mode in each membrane (see Figure 63).

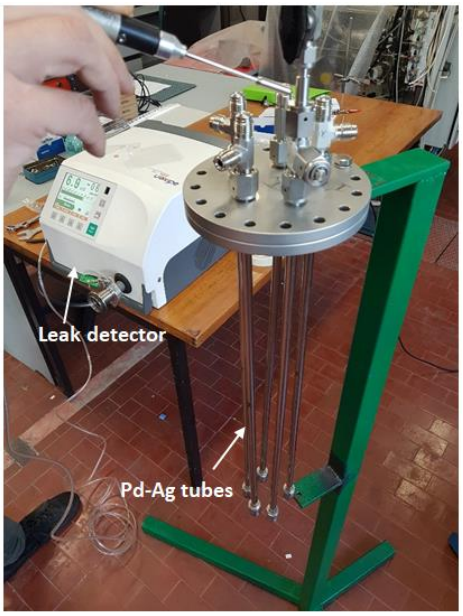

Figure 63. Picture during the leak test of the Pd-Ag membranes.

Particularly, the lumen of the membranes have been filled with helium at 5 bar, while the sniffer has been placed all along the membranes and in the connections. The mean values of the measured leaks for each membrane is reported in Table 15.

Table 15. Mean leakage value measured in each membrane.

Membrane	**Mean leakage value, mbar L/s**
1	7×10^{-6}
2	9×10^{-6}
3	9×10^{-6}
4	8×10^{-6}
5	7×10^{-6}
6	7×10^{-6}
7	8×10^{-6}
8	8×10^{-6}
9	7×10^{-6}
10	9×10^{-6}

After the leak test of the Pd-Ag tubes, the two flanges holding the 10 membranes have been fastened to the cylinder. In the outer part of the cylinder, there is the heating system and a layer of insulated material (see Figure 64, left side). The membrane module has been completed by connecting the tubes and the valves in the inlet and outlet side of each membrane (see Figure 64).

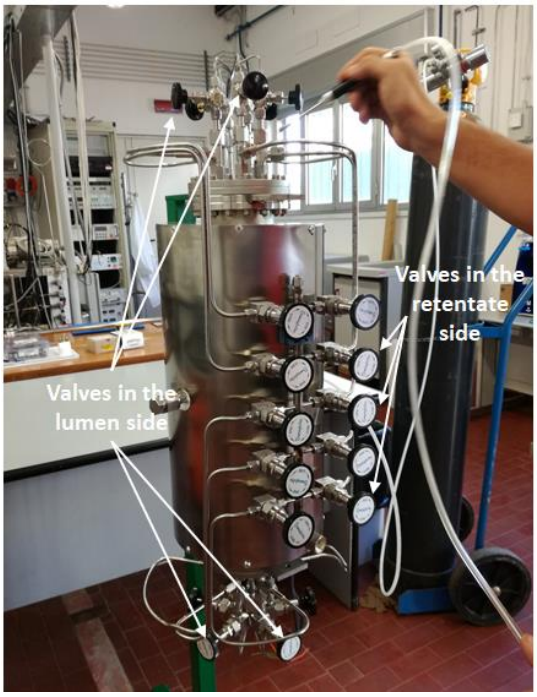

Figure 64. Picture of the membrane module.

4.5 Experimental schedule

During the commissioning phase the leak tight of the Pd-Ag membranes and of the shell module will be checked at room temperature and after several heating-cooling cycles. Then few He-H_2 permeation tests will be carried out to assess the permeation efficiency of the module and also the sealing behaviour under hydrogenation cycles. Finally tests with the ternary mixture will be performed. During such tests, the main objective is to assess the decontamination efficiency of the module and also the composition of the retentate stream. Particularly the conditions illustrated in Table 16 will be investigated.

Table 16. Experimental conditions for the tests with the ternary mixture.

He (~45 mol.%) – H_2 (~45 mol. %) H_2O (~ 10 mol.%).				
He, mol h^{-1} (sccm) [Nm^3 h^{-1}]	**H_2, mol h^{-1} (sccm) [Nm^3 h^{-1}]**	**H_2O, mol h^{-1} (g h^{-1}) [kg d^{-1}]**	**T reactor, K**	**P lumen, bar**
13.2 (5000) [0.3]	13.2 (5000) [0.3]	2.77 (50) [1.2]	573-623	2-3-4

He (~50 mol.%) – H_2 (~50 mol. %) H_2O (~1 mol.%).				
He, mol h^{-1} (sccm) [Nm^3 h^{-1}]	**H_2, mol h^{-1} (sccm) [Nm^3 h^{-1}]**	**H_2O, mol h^{-1} (g h^{-1}) [kg d^{-1}]**	**T reactor, K**	**P lumen, bar**
13.2 (5000) [0.3]	13.2 (5000) [0.3]	0.277 (5) [0.12]	573-623	2-3-4

4.6 Preliminary commissioning

After its assembly, the MeSMeR facility has been filled with helium to check its leak tightness with the leak test. Then few leak tests have been performed at high temperature (about 300 °C) and ambient temperature by pressurising the facility with helium and measuring the pressure drops vs. time with the baratron pressure sensors installed in the facility. The graphs in Figure 65 and Figure 66 illustrate the results of the leak tests performed at about 300 °C and at ambient temperature, respectively. In particular, the green and the red symbols indicate the pressure measured in the gas line and in the lumen side, while the blue symbols are the temperature measured by the thermocouples in the middle of the shell side. In the leak test at 300 °C, the pressure inside the entire facility was practically constant meaning that no leaks are present. With regard the test at ambient temperature, we can notice a very small decrease in the pressure values, which is fully justified by the decrease of the temperature.

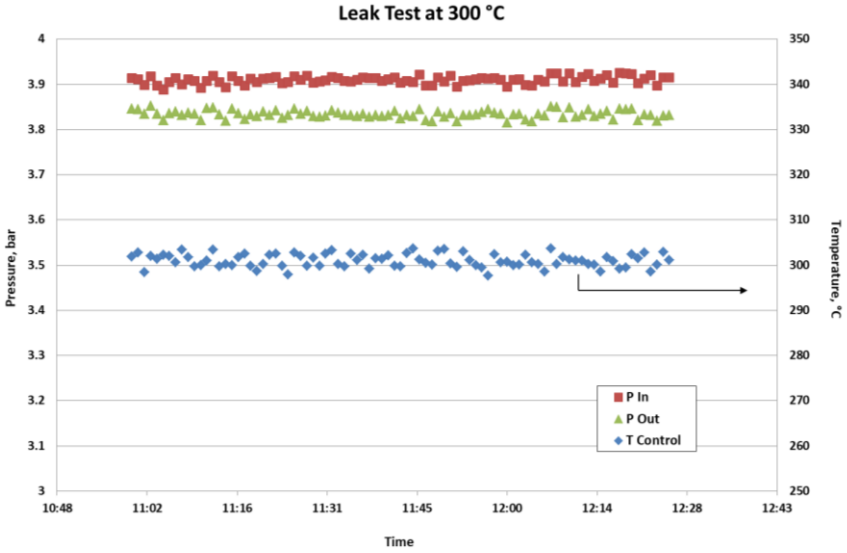

Figure 65. Results of the leak test on MesMeR performed at about 300 °C.

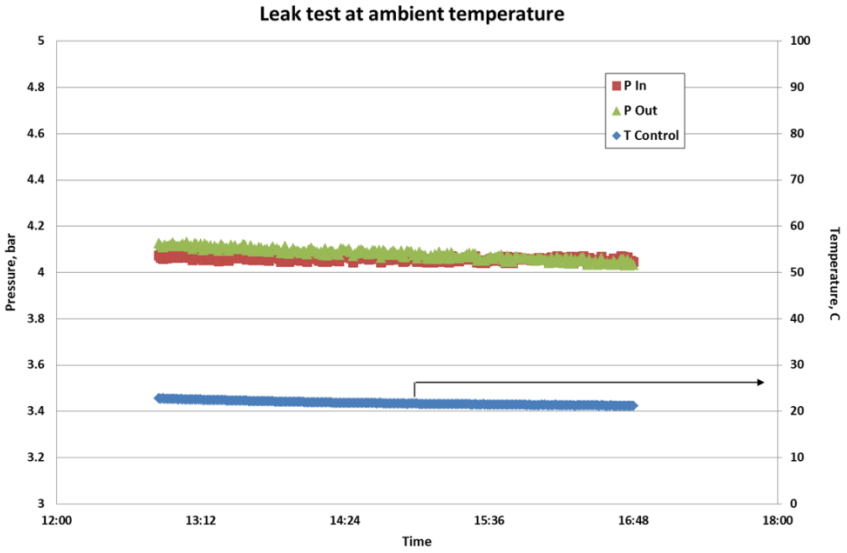

Figure 66. Results of the leak test on MesMeR performed at ambient pressure.

5. Conclusion and prospective

In this dissertation, permeation and reaction tests performed in several condition on a single Pd-Ag membrane reactor, in view of the next nuclear fusion fuel cycles, have been summarized and compared (Chapter 5). The experimental results have been performed to assess the feasibility of membrane technologies in tritium recovery system of the HCPB DEMO TERS. Tritium will be present in form of Q_2 or Q_2O. In order to recover tritium in both forms via Pd-Ag membrane technologies, permeation tests and reaction tests have been performed, respectively, in a single-tube membrane.

One of the results was that the low tritium content in He purge gas of the HCPB blanket does not allow to directly separate hydrogen isotopes via membrane permeators or CMRs therefore, in the back-up DEMO HCPB solution, a pre-concentration stage, probably operated Via zeolite membranes, is necessary.

Regarding the tritium removal from tritiated water some experiments have been performed by using heavy water. Such experiments have been carried out in a single tube CMR. In particular, the decontamination capability of the WGS and IS reactions have been evaluated by using two different catalysts and by operating at several operating conditions. WGS reactions has been performed with high water decontamination factor (up to 80% in a single stage) using catalysts that allowed to have a very low production of methane (less than 2% in the worst case and under 1% in the best case).

A middle-scale membrane reactor have been designed and commissioned (Chapter 6). The new multi-tube configuration is very compact (volume of about 10600 cm^3 containing 10 Pd-Ag tubes) since the Pd-Ag tubes are connected to the both sides of a cylinder which forms the reactor shell. Tests on middle-scale reactors, in view of DEMO, are necessary to validate the scalability of the single-tube performances and allow to gain experience on the engineering and operation procedure. Furthermore, in case of a good scalability of the single-tube, a ready (back-up) solution will be available in few years for the HCPB DEMO blanket. On the contrary, if the scalability would affect the tritium removal performances in Pd-Ag membrane separation and reaction, the work presented could be a primary step towards a better optimization of the multi-tube engineering concept.

By adopting specific tools (structural, thermal, fluid dynamics etc.), a deeper optimization and understanding of the influence of other variables, such as the fluid dynamic one, that could affect the performances of a multi-tube membrane reactor, could be of interest in view of a DEMO-scale tritium extraction process.

Additionally, many efforts may be put on the improvement of the catalysts packing and on the simplification of the engineering for a more accessible maintenance operations and reactors handling.

References

[1] The Road to Fusion Electricity, EUROfusion, https://www.euro-fusion.org/eurofusion/the-road-to-fusion-electricity (accessed November 13, 2017).

[2] G F Matthews and EFDA-JET contributors, JET ITER-like wall: overview and experimental programme, *Physica Scripta*, (2011).

[3] J. Paméla *et al*, An ITER-like wall for JET, *Journal of Nuclear Materials*. 363–365 (2007). doi:10.1016/j.jnucmat.2006.12.056.

[4] D. Maisonnier *et al.*, Power plant conceptual studies in Europe, *Nuclear Fusion*, 47 (2007).

[5] J. Rand *et al.*, Physics of Fusion Fuel Cycles: Nuclear Technology, Vol 2, No 1, http://www.tandfonline.com/doi/abs/10.13182/FST2-1-9 (accessed November 15, 2017).

[6] G.L. Kulcinski *et al.*, Nuclear fusion: Advanced fuels under debate, *Nature* 396 (1998). doi:10.1038/25456.

[7] M. Zucchetti, L.E. Sugiyama, Advanced Fuel Cycles for Fusion Reactors: Passive Safety and Zero-Waste Options, *J. Phys.* 41 (2006) 496. doi:10.1088/1742-6596/41/1/055.

[8] Deuterium: a precious gift from the Big Bang, ITER, http://www.iter.org/newsline/167/631 (accessed November 13, 2017).

[9] J.R. Gat, R. Gonfiantini, Stable isotope hydrology. Deuterium and oxygen-18 in the water cycle, (1981). http://inis.iaea.org/Search/search.aspx?orig_q=RN:13677657 (accessed November 13, 2017).

[10] T.Tanabe, Tritium fuel cycle in ITER and DEMO: Issues in handling large amount of fuel, *Journal of Nuclear Materials,* 438, July 2013, Pages 519-526

[11] Y. Igitkhanov, A new concept to achieve a higher fuel burn-up fraction in a DEMO reactor, 27th IEEE Symposium on Fusion Engineering (4-8 June 2017)

[12] T. Tanabe, Tritium: Fuel of Fusion Reactors, *Springer*, 2016.

[13] Tritium Handling and Safe Storage, DOE Technical Standards Program, https://www.standards.doe.gov/standards-documents/1100/1129-AStd-2015 (accessed November 23, 2017).

[14] S.B. Kim, N. Baglan, P.A. Davis, Current understanding of organically bound tritium (OBT) in the environment, *Journal of Environmental Radioactivity*, 126 (2013) 83–91, doi:10.1016/j.jenvrad.2013.07.011.

[15] Q.A. Acton, Radioisotopes: Advances in Research and Application, (2012). https://books.google.it/books?id=ay_4tH6gP1AC

[16] R.L. Michel, Tritium in the Hydrologic Cycle, Isotopes in the Water Cycle: Past, Present and Future of a Developing Science, *Springer Netherlands*, Dordrecht, 2005: pp. 53–66. doi:10.1007/1-4020-3023-1_5.

[17] I.A.E. Agency, O.N.E. Agency, Behaviour of tritium in the environment: proceedings of the International Symposium on the Behaviour of Tritium in the Environment, *International Atomic Energy Agency*, 1979.

[18] N.Ghirelli, S.Tosti, Tritium in Fusion: Production, Uses and Environmental Impact by Silvano, Tosti (Editor)/ Ghirelli, Nicholas (Editor): *Nova Science Pub Inc* (2016). http://www.abebooks.co.uk/Tritium-Fusion-Production-Uses-Environmental-Impact/17328606312/bd (accessed October 4, 2016).

[19] P. Gierszewski, Tritium supply for near-term fusion devices, *Fusion Engineering and Design*. 10 (1989) 399–403. doi:10.1016/0920-3796(89)90083-5.

[20] S. Jiang, M. He, Evidence for tritium production in the Earth's interior, *Chin. Sci. Bull*. 53 (2008) 540–547. doi:10.1007/s11434-008-0032-z.

[21] M. Ni, Y. Wang, B. Yuan, J. Jiang, Y. Wu, Tritium supply assessment for ITER and DEMOnstration power plant, *Fusion Engineering and Design*. 88 (2013) 2422–2426. doi:10.1016/j.fusengdes.2013.05.043.

[22] W.M. Stacey, Nuclear Reactor Physics, John Wiley & Sons, 2007.

[23] K.A. Solomon, Generating Tritium Using Civilian Reactors, (1992). https://www.rand.org/pubs/notes/N3203-1.html (accessed November 29, 2017).

[24] M.B. Kalinowski, International Control of Tritium for Nuclear Nonproliferation and Disarmament, *CRC Press*, 2004.

[25] Tritium and Enriched Uranium Management Plan Through 2060. http://fissilematerials.org/library/2015/10/tritium_and_enriched_uranium_m.html (accessed December 8, 2017).

[26] M.C. Kovari, Assessment of the tritium resource available to the fusion community, EuroFusion Report, 2016.

[27] G. Federici *et al.*, Overview of the design approach and prioritization of R&D activities towards an EU DEMO, Fusion Engineering and Design. 109–111 (2016) 1464–1474. doi:10.1016/j.fusengdes.2015.11.050.

[28] A. Hollingsworth, A review of tritium accountancy techniques, EuroFusion Report, 2012

[29] D. Demange *et al.*, Overview of R&D at TLK for process and analytical issues on tritium management in breeder blankets of ITER and DEMO, *Fusion Engineering and Design*. 87 (2012) 1206–1213. doi:10.1016/j.fusengdes.2012.02.105.

[30] Z. Köllö *et al.*, Calibrating a gas chromatograph to measure tritium using calorimetry, *Fusion Engineering and Design*, 84, 7–11, 2009, 1073-1075, https://doi.org/10.1016/j.fusengdes.2008.11.106.

[31] K. Isobe *et al.*, R&D activities of tritium technologies on Broader Approach in Phase 2-2, *Fusion Engineering and Design*. 98–99 (2015) 1792–1795. doi:10.1016/j.fusengdes.2015.06.075.

[32] D.J. Brassington, Photo-acoustic detection and ranging-a new technique for the remote detection of gases, *Journal of Physics D: Applied Physics.* 15 (1982) 219.

[33] G.L. Jackson, V.S. Chan, R.D. Stambaugh, An Analytic Expression for the Tritium Burnup Fraction in Burning-Plasma Devices, *Fusion Science and Technology*, 64 (2013) 8–12. doi:10.13182/FST13-A17042.

[34] M. Glugla *et al.*, The ITER tritium systems, *Fusion Engineering and Design*. 82 (2007) 472–487. doi:10.1016/j.fusengdes.2007.02.025.

[35] N. Taylor *et al.*, Resolving safety issues for a demonstration fusion power plant, *Fusion Engineering and Design*. 124 (2017) 1177–1180. doi:10.1016/j.fusengdes.2017.02.018.

[36] C. Day, T. Giegerich, The Direct Internal Recycling concept to simplify the fuel cycle of a fusion power plant, *Fusion Engineering and Design*. 88 (2013) 616–620. doi:10.1016/j.fusengdes.2013.05.026.

[37] M. Ionescu-Bujor, KIT - PL FUSION -Fuel Cycle, (2015). http://www.fusion.kit.edu/english/89.php (accessed November 10, 2017).

[38] D. Demange, S. Stämmler, M. Kind, A new combination of membranes and membrane reactors for improved tritium management in breeder blanket of fusion machines, *Fusion Engineering and Design*. 86 (2011) 2312–2316. doi:10.1016/j.fusengdes.2010.12.083.

[39] G. Federici *et al.*, European DEMO design strategy and consequences for materials, *Nucl. Fusion*. 57 (2017) 092002. doi:10.1088/1741-4326/57/9/092002.

[40] S. Tosti, G. Bruni, M. Incelli, A. Santucci, Ceramic membranes for processing plasma enhancement gases, *Fusion Engineering and Design*. 124 (2017) 928–933. doi:10.1016/j.fusengdes.2017.01.010.

[41] B. Bornschein, C. Day, D. Demange, T. Pinna, Tritium management and safety issues in ITER and DEMO breeding blankets, *Fusion Engineering and Design*. 88 (2013) 466–471. doi:10.1016/j.fusengdes.2013.03.032.

[42] B. Bornschein, M. Glugla, K. Günther, T.L. Le, K.H. Simon, S. Welte, Successful experimental verification of the tokamak exhaust processing concept of ITER with the CAPER facility, *Fusion Science and Technology*. 48 (2005) 11–16.

[43] M. Glugla, L. Dörr, R. Lässer, D. Murdoch, H. Yoshida, Recovery of tritium from different sources by the ITER Tokamak exhaust processing system, *Fusion Engineering and Design*. 61–62 (2002) 569–574. doi:10.1016/S0920-3796(02)00250-8.

[44] M. Glugla *et al.* , ITER fuel cycle R&D: Consequences for the design, *Fusion Engineering and Design*. 81 (2006) 733–744. doi:10.1016/j.fusengdes.2005.07.038.

[45] B. Bornschein, M. Glugla, K. Günther, R. Lässer, T.L. Le, K.H. Simon, S. Welte, Tritium tests with a technical PERMCAT for final clean-up of ITER exhaust gases, *Fusion Engineering and Design*. 69 (2003) 51–56. doi:10.1016/S0920-3796(03)00234-5.

[46] Y Iwai *et al.*, H-D-T cryogenic distillation experiments at TPL/JAERI in support of ITER, *Fusion Engineering and Design*, 61–62 (2002), 553-560, https://doi.org/10.1016/S0920-3796(02)00175-8.

[47] H. Yoshida, M. Glugla, T. Hayashi, R. Lässer, D. Murdoch, M. Nishi, R. Haange, Design of the ITER tritium plant, confinement and detritiation facilities, *Fusion Engineering and Design.* 61–62 (2002) 513–523. doi:10.1016/S0920-3796(02)00105-9.

[48] M. Glugla, R. Lässer, L. Dörr, D.K. Murdoch, R. Haange, H. Yoshida, The inner deuterium/tritium fuel cycle of ITER, *Fusion Engineering and Design*. 69 (2003) 39–43. doi:10.1016/S0920-3796(03)00231-X.

[49] S.-H. Yun *et al*., Risk-based multi-criteria design concept of the ITER SDS getter bed, *Fusion Engineering and Design*. 89 (2014) 1495–1499. doi:10.1016/j.fusengdes.2014.04.081.

[50] M. Glugla *et al.*,, The tritium fuel cycle of ITER-FEAT, *Fusion Engineering and Design.* 58–59 (2001) 349–353. doi:10.1016/S0920-3796(01)00356-8.

[51] A. B. Deme *et al.*, Experimental Investigation of ZrCo Getter Beds as Candidate Process for the Tritium Extraction Systems of the European Test Blanket Modules, *Fusion Science and Technology*. 71 (2017) 527–531. doi:10.1080/15361055.2017.1288976.

[52] H.A. Boniface, N.V. Gnanapragasam, D.K. Ryland, S. Suppiah, A. Perevezentsev, Water Detritiation System for ITER: Evaluation of Design Parameters, *Fusion Science and Technology.* 71 (2017) 241–245. doi:10.1080/15361055.2017.1290970.

[53] S. Welte, I. Cristescu, H. Dittrich, N. Lohr, C. Melzer, R. Michling, C. Plusczyk, P. Schaefer, Setup and commissioning of a combined water detritiation and isotope separation experiment at the Tritium Laboratory Karlsruhe, Fusion Engineering and Design. 88 (2013) 2251–2254. doi:10.1016/j.fusengdes.2013.03.061.

[54] I. Cristescu et al., Design and R&D activities of TriPla-CA Consortium in support of ITER Tritium Plant development, *Fusion Engineering and Design*. 89 (2014) 1524–1528. doi:10.1016/j.fusengdes.2014.03.067.

[55] S. Welte et al., Construction and commissioning of an ITER sized Pd/Ag permeator for a water detritiation experiment, *Fusion Engineering and Design*, 84, 7–11 (2009) 1969-1972, https://doi.org/10.1016/j.fusengdes.2009.02.027.

[56] R. Michling, I. Cristescu, L. Dörr, S. Welte, W. Wurster, Modification, enhancement and operation of a water detritiation facility at the Tritium Laboratory Karlsruhe,

Fusion Engineering and Design. 84 (2009) 338–343. doi:10.1016/j.fusengdes.2009.03.003.

[57] I.R. Cristescu, I. Cristescu, L. Doerr, M. Glugla, D. Murdoch, Tritium inventories and tritium safety design principles for the fuel cycle of ITER, *Nucl. Fusion*. 47 (2007) S458. doi:10.1088/0029-5515/47/7/S08.

[58] S. Konishi, M. Glugla, T. Hayashi, Fuel cycle design for ITER and its extrapolation to DEMO, *Fusion Engineering and Design.* 83 (2008) 954–958. doi:10.1016/j.fusengdes.2008.06.060.

[59] L.M. Giancarli *et al.*, Overview of the ITER TBM Program, Fusion Engineering and Design. 87 (2012) 395–402. doi:10.1016/j.fusengdes.2011.11.005.

[60] L.V. Boccaccini e*t al.*,Objectives and status of EUROfusion DEMO blanket studies, Fusion Engineering and Design. 109–111 (2016) 1199–1206. doi:10.1016/j.fusengdes.2015.12.054.

[61] C. Bachmann et al., Issues and strategies for DEMO in-vessel component integration, Fusion Engineering and Design. 112 (2016) 527–534. doi:10.1016/j.fusengdes.2016.05.040.

[62] S. Konishi *et al.*, Functional materials for breeding blankets—status and developments, Nucl. Fusion. 57 (2017) 092014. doi:10.1088/1741-4326/aa7e4e.

[63] A.R. Raffray, M. Akiba, V. Chuyanov, L. Giancarli, S. Malang, Breeding blanket concepts for fusion and materials requirements, Journal of Nuclear Materials. 307–311 (2002) 21–30. doi:10.1016/S0022-3115(02)01174-1.

[64] K. Tsuchiya *et al.*, Development of advanced tritium breeders and neutron multipliers for DEMO solid breeder blankets, Nucl. Fusion. 47 (2007) 1300. doi:10.1088/0029-5515/47/9/029.

[65] F. Hernández et al., A new HCPB breeding blanket for the EU DEMO: Evolution, rationale and preliminary performances, Fusion Engineering and Design, 124 (2017), 882-886, https://doi.org/10.1016/j.fusengdes.2017.02.008.

[66] G. Zhou et al., Preliminary structural analysis of the new HCPB blanket for EU DEMO reactor, International Journal of Hydrogen Energy, 41, 17(2016), 7053-7058, https://doi.org/10.1016/j.ijhydene.2016.01.064.

[67] R. Knitter, B. Löbbecke, Reprocessing of lithium orthosilicate breeder material by remelting, Journal of Nuclear Materials. 361 (2007) 104–111. doi:10.1016/j.jnucmat.2006.11.005.

[68] J.-C. Jaboulay, G. Aiello, J. Aubert, A. Morin, M. Troisne, Nuclear analysis of the HCLL blanket for the European DEMO, Fusion Engineering and Design. 124 (2017) 896–900. doi:10.1016/j.fusengdes.2017.01.050.

[69] G. Aiello, J. Aubert, N. Jonquères, A. Li Puma, A. Morin, G. Rampal, Development of the Helium Cooled Lithium Lead blanket for DEMO, Fusion Engineering and Design. 89 (2014) 1444–1450. doi:10.1016/j.fusengdes.2013.12.036.

[70] E. Martelli *et al.*, Advancements in DEMO WCLL breeding blanket design and integration, Int. J. Energy Res. (n.d.) n/a-n/a. doi:10.1002/er.3750.

[71] R.A. Causey et al., Tritium Barriers and Tritium Diffusion in Fusion Reactors

[72] S. Smolentsev et al., Dual-coolant lead–lithium (DCLL) blanket status and R&D needs, Fusion Engineering and Design, 100 (2015), 44-54, https://doi.org/10.1016/j.fusengdes.2014.12.031.

[73] M. Abdou *et al.*, Blanket/first wall challenges and required R&D on the pathway to DEMO, Fusion Engineering and Design. 100 (2015) 2–43. doi:10.1016/j.fusengdes.2015.07.021.

[74] B. Garcinuño *et al.*, Design and fabrication of a Permeator Against Vacuum prototype for small scale testing at Lead-Lithium facility, Fusion Engineering and Design. 124 (2017) 871–875. doi:10.1016/j.fusengdes.2017.02.060.

[75] F. Okino, P. Calderoni, R. Kasada, S. Konishi, Feasibility analysis of vacuum sieve tray for tritium extraction in the HCLL test blanket system, Fusion Engineering and Design. 109–111 (2016) 1748–1753. doi:10.1016/j.fusengdes.2015.10.004.

[76] D. Demange *et al.*, Tritium extraction technologies and DEMO requirements, Fusion Engineering and Design. 109–111 (2016) 912–916. doi:10.1016/j.fusengdes.2016.01.053.

[77] F. Hernández, P. Pereslavtsev, Q. Kang, P. Norajitra, B. Kiss, G. Nádasi, O. Bitz, A new HCPB breeding blanket for the EU DEMO: Evolution, rationale and preliminary performances, Fusion Engineering and Design. 124 (2017) 882–886. doi:10.1016/j.fusengdes.2017.02.008.

[78] E. Proust, L. Anzidei, M. Dalle Donne, U. Fischer, T. Kuroda, Solid breeder blanket design and tritium breeding, Fusion Engineering and Design. 16 (1991) 73–84. doi:10.1016/0920-3796(91)90184-R.

[79] G.E. Shatalov *et al.*, Breeder and test blankets in ITER, Fusion Engineering and Design. 16 (1991) 85–93. doi:10.1016/0920-3796(91)90185-S.

[80] A. Froio, C. Bachmann, F. Cismondi, L. Savoldi, R. Zanino, Dynamic thermal-hydraulic modelling of the EU DEMO HCPB breeding blanket cooling loops, Progress in Nuclear Energy. 93 (2016) 116–132. doi:10.1016/j.pnucene.2016.08.007.

[81] T. Hoshino, M. Dokiya, T. Terai, Y. Takahashi, M. Yamawaki, Non-stoichiometry and its effect on thermal properties of Li2TiO3, Fusion Engineering and Design. 61–62 (2002) 353–360. doi:10.1016/S0920-3796(02)00216-8.

[82] T. Hoshino *et al.*, Development of advanced tritium breeding material with added lithium for ITER-TBM, Journal of Nuclear Materials. 417 (2011) 684–687. doi:10.1016/j.jnucmat.2010.12.128.

[83] T. Hoshino, Pebble fabrication of super advanced tritium breeders using a solid solution of Li2+xTiO3+y with Li2ZrO3, Nuclear Materials and Energy, 9 (2016), 221-226, https://doi.org/10.1016/j.nme.2016.05.004.

[84] Francisco A. Hernández González, HCPB Design Report 2015, 17-Jun-16.

[85] J. Reimann, S. Hermsmeyer, Thermal conductivity of compressed ceramic breeder pebble beds, Fusion Engineering and Design. 61–62 (2002) 345–351. doi:10.1016/S0920-3796(02)00165-5.

[86] S. Yagi, D. Kunii, Studies on heat transfer near wall surface in packed beds, AIChE Journal. 6 (1960) 97–104. doi:10.1002/aic.690060119.

[87] B. Bornschein, C. Day, D. Demange, T. Pinna, Tritium management and safety issues in ITER and DEMO breeding blankets, Fusion Engineering and Design. 88 (2013) 466–471. doi:10.1016/j.fusengdes.2013.03.032.

[88] A. Santucci, M. Incelli, M. Sansovini, S. Tosti, Catalytic membrane reactor for tritium extraction system from He purge, Fusion Engineering and Design. doi:10.1016/j.fusengdes.2016.02.028.

[89] I. Cristescu, Extrapolation at DEMO scale of the HCPB TER system based on cryogenic trapping, EUROFusion, 13-Jun-17.

[90] D. Demange, L.V. Boccaccini, F. Franza, A. Santucci, S. Tosti, R. Wagner, Tritium management and anti-permeation strategies for three different breeding blanket options foreseen for the European Power Plant Physics and Technology Demonstration reactor study, Fusion Engineering and Design. 89 (2014) 1219–1222. doi:10.1016/j.fusengdes.2014.04.028.

[91] D. Demange, O. Borisevich, N. Gramlich, R. Wagner, S. Welte, Zeolite membranes and palladium membrane reactor for tritium extraction from the breeder blankets of ITER and DEMO, Fusion Engineering and Design, 88 (2013), 9–10, 2396-2399, https://doi.org/10.1016/j.fusengdes.2013.05.102.

[92] O. Borisevich, R. Antunes, D. Demange, Experimental study of permeation and selectivity of zeolite membranes for tritium processes, Fusion Engineering and Design. 98–99 (2015) 1755–1758. doi:10.1016/j.fusengdes.2015.04.015.

[93] M. Simplício, M.D. Afonso, O. Borisevich, X. Lefebvre, D. Demange, Permeation of single gases and binary mixtures of hydrogen and helium through a MFI zeolite hollow fibres membrane for application in nuclear fusion, Separation and Purification Technology. 122 (2014) 199–205. doi:10.1016/j.seppur.2013.10.034.

[94] M.P. Rohde, G. Schaub, S. Khajavi, J.C. Jansen, F. Kapteijn, Fischer–Tropsch synthesis with in situ H2O removal – Directions of membrane development, Microporous and Mesoporous Materials. 115 (2008) 123–136. doi:10.1016/j.micromeso.2007.10.052.

[95] S. Khajavi, F. Kapteijn, J.C. Jansen, Synthesis of thin defect-free hydroxy sodalite membranes: New candidate for activated water permeation, Journal of Membrane Science. 299 (2007) 63–72. doi:10.1016/j.memsci.2007.04.027.

[96] D. Demange, R. Antunes, O. Borisevich, L. Frances, D. Rapisarda, A. Santucci, M. Utili, Tritium extraction technologies and DEMO requirements, Fusion Engineering and Design. (n.d.). doi:10.1016/j.fusengdes.2016.01.053.

[97] Y. Kawamura, M. Enoeda, T. Yamanishi, M. Nishi, Feasibility study on the blanket tritium recovery system using the palladium membrane diffuser, Fusion Engineering and Design. 81 (2006) 809–814. doi:10.1016/j.fusengdes.2005.09.035.

[98] S. Tosti, L. Bettinali, V. Violante, Rolled thin Pd and Pd–Ag membranes for hydrogen separation and production, International Journal of Hydrogen Energy. 25 (2000) 319–325. doi:10.1016/S0360-3199(99)00044-0.

[99] Hatlevik, S.K. Gade, M.K. Keeling, P.M. Thoen, A.P. Davidson, J.D. Way, Palladium and palladium alloy membranes for hydrogen separation and production: History, fabrication strategies, and current performance, Separation and Purification Technology. 73 (2010) 59–64. doi:10.1016/j.seppur.2009.10.020.

[100] N. Hilal, A.F. Ismail, C. Wright, Membrane Fabrication, CRC Press, 2015.

[101] F. Gallucci, E. Fernandez, P. Corengia, M. van Sint Annaland, Recent advances on membranes and membrane reactors for hydrogen production, Chemical Engineering Science. 92 (2013) 40–66. doi:10.1016/j.ces.2013.01.008.

[102] A. Arratibel Plazaola, D.A. Pacheco Tanaka, M. Van Sint Annaland, F. Gallucci, Recent Advances in Pd-Based Membranes for Membrane Reactors, Molecules. 22 (2017) 51. doi:10.3390/molecules22010051.

[103] S. Tosti, Supported and laminated Pd-based metallic membranes, International Journal of Hydrogen Energy. 28 (2003) 1445–1454. doi:10.1016/S0360-3199(03)00028-4.

[104] W. Koros, Y. Ma, T. Shimidzu, Terminology for membranes and membrane processes, J. Membr. Sci. 120 (1996) 149–159.

[105] S. Tosti, A. Basile, L. Bettinali, F. Borgognoni, F. Chiaravalloti, F. Gallucci, Long-term tests of Pd–Ag thin wall permeator tube, Journal of Membrane Science. 284 (2006) 393–397. doi:10.1016/j.memsci.2006.08.006.

[106] S. Tosti, F. Borgognoni, A. Santucci, Electrical resistivity, strain and permeability of Pd–Ag membrane tubes, International Journal of Hydrogen Energy. 35 (2010) 7796–7802. doi:10.1016/j.ijhydene.2010.05.088.

[107] J. Zaman, A. Chakma, Inorganic membrane reactors, Journal of Membrane Science. 92 (1994) 1–28. doi:10.1016/0376-7388(94)80010-3.

[108] S. Yun, S. Ted Oyama, Correlations in palladium membranes for hydrogen separation: A review, Journal of Membrane Science. 375 (2011) 28–45. doi:10.1016/j.memsci.2011.03.057.

[109] J. Shu, B.P.A. Grandjean, A.V. Neste, S. Kaliaguine1, Catalytic palladium-based membrane reactors: A review, Can. J. Chem. Eng. 69 (1991) 1036–1060. doi:10.1002/cjce.5450690503.

[110] S. Tosti, C. Rizzello, 24 - Membranes for nuclear power applications, in: Advanced Membrane Science and Technology for Sustainable Energy and Environmental Applications, Woodhead Publishing, 2011: pp. 769–791. http://www.sciencedirect.com/science/article/pii/B9781845699697500242 (accessed September 1, 2016).

[111] S. Tosti, A. Basile, G. Chiappetta, C. Rizzello, V. Violante, Pd–Ag membrane reactors for water gas shift reaction, Chemical Engineering Journal. 93 (2003) 23–30. doi:10.1016/S1385-8947(02)00113-4.

[112] S. Tosti, Overview of Pd-based membranes for producing pure hydrogen and state of art at ENEA laboratories, International Journal of Hydrogen Energy. 35 (2010) 12650–12659. doi:10.1016/j.ijhydene.2010.07.116.

[113] D. Demange, M. Glugla, K. Günther, T.L. Le, K.H. Simon, R. Wagner, S. Welte, Counter-current isotope swamping in a membrane reactor: The PERMCAT process and its applications in fusion technology, Catalysis Today. 156 (2010) 140–145. doi:10.1016/j.cattod.2010.02.033.

[114] M. Glugla, A. Perevezentsev, D. Niyongabo, R.-D. Penzhorn, A. Bell, P. Herrmann, A Permcat reactor for impurity processing in the JET Active Gas Handling System, Fusion Engineering and Design. 49–50 (2000) 817–823. doi:10.1016/S0920-3796(00)00209-X.

[115] D. Demange, S. Welte, M. Glugla, Experimental validation of upgraded designs for PERMCAT reactors considering mechanical behaviour of Pd/Ag membranes under H2 atmosphere, Fusion Engineering and Design. 82 (2007) 2383–2389. doi:10.1016/j.fusengdes.2007.05.049.

[116] S. Tosti, L. Bettinali, F. Borgognoni, D.K. Murdoch, Mechanical design of a PERMCAT reactor module, Fusion Engineering and Design. 82 (2007) 153–161. doi:10.1016/j.fusengdes.2006.08.003.

[117] S. Welte, D. Demange, R. Wagner, Mechanical design and first experimental results of an upgraded technical PERMCAT reactor for tritium recovery in the fuel cycle of a fusion machine, Fusion Engineering and Design. 85 (2010) 1320–1325. doi:10.1016/j.fusengdes.2010.03.033.

[118] Method for the production of hydrogen-containing gaseous mixtures, n.d. http://www.google.com/patents/US6685754 (accessed January 5, 2018).

[119] Permselective membrane type reactor and method for hydrogen production, n.d. http://www.google.com/patents/US20080226544 (accessed January 5, 2018).

[120] S. Tosti, A. Basile, L. Bettinali, F. Borgognoni, F. Gallucci, C. Rizzello, Design and process study of Pd membrane reactors, International Journal of Hydrogen Energy. 33 (2008) 5098–5105. doi:10.1016/j.ijhydene.2008.05.031.

[121] E. Carella, C. Moreno, F.R. Urgorri, D. Rapisarda, Á. Ibarra, Tritium modelling in HCPB breeder blanket at a system level, Fusion Engineering and Design. (2017). doi:10.1016/j.fusengdes.2017.01.051.

[122] S. Tosti, C. Rizzello, F. Borgognoni, N. Ghirelli, A. Santucci, P. Trabuc, Design of Pd-based membrane reactor for gas detritiation, Fusion Engineering and Design. 86 (2011) 2180–2183. doi:10.1016/j.fusengdes.2010.11.021.

[123] M. Incelli, A. Santucci, S. Tosti, M. Sansovini, M. Carlini, Heavy water decontamination tests through a Pd-Ag membrane reactor: Water Gas Shift and Isotopic Swamping performances, Fusion Engineering and Design. 124 (2017) 692–695. doi:10.1016/j.fusengdes.2017.06.021.

[124] J.G. Bayly, V.B. Kartha, W.H. Stevens, The absorption spectra of liquid phase H2O, HDO and D2O from 0·7 μm to 10 μm, Infrared Physics. 3 (1963) 211–222. doi:10.1016/0020-0891(63)90026-5.

[125] O.D. Bonner, J.D. Curry, Infrared spectra of liquid H2O and D2O, Infrared Physics. 10 (1970) 91–94. doi:10.1016/0020-0891(70)90003-5.

[126] S.Y. Venyaminov, F.G. Prendergast, Water (H2O and D2O) Molar Absorptivity in the 1000–4000 cm−1Range and Quantitative Infrared Spectroscopy of Aqueous Solutions, Analytical Biochemistry. 248 (1997) 234–245. doi:10.1006/abio.1997.2136.

[127] M. Vadrucci, F. Borgognoni, A. Moriani, A. Santucci, S. Tosti, Hydrogen permeation through Pd–Ag membranes: Surface effects and Sieverts' law, International Journal of Hydrogen Energy. 38 (2013) 4144–4152. doi:10.1016/j.ijhydene.2013.01.091.

[128] A. Santucci, F. Borgognoni, M. Vadrucci, S. Tosti, Testing of dense Pd–Ag tubes: Effect of pressure and membrane thickness on the hydrogen permeability, Journal of Membrane Science. 444 (2013) 378–383. doi:10.1016/j.memsci.2013.05.058.

[129] A. Basile, G. Chiappetta, S. Tosti, V. Violante, Experimental and simulation of both Pd and Pd/Ag for a water gas shift membrane reactor, Separation and Purification Technology. 25 (2001) 549–571. doi:10.1016/S1383-5866(01)00168-X.

[130] C.A. Cornaglia, S. Tosti, J.F. Múnera, E.A. Lombardo, Optimal Pt load of a Pt/La2O3·SiO2 highly selective WGS catalyst used in a Pd-membrane reactor, Applied Catalysis A: General. 486 (2014) 85–93. doi:10.1016/j.apcata.2014.08.018.

[131] Claudio Rizzello et al., Simulazione di un reattore a membrana per processi di detriziazione in fase gassosa

[132] S. Tosti, L. Bettinali, V. Violante, Rolled thin Pd and Pd–Ag membranes for hydrogen separation and production, International Journal of Hydrogen Energy. 25 (2000) 319–325. doi:10.1016/S0360-3199(99)00044-0.